ÉCOLE DE TECHNOLOGIE SUPÉRIEURE
UNIVERSITÉ DU QUÉBEC

THESIS PRESENTED TO
ÉCOLE DE TECHNOLOGIE SUPÉRIEURE

IN PARTIAL FULFILLMENT OF THE REQUIREMENTS FOR
THE DEGREE OF DOCTOR OF PHILOSOPHY
Ph.D.

BY
Faten M'HIRI

ANGIOGRAPHIC IMAGE ANALYSIS FOR THE DIAGNOSIS OF CORONARY
DISEASE IN YOUNG PATIENTS

MONTREAL, 29 JUNE 2016

BOARD OF EXAMINERS

THIS THESIS HAS BEEN EVALUATED

BY THE FOLLOWING BOARD OF EXAMINERS:

M. Luc Duong, thesis director
Département de génie logiciel et des technologies de l'information, École de technologie
supérieure

M. Mohamed Cheriet, co-advisor
Département de la génie de la production automatisée, École de technologie supérieure

M. Éric Wagnac, committee president
Département de génie mécanique, École de technologie supérieure

M. Tien Dai Bui, external examiner
Department of Computer Science and Software Engineering, Concordia University

Mme. Sylvie Ratté, invited examiner
Département de génie logiciel et des technologies de l'information, École de technologie
supérieure

THIS THESIS WAS PRESENTED AND DEFENDED

IN THE PRESENCE OF A BOARD OF EXAMINERS AND THE PUBLIC

ON 24 MAY 2016

AT ÉCOLE DE TECHNOLOGIE SUPÉRIEURE

"A man will continue to have knowledge as long as he is seeking knowledge.

If he assumes that he has knowledge, then he has become ignorant."

Ibn Al-Mubarak

Je tiens à remercier mes parents Sabah et Radhi Mhiri, pour être des parents formidables, toujours ouverts et à l'écoute. Merci à toi maman de m'apprendre à être patiente mais toujours déterminée. Merci, papa de m'avoir toujours dit que dans la vie on peut tout faire tant qu'on a la volonté. Votre décision de quitter la Tunisie pour nous et de venir reconstruire une nouvelle vie au Canada, alors que vous aviez tout en Tunisie, est une preuve pour moi que tout est possible... même avoir plusieurs vies dans une vie. Merci à mon frère Fares qui m'inspire malgré son jeune âge: merci pour ton humour décalé et ta joie de vivre.

Merci à mon mari et meilleur ami Habib Sakka, qui a été d'un soutien inconditionnel et indéfectible: Merci de croire en moi et de m'encourager à me dépasser et à devenir meilleure et merci de toujours garder ton sens de l'humour.

Je suis reconnaissante envers toute ma famille Mhiri et Fantar, qui m'a toujours encouragée dans la poursuite de mes études, et aux nouveaux membres de ma famille: tata Fatma, tonton Lotfi, Aicha et toute la famille Sakka. Merci pour votre accueil, votre générosité sans faille et vos encouragements.

Merci aussi à tous mes amis d'ici et d'ailleurs: Emira, Rania, Asma, Juliette et Anne Marie. Je suis reconnaissante aux employés de l'ETS, avec lesquels j'ai eu le plaisir de travailler, et à mes camarades du club Tributerre de m'avoir poussé à sortir du laboratoire et à mieux apprécier la vie étudiante. Merci aux techniciens du département LOG/TI à l'ETS et aux techniciennes de Sainte Justine et au reste de l'équipe de cardiologie.

I thank the young patients of Sainte Justine and their families. This work is dedicated to them.

ANGIOGRAPHIC IMAGE ANALYSIS FOR THE DIAGNOSIS OF CORONARY DISEASE IN YOUNG PATIENTS

Faten M'HIRI

ABSTRACT

Congenital heart disease (CHD) is the leading cause of birth defects worldwide. In Canada, about 1 in 100 of newborns are with CHD. New methods and protocols to both diagnose and treat CHD are needed. To diagnose or treat newborns or young patients, cardiologists often use percutaneous catheter-based interventions (PCI). PCI is based on using a real-time two-dimensional X-ray moving sequence to navigate inside the patient's heart. This moving sequence will display the artery of the patient during one or more cardiac cycles. During one cardiac cycle, the diameter of a healthy coronary artery (CA) changes: it expands in diastole, when the blood flow in the artery increases, and it shrinks in systole. Capturing these diameter changes is one of the measures used to evaluate the state of the CA as an indicator for a vascular disease. These measurements are usually done manually on X-ray frames or using other image modalities such as ultrasounds. This research sheds new light on an automatic method that can guide the diagnosis of coronary arteries from 2D X-ray sequences. Measuring CA diameter automatically in the X-ray sequence is not a straightforward task. First, a segmentation step is needed to extract CA in 2D X-ray angiograms. Second, the CA is tracked during the moving sequence. Finally, with the segmented and tracked CA, an automatic method measures the diameters of CA at each frame of the sequence and an assessment of diameter variations during the sequence is presented. Each step presents different challenges regarding : the complexity of CA structure, the lack of contrast in the images, the presence of motion artifacts, and the small variations of diameters from one frame to the next. This work introduces new methods for segmentation, tracking and diameter measurements. Our project is held in collaboration with the cardiology department at Sainte Justine's children hospital. The methods developed in this research have been tested and evaluated on a dataset of X-ray sequences of young patients. Qualitative and quantitative results show the efficiency of the methods from segmenting and tracking to measuring the diameter's variation from X-ray moving sequence.

L'ANALYSE D'IMAGE ANGIOGRAPHIQUES POUR LE DIAGNOSTIQUE DES PATHOLOGIES CORONARIENNE EN PÉDIATRIE

Faten M'HIRI

RÉSUMÉ

Les cardiopathies coronariennes sont parmi les malformations congénitales les plus observées chez l'enfant et les nouveau-nés. Au Canada, un nouveau né sur 100 est atteint de cardiopathie congénitale. Aujourd'hui, il existe un réel besoin de nouvelles méthodes et protocoles pour diagnostiquer et traiter ces cardiopathies. Pour traiter ou faire le diagnostique de ces cardiopathies, des interventions coronariennes percutanées (ICP) sont réalisées. Les ICP sont guidées par une séquence de radiographies 2D prises en temps-réel durant un ou plusieurs cycles cardiaques. Durant un cycle cardiaque, le diamètre d'une artère coronaire saine change: ce diamètre va se dilater en diastole quand le flux sanguin croit à l'intérieur de l'artère et se contracter en systole. Cette variation de diamètre est l'une des mesures utilisées pour évaluer l'état de l'artère coronaire (AC) comme indicateur de pathologie vasculaire. Cette mesure est souvent calculée manuellement à partir d'une image de la séquence radiographique ou encore en utilisant d'autres modalités d'imagerie comme l'échographie. Cette recherche présente une nouvelle contribution sur une méthode qui guidera le diagnostique des artères coronaires à partir des séquences de radiographies 2D. Mesurer automatiquement le diamètre d'une artère coronaire dans une séquence radiographique est une tâche complexe. D'abord, une étape de segmentation est nécessaire pour extraire l'AC dans la séquence radiographique. Ensuite, l'artère est traquée durant la séquence en mouvement. Finalement, en utilisant le résultat de segmentation et de suivi de l'artères, une méthode automatique de mesure de diamètre est appelée pour évaluer les variations de diamètres. Chaque étape présente différents défis reliés à: la complexité de la structure des AC, au niveau de contraste limité dans certaines images, à la présence d'artéfacts de mouvement, et à la faible variation de diamètre d'AC d'une image à la suivante. Cette recherche introduit de nouvelles méthodes pour la segmentation, le suivi et la mesure de diamètre à partir de séquence de radiographie 2D. Notre projet est réalisé avec la collaboration du département de cardiologie du CHU Sainte Justine. Les méthodes développées ont été testées et évaluées sur une base de données de radiographies de jeunes patients. Les résultats qualitatifs et quantitatifs montrent l'efficacité des méthodes de segmentation et suivi et celle de la mesure des variations de diamètre à partir des séquence radiographiques.

Mots clés: Segmentation, artères coronaires, méthodes basées sur les graphes, angiographies, suivi du mouvement, cardiologie, détection de vaisseaux sanguins, radiographies

CONTENTS

LIST OF TABLES

LIST OF FIGURES

LIST OF ABREVIATIONS

AC   Active Contour method

AUC   Area under the ROC curve

CA   Coronary Arteries

CHD   Congenital Heart Defect/Disease

CT   Computed Tomography

Cx   Circumflex Coronary Artery

ECG   Electrocardiography

GC   Graph cuts method

LAD   Left Anterior Descending Artery

MAPCAs   major aortopulmonary collateral arteries

MSCT   Multi-Slice Computer Tomography

PCI   Percutaneous coronary intervention

RCA   Right Coronary Artery

ROC   Receiver Operating Characteristic

RW   Random Walker method

SP   Superpixel

TVW   Temporal Vessel Walker method

TVWSP   Temporal Vessel Walker method with Superpixels

VW   Vessel Walker method

VWSP	Vessel Walker method with Superpixels
2D	Two dimensions
3D	Three dimensions

INTRODUCTION

Congenital heart disease (CHD) is the leading cause of birth defects worldwide (Peter WG *et al.* (2010)). In Canada, about 1 in 100 of newborns have CHD. According to the Canadian Congenital Heart Alliance (2010) (CCHA), the survival rate of these newborns to adulthood increased from 20% to 90%, in 60 years. However, as mentioned by the CCHA, more work has to be done in the area of heart disease research and CHD in particular. Therefore, new methods and protocols to both diagnose and treat CHD are needed.

CHD leads to malformations at different structures in the heart, including coronary arteries. Indeed, these arteries can be affected in several ways, showing pathologies such as stenosis (a narrowing of the artery) or aneurysms (an enlargement of the artery).

To diagnose or treat young patients with pathological coronary arteries, cardiologists often use percutaneous catheter-based interventions (PCI). PCI is preferred to open heart surgery, especially with young patients. These procedures involve the insertion of a catheter through the vascular system and are guided by real-time two-dimensional (2D) X-ray moving sequence to navigate inside the patient's heart. These 2D X-ray sequences, also called fluoroscopy or angiogram sequences, can be used to evaluate the distensibility of coronary arteries. Distensibility is one accurate indicator of cardiovascular disease by assessing blood vessels elasticity. More precisely, the distensibility index measures how the vessel's diameter stretches or dilates as the blood flow increases or decreases. The artery's diameter variation during the cardiac cycle is a key indicator of healthy or pathological arteries. For example, a low distensibility measure indicates a small variation of the diameter and a possible artery wall stiffness due to a vascular disease. Therefore, measuring coronary arteries (CA) diameter variation along the X-ray sequence is essential to compute distensibility index.

Diameter measurements are usually done manually by a technical expert. However, manual measurement lacks precision and shows inter and intra oberver variability. Other measurements techniques are proposed in the literature or in existing software (Gronenschild *et al.* (1994) and PIEMedical and Medis) to semi-automatically segment part of a vessel. These software work

on one single X-ray frame and do not evaluate the vessel diameter along the moving sequence. Moreover, most of the existing works that assess the distensibility measure are applied on other imaging modalities, such as ultrasound. The present research explores, the possibility of computing the distensibility measure automatically from 2D X-ray sequence. To the best of our knowledge, this is the first study that involves a temporal analysis of the diameter variation of the coronary artery during the cardiac sequence, **automatically** and based on a **monoplane 2D X-ray** angiographic sequence.

Measuring the diameter of an artery during the X-ray sequence is not a straightforward task. First, the coronary arteries are segmented from 2D X-ray angiograms. Second, a coronary artery is tracked in time during the moving sequence to capture the diameter changes. Finally, using the segmentation and tracking result, the measurement of the artery's diameter at each frame must be precise to compute the distensibility index. This thesis focus on each one of the mentioned 3 steps that lead to measuring distensibility. The following section presents the outline of the manuscript to describe our work.

0.1. Manuscript Overview

First, the manuscript starts by detailing the research problem and objectives within the defined clinical context. Then, the second chapter presents the clinical context, as well as the existing works on the topics of: medical image segmentation, structure tracking and the quantification of vascular structures.

The three following chapters can be read independently, since each of them represents one research objective and describes the proposed method to reach each objective with the corresponding experimental results.

Chapter 3 introduces our first contribution in segmenting tubular structure in general and coronary arteries in particular from 2D X-ray images. Automatic segmentation of arteries is a key step before measuring its physiological properties. However, segmenting arteries from 2D angiograms is challenging due to the complexity of the structure and the artifacts within

the image. We propose a new method that combines prior information (using intensity and topological information) together with an existing segmentation approach, the random walks by Grady *et al.* (2006a). This combination leads to our first contribution: the Vessel Walker method for vessel segmentation.

In chapter four, the manuscript presents the second research objective, where temporal information is added to not only segment but also to track one coronary artery in the X-ray sequence. Such step provides the necessary information to assess the dynamics of the vessel during the cardiac cycle. To do so, it is important to track and segment the artery accurately, while dealing with the complex cardiac and respiratory motions. We propose a new spatio-temporal algorithm for segmenting a specific coronary artery and tracking it in the X-ray moving sequence. This algorithm uses a modified version of the Vessel Walker, with temporal information, leading to a Temporal Vessel Walker for coronary artery segmentation and tracking.

Chapter 5 uses the two previous contributions to compute the diameter changes of an artery during the moving sequence. Such computations provide the cardiologist with the necessary information to evaluate the artery's elasticity by measuring its distensibility index. To do so, an accurate measurement of the artery's width during the cardiac cycle is necessary. These measurements are based on precise segmentation results to capture the diameter changes. The fifth chapter presents the pipeline for measuring distensibility index: First, the method automatically segment the vessel of interest (or part of a vessel that a cardiologist wants to evaluate). Then, the vessel is tracked and segmented in the moving sequence. Finally, the diameters of the vessel at each frame of the sequence are computed automatically. We believe that this contribution is the first to tackle distensibility measurement in this specific context, where the diameter of a coronary artery is computed automatically during the cardiac cycle using only a monoplane 2D X-ray sequence.

Finally, the last chapter summarizes the work accomplished and gives perspectives for future work.

CHAPTER 1

RESEARCH PROBLEM

1.1   Problem statement

According to the World Health Organization (WHO (2014)), cardiovascular disease is the number one cause of mortality in the world. More specifically, congenital heart defects (CHD) are culpable for the high rate of mortality among newborns and children (Peter WG *et al.* (2010)). CHD often affects the coronary arteries showing pathologies such as stenosis (a narrowing of the artery) or aneurysms (an enlargement of the artery). One popular procedure used to diagnose or treat CHD are percutaneous catheter-based interventions (PCI). As shown in Figure 1.1, these procedures involve the insertion of a catheter through the vascular system and are guided by a real-time 2D X-ray angiogram (or fluoroscopy). Since blood vessels are invisible to X-rays as shown in the first image in Figure 1.2, a contrast agent is injected through the vessels to depict them, during PCI (Figure 1.2b).

Arterial distensibility is one of the most accurate measures used by cardiologists to diagnose CHD Cheung *et al.* (2002). This measure evaluates the elasticity of a blood vessel to expand and contract with cardiac contraction (systole) and relaxation (diastole) (Godia *et al.* (2007)). Having a low distensibility measure can be an indicator of an artery wall stiffness and, therefore, of a vascular disease. This measure evaluates the vessel's diameter changes in response to cardiac work. Hence, a precise measurement of a blood vessel's diameter during the cardiac cycle is critical to compute the distensibility, and to help the detection of cardiovascular diseases.
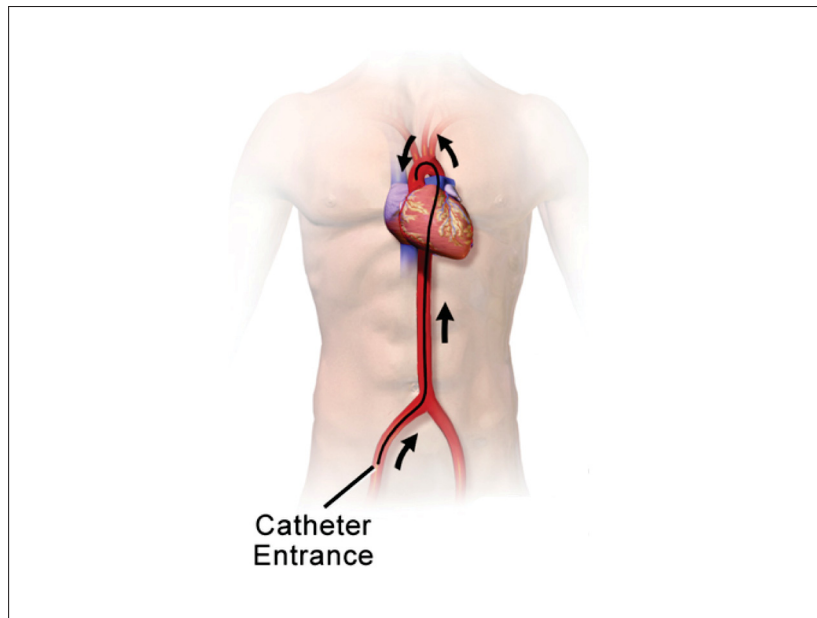
Figure 1.1   Percutaneous catheter-based intervention : the catheter (the black tube) is inserted from a blood vessel in the groin and is advanced into the heart.
Image Adapted from "Balloon-tipped catheter" used under Creative Common by Bruce Blaus (BruceBlaus (2016)).

a) frame with no contrast agent   b) frame with contrast agent
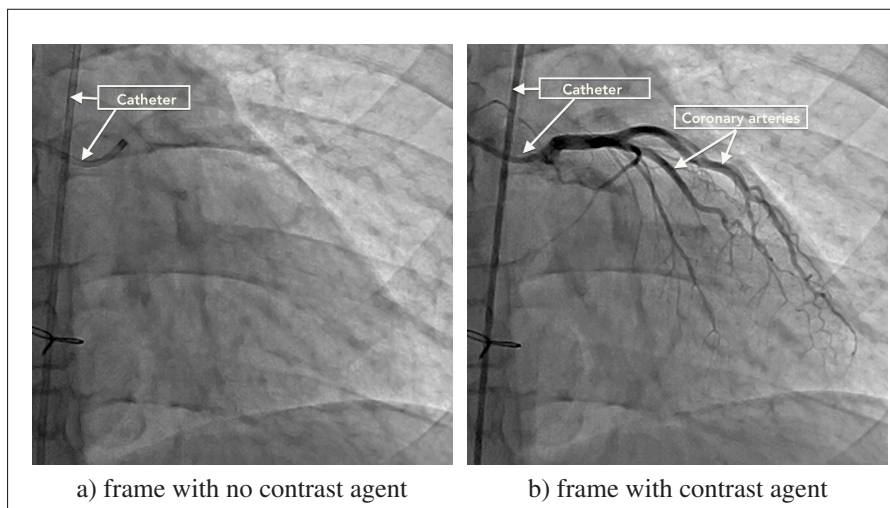
Figure 1.2   X-ray frame without the contrast agent (left) and the same X-ray after the injection of the contrast agent (right).

This research focus on the evaluation of diameter changes during the cardiac cycle automatically from monoplane 2D X-ray sequences. An overview of the research questions and objectives is presented in Figure 1.3 and they are detailed in the following. The general research question is :

Can we evaluate the changes of coronary artery's diameter, directly from monoplane 2D X-ray moving sequences?
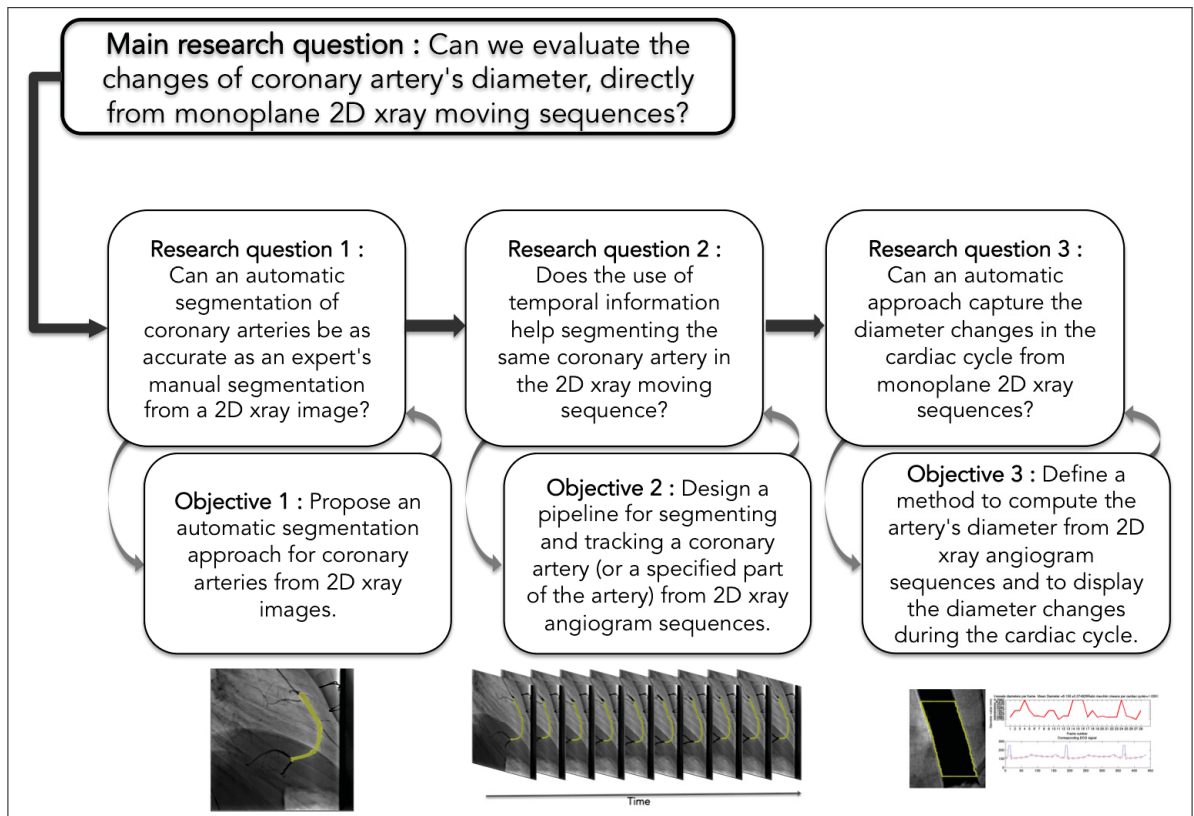
Figure 1.3 Overview of research questions and objectives.

Extracting coronary arteries automatically from angiogram is necessary before computing vessel diameter. Different works proposed automatic methods for vascular segmentation. However, it is still an open research topic. Moreover, segmenting vessels from 2D X-ray angiograms represents a different challenge than segmenting vessels from other imaging modalities such as Magnetic Resonance Imaging (MRI) or Multi-Slice Computer Tomography (MSCT). Fur-

thermore, other imaging techniques can beneficiate from better prior (eg. the Hounsfield unit in MSCT is used to detect vessels). Such information cannot be used in 2D X-rays. Besides processing 2D images can be challenging due to vessel overlap or low contrast in some regions. The issue to consider at this step is: ***Can an automatic segmentation of coronary arteries be as accurate as an expert's manual segmentation from a 2D X-ray image?***

Additionally, X-ray angiograms are real-time moving sequences that capture not only the structure of the coronary artery but also its motion in time. To compute the diameter changes during the cardiac cycle, one has to segment and track simultaneously the same artery in the moving sequence. Both respiratory and cardiac motions have to be considered during tracking, since these motions affect the coronary arteries' shape as well as their location. The second step of our research is to segment the same artery (or part of an artery) in the X-ray moving sequence. This leads to the second research question: ***Does the use of temporal information helps in segmenting the same coronary artery in the 2D X-ray moving sequence?***

Finally, the segmented and tracked coronary artery has a diameter that changes according to the level of blood flow within it. Indeed, a healthy artery's wall would expand, when there is an important level of blood flow, and shrinks, when the flow decreases. Distensibility is one accurate indicator of cardiovascular disease by evaluating the elasticity and the condition of an artery. Such measure needs a precise computation of the artery's diameter during the cardiac cycle. These measurements are often computed using other imaging modalities such as ultrasound or biplane X-ray sequences. Our third research question is: ***Can an automatic approach capture the diameter changes in the cardiac cycle from monoplane 2D X-ray sequences?***

Challenges

Our research focus on the segmentation, tracking and measurement of coronary arteries from monoplane 2D X-ray angiograms. Different challenges should be considered:

- Coronary arteries (CA) are complex tubular structures : They are thin elongated structures with various diameters and bifurcations. This makes the segmentation step challenging

especially with young patients, where the vessels are smaller than in adults. Moreover, 2D X-ray angiograms are a projection of a three-dimensional structure in a two-dimensional plane. The projection causes the loss of depth information, where two vessels at different levels of depth would be pictured as overlapping in the 2D angiogram. Furthermore, since a contrast agent is injected to depict coronary arteries, this agent disappears as it moves, with the blood flow, through the arteries. This causes the contrast to decrease during the X-ray sequence.

- Coronary arteries are moving structures in the angiography sequence : Indeed, they are influenced by respiratory and cardiac motions which makes their position and shape changes in the sequence.

- Coronary arteries are thin structures: therefore they have small diameter (with a diameter as small as 1 mm in newborns and 4.5 mm in teenagers (Oberhoffer *et al.* (1989))) and the variability of the diameter during the cardiac cycle is smaller (can be less than 1 mm). The extraction and the measurement of the arteries have to be precise enough to capture this variability.

- This research is conducted on a pediatric population which implies: small vascular structures, a faster heart rate than an adult's and a restricted injection doses of the contrast agent. Besides, some X-rays of patients that have been previously operated, depict sternal sutures. These are dark and tubular structures that can be misperceived as blood vessel by a segmentation method.

- Dataset availability: To our best knowledge, no dataset of 2D X-ray angiogram sequence is available with the corresponding ground truth data. Therefore, a first step in this research is to construct a dataset of angiograms with the collaboration of Sainte-Justine's Children Hospital after the approval of the Sainte-Justine's Institutional Ethics Review Board. Moreover, to evaluate quantitatively the accuracy of the computed results, a ground truth of this dataset has to be built with the help of technicians and cardiologists at Sainte-Justine's Hospital.

Clinical application

This work is conducted with the collaboration of two cardiologists from CHU Sainte Justine's Cardiology Department : Dr. Joaquim Miró and Dr. Nagib Dahdah and their team. All the data collected and the results obtained are supervised and validated by two experts from Sainte Justine.

1.2 Research hypothesis

The work proposes a new automatic method for evaluating coronary arteries to guide the diagnosis of heart disease in the pediatric population. This section highlights the hypothesis that are investigated in the research :

Hypothesis 1 : *An automatic method to extract coronary arteries from 2D angiograms can be as accurate as an expert's manual segmentation.*

Automatic segmentation of vascular structures remains an open research topic despite the fact that different works have tackled this problem. Yet it is still a challenging task due to the nature of the structure. Besides, the segmentation method depends on the imaging modality that is used. This work seeks for an automatic segmentation method able to extract the lumen of vascular structures as accurately as a segmentation expert.

Hypothesis 2 : *Using temporal information in 2D X-ray moving sequence helps segmenting and tracking a specific coronary artery.*

Coronary arteries are moving structures. Temporal information can be used to segment and track the same artery in the angiography sequence. The segmentation result at one frame can be used as a temporal prior for segmenting the rest of the frames. Extracting the same coronary artery in the moving sequence will provide important information regarding the elasticity of the artery or the presence of deformations.

Hypothesis 3 : *Distensibility measure can be computed directly from monoplane 2D X-ray angiograms.*

Distensibility is based on evaluating the coronary arteries' diameter changes in the cardiac cycle. It is often computed using other imaging modalities such as ultrasound images (Godia *et al.* (2007)), MRI or biplane X-ray sequences. This hypothesis evaluates whether distensibility measure can be computed automatically from monoplane 2D X-rays. To do so, the segmentation and tracking result is used to compute the diameter of the vessel at each frame of the sequence. The measurement of the artery should be precise to capture the diameter changes and obtain thereby the distensibility measure.

1.3 Research objectives

To evaluate each hypothesis, this section defines our research objectives.

1.3.1 Segmentation of coronary arteries from 2D X-ray angiogram

Objective 1 : Propose an automatic segmentation approach for coronary arteries from 2D X-ray images.

The result should be as precise as a manual segmentation and improve other existing segmentation approaches. To do so, we take into account the observed limitations in 2D angiograms (vessel overlap, low contrast level, presence of other dark tubular structures, etc.). There are different information that can be used to characterize coronary arteries : using intensity information, topological information or local information within a neighbourhood. A combination of these characteristics can bring to an accurate segmentation result. To reach this objective, we propose different segmentation approaches either using active contours (M'hiri *et al.* (2012b)) or normalized cut (M'hiri *et al.* (2012a)). However, a new segmentation approach named "Vessel Walker" (M'hiri *et al.* (2013)) has shown a better performance to segment the coronary artery tree. This work is further presented in Chapter 3 of the manuscript.

1.3.2 Spatio-temporal segmentation (or segmentation and tracking) of coronary arteries in 2D X-ray angiogram sequences

Objective 2 : Design a pipeline for segmenting and tracking a coronary artery (or a specified part of the artery) from 2D X-ray angiogram sequences.

Both respiratory and cardiac motions should be considered while segmenting and tracking the artery. The result should be as accurate as a manual ground truth. The method should consider respiratory and cardiac motions to track the coronary arteries. Moreover, the method has to consider that the intensity level changes from one frame to the following, as the contrast agent disappears. We propose a new spatio-temporal segmentation model that uses temporal prior to segment and track an artery. The model has encouraging quantitative, and qualitative results in comparison with existing works. The proposed pipeline, focus on tracking and segmenting one artery of interest, defined by the cardiologist. The result enhances other existing vessel-tracking method introduced by Dubuisson-Jolly *et al.* (1998). The final framework is presented in Chapter 4 of this manuscript.

1.3.3 Evaluation of coronary artery's distensibility measure

Objective 3 : Define a method to compute the artery's diameter from 2D X-ray angiogram sequences and to display the diameter changes during the cardiac cycle.

The diameter measurements have to be precise to capture the variations during the cardiac cycle. Moreover, the method should process the artery that a cardiologist wants to evaluate. To assess the precision of the solution, the method should be tested on simulated angiogram sequence and on large vessels such as the aorta (since the diameter changes are bigger and easier to capture). Finally, the method has to be evaluated on a dataset of patient's angiograms displaying coronary arteries. The proposed solution uses the spatio-temporal model that solves objective 2. We define a method to measure vessels' diameters through the cardiac sequence. The diameter values computed along the cardiac cycle and the blood pressure values can be used to estimate arterial distensibility. The proposed method is presented in Chapter 5.

CHAPTER 2

LITERATURE REVIEW

2.1 Clinical context

2.1.1 Anatomy of the heart
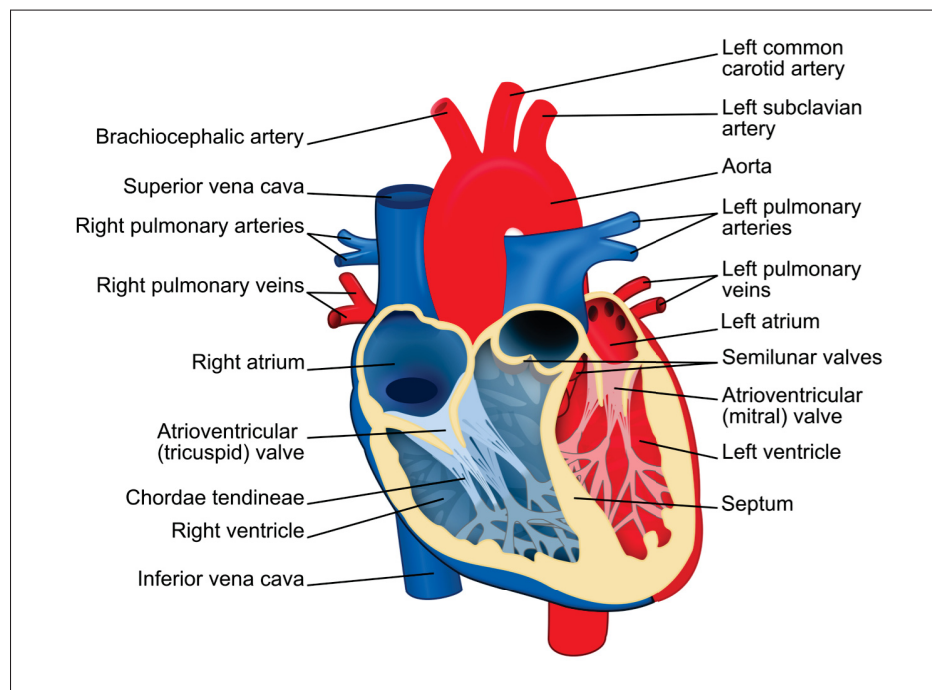
Figure 2.1   Anatomy of the heart : the four chambers of the heart.
Image Adapted from "Human heart diagram" used under Creative
Common created by ZooFari (ZooFari (2010)).

The cardiovascular system is responsible for the blood circulation in the body. The heart is the principal organ in this system. It pumps blood around the body to distribute oxygen and nutrients and to remove carbon dioxide and waste products. Located between the lungs in the middle of the chest, the heart is divided in four chambers : the left and right atria are the upper chambers and the left and right ventricles are the lower ones (Fig. 2.1). It is surrounded by a double-layered sac called the pericardium.

The coronary arteries play a crucial part in delivering oxygen and nutrients to the heart. They encircle the surface of the heart forming a *crown*. The coronary arteries are divided in two main arteries: the right coronary artery (RCA) and the left coronary artery which bifurcates into the left anterior descending (LAD) and the circumflex artery (CX) (Fig. 2.2).

The cardiac function is regulated by the cardiac cycle. One heart bump refers to one cardiac cycle. This cycle is defined by two stages. The diastole stage is when the heart's cavities are dilated and filled with blood. It is followed by the systole, when the heart contracts and the blood is pumped out into the aorta.
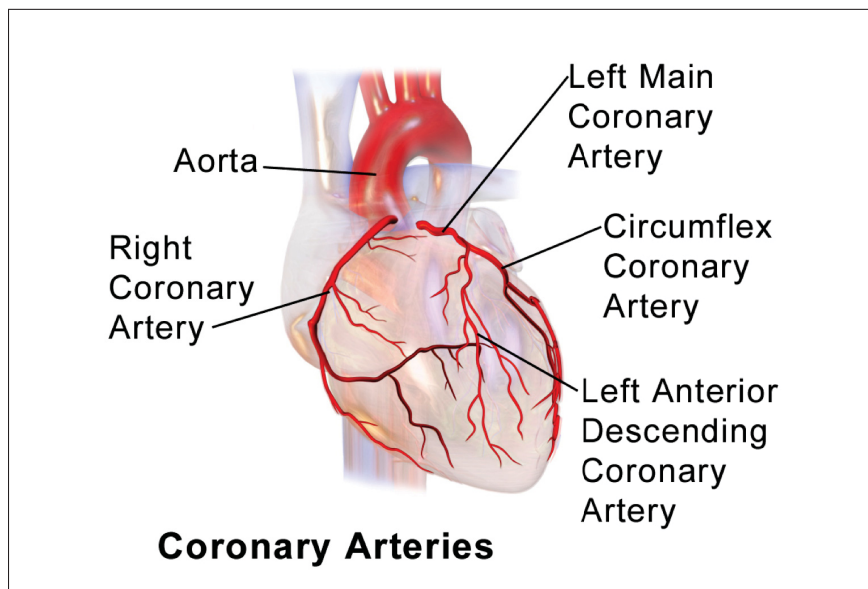
Figure 2.2   Anatomy of the heart : Coronary arteries.
Image Adapted from "Illustration of coronary arteries" used under
Creative Common by Bruce Blaus (BruceBlaus (2013)).

2.1.2   Heart defects

Coronary artery disease is the most common of heart disease affecting the blood circulation. Some of the diseases affecting the heart and its arteries are:

- Atherosclerosis: when the arteries are narrowed or blocked, causing stenosis. This leads to a poor blood circulation.

- Tetralogy of fallot: A congenital heart defect that creates a deviation of the blood flow and a low oxygenation of the blood. This can lead to anomalies in the coronary arteries.

- Kawasaki disease: A children's disease can cause aneurysms in the coronary arteries, which are abnormal dilation of the arteries' walls.

Heart diseases are treated with medication, surgery or non-surgical procedures. The latter is mostly preferred to surgery since they are less dangerous for young patients.

2.1.3 Cardiac catheterization for coronary aretries treatment

Cardiac catheterizations, such as PCI, are non-surgical procedures used for the diagnosis or treatment of coronary arteries. A catheter, which is a thin tube, is inserted through the vascular system to the location of the heart and the targeted coronary arteries (Figure 1.1). The imaging modality used for navigation guidance during percutaneous procedures is real-time two-dimensional X-ray angiography. Since blood vessels are invisible through X-rays, a radiopaque contrast agent is injected at key times through the catheter to depict coronary arteries (1.2). The X-ray angiography helps not only for navigation guidance but also for evaluating the dynamics of the coronary arteries. However, these X-rays have some limitations:

- The presence of Poisson noise that can degrade the image quality (Cesarelli *et al.* (2013)).

- The limited contrast depending on the injection of the contrast agent.

- The artery may not be visible in totality but gradually in time as the contrast agent is moving with the blood flow.

- The presence of stents, surgical pins and the catheter that can affect the segmentation result.

- The representation of a complex 3D structure (coronary tree) projected into a 2D plane (leading to the loss of depth information).

2.2 Segmentation

Segmentation is defined as the "*task of decomposing image data into meaningful structures that are relevant for a specific task*" (Preim and Bartz (2007)). Indeed, segmentation depends on the nature of the structure of interest and on the imaging modality. A segmentation method is evaluated on four terms: "Robustness, Accuracy, Reproducibility and Speed" (Preim and Bartz (2007)).

An accurate, robust and repeatable segmentation of vessels from the 2D angiograms is paramount to obtain either biophysical measurement of the vessels or a good registration or reconstruction for navigation guidance. As mentioned by various research, a weak segmentation can greatly affect other results. Rivest-Henault *et al.* (2012) mentions that a poor 2D segmentation affects the performance of their 2D-3D coronary artery registration method. Additionally, Hipwell *et al.* (2003) claims that the robustness of their registration algorithm depends on the segmentation result of the vascular structure.

Two categories of basic approaches are known in image segmentation : First, edge-based approach that search for object's borders such as Canny (1986) edge detector. Second, region-based approach that consider the structure of interest as a homogeneous region. Edge-based approaches can bring accurate segmentation result thanks to its local-based nature. However, it can be sensitive to noise and can return discontinuous object boundaries. On the other hand, region-based techniques rely on a global approach to segment an image such as the threshold-based method of Otsu (1979), the region-growing method of Wong *et al.* (2009) or the watershed segmentation of Serra (1982).

Since the late 1980 's, segmentation problems are formulated as the minimization of an energy function (Geman and Geman (1984) and Mumford and Shah (1989)). This function is usually divided into a data term and a smoothness term. The optimal segmentation result is the one that puts this energy to its minimum. Today, most modern segmentation approaches are based on this energy formulation (Lombaert (2012)).

An ideal segmentation solution is the one that can be computed automatically, where no user interaction is needed. Such method can hardly exist, especially in medical images, where there are different anatomical structures and where some anomalies may be observed due to the presence of pathologies or to imaging artifacts. As denoted by Lombaert (2012), a unique automatic solution cannot be efficient to handle all these different cases.

In the context of vessel segmentation from X-rays, several works have been proposed. They either rely on a previously defined prior model or on some manual initialization. The research in this field remains an open topic. Kirbas and Quek (2004) and Lesage *et al.* (2009) review various segmentation techniques, both in 2D and in 3D. In their review, Lesage *et al.* (2009) concludes that while vascular segmentation is still a challenging task, techniques that use a prior appearance model and those based on a combination of existing models are more suitable to enhance the efficiency of the results.

Extraction approaches are categorized in two families of methods: variational approaches and graph-based approaches. They are discussed in the second subsection. Prior appearance models can be defined, for instance, based on intensity features or topological feature. One of the most efficient topological features in vessel segmentation is described in the following subsection.

2.2.1 Topological features for vascular structures

Special filters have been proposed in the literature to highlight tubular structures, such as blood vessels. One of the well-performing methods is the Hessian-based filter. Introduced by Sato *et al.* (1998) and Frangi *et al.* (1998), these techniques analyze the eigenvalues and eigenvectors of the Hessian matrix of the image. Frangi's work is an extension of Sato's method for vessel enhancement in X-ray angiography. A recent work of Rivest-Henault and Cheriet (2013) introduced a 3D curvilinear structure detection filter which brings robust performance in detecting vessel-like structures despite the presence of bifurcations.

In the formulation of Frangi *et al.* (1998), the method is based on the analysis of the Hessian matrix computed using convolutions by Gaussian masks at different scales in order to extract different vessels of different diameters. For a specific scale σ, the Hessian matrix of the image $\mathscr{I}$ is computed. For each pixel p_i from $\mathscr{I}$, the technique computes the two smallest eigenvalues λ_1, λ_2 of the Hessian matrix at scale σ: with $|\lambda_1| \leq |\lambda_2|$ and $\vec{u}_1, \vec{u}_2$ are their corresponding normalized eigenvectors. Pixel p_i belongs to a tubular structure if $|\lambda_1|$ is close to 0 and $|\lambda_1|$ is lower than $|\lambda_2|$. The direction of the curvature (i.e along the vessel) is indicated by the smallest eigenvector $\vec{u}_1$. Frangi's method returns a vesselness value $b_{i,\sigma} \in [0,1]$ for each pixel p_i at a scale σ. The measure $b_{i,\sigma}$ expresses a probability-like value that pixel p_i belongs to a tubular structure at scale σ and is computed as follows:

$$
b_{i,\sigma} = \begin{cases} 0, & \text{if } \lambda_2 < 0 \\ \exp(-\frac{R_B^2}{2\beta^2})(1 - \exp(\frac{S^2}{2c^2})) & \text{otherwise,} \end{cases} \tag{2.1}
$$

where $R_B = \lambda_1/\lambda_2$ is a measure of *blobness*. The value of $S = \sqrt{\lambda_1^2 + \lambda_2^2}$ distinguishes background pixels and $\beta, c > 0$ are controlling parameters. Once $b_{i,\sigma}$ is computed at different scales σ for a pixel p_i, the technique extracts the maximum response $b_{i,\sigma}$ value among all tested scales. This vesselness filter returns a high vesselness value at the centerline location of the vessel and a lower value near the borders. Their ability to highlight vessel-like structures in the image have been used in several applications. The filter is usually used as a preprocessing step or as a topological feature to extract vessels. Rudyanto *et al.* (2014) noticed that the most efficient segmentation techniques are the ones based on vesselness approaches.

However, it is difficult to segment vessels using only vesselness filters. Indeed, Hessian-based methods is measure to highlight vessel's centerline and not vessel's lumen. Therefore, applying a simple threshold on the filter's result may generate disconnected regions, not providing sufficient robustness for vessel lumen identification. Moreover, as noticed by Lesage *et al.* (2009), these filters can be sensitive to local deformations in the vessel, such as bifurcation or the sudden change of vessel's diameter (i.e. in the presence of a stenosis or an aneurysm in

the vessel). In the recent literature, they are usually combined with other methods or filters to overcome the limitations of vesselness filters, while appreciating their ability to enhance vascular structures (Freiman *et al.* (2009); Hernández-Vela *et al.* (2012)).

2.2.2 Segmentation methods for vascular structures

Various researches have addressed the problem of coronary arteries segmentation or vessel segmentation in general. These researches can be categorized in two families of approaches: variational approaches, such as levelsets, and graph-based (or combinatorial) approaches, such as graph-cuts. The latter have the advantage to represent connectivity information between pixels.

2.2.2.1 Variational approaches

Variational approaches have been widely applied in medical images. Such methods rely on a defined model to segment the structure of interest. They include information about the size, shape and intensity distributions of the structure. Deformable models is a well-known variational approach, where a contour is initialized and is later deformed, under computed forces until it covers the foreground structure.

Variational approaches based on region growing have been proposed for vessel lumen segmentation, such as the work of Zhao *et al.* (2014) and active contours by Zhao *et al.* (2015b). These methods have the advantage of returning a well-connected region. However, they are sensitive to the initial seed location and to the complex topology of vascular tree, and can have topological problems leading to a high rate of false positives and false negatives (Sun *et al.* (2012)).

Levelsets can be used to solve variational models. The method defines a wavefront propagating towards the object of interest (i.e. the boundaries of the foreground). The motion of the wavefront is guided by information extracted from the image, such as intensity distribution and the image's gradient (Preim and Bartz (2007)). The contour, initialized at a dimension n, is

considered as the zero levelset of a function Φ at a higher dimension $(n+1)$. The displacement of the contour is computed using the level set function Φ and it evolves following vector N, which is the normal to the contour, and under a speed function F_I, defined depending on the nature of the image and the targeted object.

Levelsets have been used in various medical images applications. Sun *et al.* (2012) used them to segment blood vessels in 2D angiograms. Their model use local morphology features within the levelset formulation acheiving robust results.

Researchers have proposed new methods to segment thin and elongated structures by including shape priors in the levelset formultation. Indeed, relying on pixel homogeneity and edge contrast can be insufficient to extract challenging structures like thin and elongated structures (Cremers (2015)). Wang *et al.* (2012) introduced a level set method guided by a 3D cylinder model. This model is generated from computed centerlines. The method shows successful results in extracting the coronary arteries in CTA. However, the authors mentioned that the method is sensitive to the initial centerline computation, which can limit the overall segmentation.

Levelsets method has a capacity to segment complex structures, which is convenient to segment coronary arteries. However, it can be computationally expensive and has to be initialized either using other techniques or manually selected seeds.

Variational approaches can be efficient in segmenting complex vascular structures yet, unlike graph-based methods, they do not guarantee repeatability. They can depend on the initialization parameters. Besides, the convergence to a global optimum is not guaranteed in methods based on levelsets (Boykov and Funka-Lea (2006)).

2.2.2.2 Graph-based approaches

Graph-based methods are combinatorial approaches that have been successfully used to solve vessel segmentation problems, such as shortest-path (Benmansour and Cohen (2011)), random

walks (**RW**) by Grady *et al.* (2006a) or graph-cuts (Shahzad *et al.* (2013); Freiman *et al.* (2009); Hernández-Vela *et al.* (2012)). These techniques have been applied to segment different vascular structures: from coronary arteries to the aorta or retinal vessels. Yet, most graph-based methods use intensity values as features to compute the segmentation. In the case of X-ray angiograms, using only intensity features can give limited solutions. Graph-based methods represent an image as a connected graph, where the pixels are nodes of the graph connected by edges. Most method uses the Laplacian matrix to define this connected graph.

Laplacian Matrix :
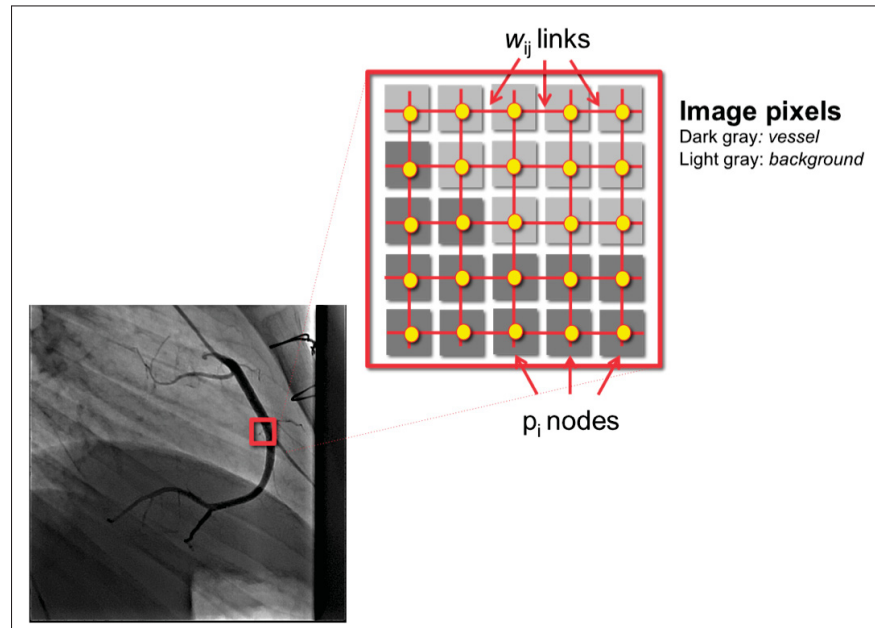
Figure 2.3   Graph representation of an image.

In a graph-based segmentation method, image $\mathscr{I}$ of size $n \times n = N$ is represented by an undirected graph $G = (V, E)$, as illustrated in Figure 2.3. V is the node set where each pixel p_i from $\mathscr{I}$ corresponds to a node v_i from V ($|V| = N$). E is the edge set that connects two neighbouring nodes to each other (i.e. a node v_i is connected to v_j by an edge e_{ij} in E, if their corresponding pixels p_i and p_j are in the vicinity of radius r). The graph is represented by the adjacency matrix $W \in \mathbb{R}^{N \times N}$, where $[W]_{ij} = w_{ij}$ is the weight of the edge e_{ij} connecting nodes v_i to v_j,

defined as:

$$
w_{ij} =
\begin{cases}
\exp\left\{-\gamma(\mathscr{I}_i - \mathscr{I}_j)^2\right\}, & \text{if } \mathrm{dist}(p_i, p_j) \leq r \\
& \text{and } i \neq j \\
0, & \text{otherwise.}
\end{cases}
\tag{2.2}
$$

$\mathscr{I}_i$ corresponds to the intensity feature (or other features) of pixel p_i and γ is a parameter controlling the effect of intensity's differences on the weight. Different distance metrics can be used to consider whether or not two pixels are neighbours : Euclidean distance, L_1 or Manhattan distance. The degree matrix $D \in \mathbb{R}^{N^2}$ is a diagonal matrix that describes the degree $[D]_{ii} = d_i$ of each node v_i from the graph G such as: $d_i = \sum_{j \neq i} w_{ij}$. Finally, image connectivity information is represented by the Laplacian matrix L which is the difference between the degree and adjacency matrices: $L = D - W$.

After computing the graph representation of the image (i.e. the Laplacian matrix), a graph-based algorithm searches for the optimal "cut" in the graph, dividing the image pixels in two subsets: foreground (i.e. the vessel lumen, opacified by the contrast agent) and background. To solve this optimization problem, different graph-based methods can be applied. Three well-performing methods are graph cuts, Laplacian eigenmaps and random walks:

a. **Graph cuts method:** Graph cuts adds to the graph G two terminal nodes s and t called the source and the sink node respectively. The method searches for the cut C that divides the graph in two subsets: the nodes that belong to the foreground region and include the source node s, and the one that belongs to the background including the sink node t. The optimal cut C contains all the edges connecting two pixels belonging to different subset. $|C|$ is the weight of the cut C and is computed as the sum of all the cut edges' weight. The optimal cut C will have the minimal weight cut $|C|$. Therefore, graph cuts are represented as an optimization challenge called the min-cut/maxflow problem. The min-cut/maxflow is formulated as the minimization of the following energy equation (Boykov and Kolmogorov (2004)):

$$
E(f) = \lambda \sum_{p \in N} D_p(f) + \sum_{(p,q) \in V} W_{p,q}(f_p, f_q).
\tag{2.3}
$$

The first term of the equation, called the data term, represents the cost of assigning the label f (i.e. background or foreground) to the pixel p. It is usually based on a apriori known feature distribution model (using manually selected seeds, for example). The second term or the smoothness term is the regularization energy that evaluates the similarity W between two neighbouring pixels p and q. Parameter $\lambda >= 0$ controls the tradeoff between the data and smoothness terms.

Graph cuts is a robust and repeatable technique. Moreover, it is independent on the initialization parameters (Grady and Alvino (2009)). It has been successfully adapted and applied on the most complex segmentation problems, especially in medical images. To segment thin and tube like structures, such as coronary arteries, using intensity information only is not sufficient. Freiman *et al.* (2009) suggested to use vesselness features with intensity information in the graph cut formulation to extract the carotid artery from 3D MSCT volume. On the other hand, Hernández-Vela *et al.* (2012) uses a graph cuts with geodesic paths and vesselness features to segment coronary arteries from 2D X-ray angiograms. Despite its efficiency and performance, the most noticed limitation of the graph cuts method is that it does not guarantee a sub-pixel accuracy, unlike variational methods. Moreover, as mentioned by Grady *et al.* (2006b), graph cuts are known to search for the smallest region surrounding foreground seeds to define the regions, which can be beneficial in some cases. The downside of such properties is the small-cut problem and hence big region needs more specified seeds.

b. **Laplacian eigenmaps:** Laplacian eigenmaps have been widely used to solve clustering problems such as segmentation, where the method aims to find two clusters in one image: A cluster of foreground pixels and one of background pixels. This method evaluates the eigenvectors of the Laplacian matrix to find clusters in the image. Von Luxburg (2007) presents a complete tutorial on how the eigenanalysis of the Laplacian matrix can solve a clustering problem. Several works have exploited the relationship between the spectral properties of the Laplacian matrix and the partitioning of the graph. The ratio-cut algorithm introduced by Hagen and Kahng (1992) is one of these works. The method solves the small-cut limitation of graph-cuts by adding the constraint that clusters should be containing a reasonably large num-

ber of nodes. The algorithm, looks for a mapping $f : \mathscr{I} \rightarrow \{0,1\}$ that minimizes the ratio between the weight of the cut $|C|$ and the number of pixels mapped to 1 (i.e. the foreground pixels). Ratio-cut is formulated as:

$$\underset{f \in \{0,1\}^n}{\text{argmin}} \quad \frac{\sum_{i=1}^{n} \sum_{j=1}^{n} w_{ij}(f_i - f_j)^2}{\sum_{i=1}^{n} f_i^2}. \tag{2.4}$$

Shi and Malik (2000) introduced another formulation to use the spectral properties of the Laplacian: The Normalized cut. Normalized cut considers both the dissimilarity between different groups and the similarity within groups. The method has successful results in segmenting images.

Laplacian eigenmaps methods succeed in segmenting continuous regions. However, they have limited results when extracting thin and elongated structures such as vascular structures. Therefore, other features in addition to intensity information must be added. Moreover, these methods have a high computational cost, depending on the image size and the sparsity of the Laplacian matrix.

c. **Random walks:** The method outperforms other graph-based method since it does not suffer from the small cut problem noticed with graph cuts (Grady *et al.* (2006b)). Moreover, it is robust to noise and the computation requires solving a set of linear equations, which is computationally faster than spectral methods. The method requires user specified seeds and it computes the path on a graph that a random walker would take to go from an unseeded pixel to the closest seeded one. Having each node (or pixel) connected to a seed makes the RW robust to noise. RW apply the minimization of real numbers instead of the binary constraint defined in graph cuts. Therefore, the method gives a "confidence value" (or probability value) instead of a straightforward binary segmentation (like graph cuts). However, random walks does not work without specified seeds, and does not support cases, where the object is formed by disconnected regions in the image. Grady (2005) modified the random walks to include a prior model, making the method independent of seeds, if needed. The method produces encouraging

results despite the variability in intensity values within regions, using an intensity profile of the different regions to be segmented. However, intensity distribution can be insufficient in some cases and other features should be used as a prior instead.

Recent graph-based works include the optimization of the boundary curvature, which is initially used by variational methods. Schoenemann *et al.* (2009) presents curvature of an object boundary on a graph and succeed in preserving thin and elongated objects. Another similar model was introduced by Nieuwenhuis *et al.* (2014). However their method may be limited when the data term from equation 2.3 is poorly defined (i.e. when object and background have similar distributions). El-Zehiry and Grady (2016) recently presented a contrast driven elastica model that overcomes this limitation and has a robust segmentation result even when the data term is poorly defined.

In general, graph-based methods are appealing, because they preserve the connectivity information during segmentation, mostly by using pixel intensities as prior. Moreover, most of the graph-based methods show robustness to noise. However, to extract thin and elongated structures like blood vessels, relying on only intensity information is not sufficient. Therefore, adding other features such as topological information (like vesselness information) to a graph-based method can give more accurate solutions.

Different methods have been proposed to combine graph-based approaches with vesselness information to segment vascular structures. Hernández-Vela *et al.* (2012) presents a solution based on graph-cuts and vesselness information together with geodesic paths to segment CA from 2D angiograms. However, some limitations are noticed regarding bifurcations or wherever there is a vessel overlap. The method proposed by Freiman *et al.* (2009) combines graph-cuts and vesselness information to segment the carotid artery from 3D MSCT-scans. The graph is computed using an estimated intensity probability distribution function. This can be robust in the case of CT-scans (thanks to the Houndsfield scale) but not for 2D X-ray angiography, where the contrast among a vessel can be limited. Moreover, both Hernández-Vela *et al.* (2012) and Freiman *et al.* (2009) use the graph cuts method, which may encounter the small-cut problem,

depending on seeds location. The random walks method stands out from the other graph-based solutions due to its robustness, flexibility and fast computations to find a segmentation solution Grady *et al.* (2006a). Additionally, the method avoids the "small-cut" problem while being computationally faster than other graph-based methods.

2.2.3 Evaluating Segmentation : validation metrics

To evaluate the performance of a segmentation method, several metrics can be computed. They all rely on comparing the segmentation result to a defined ground truth. First, Dice index measures the agreement between a computed mask (C) and a ground truth mask (G) and computed as:

$$Dice(C,G) = \frac{2 \times |C| \cap |G|}{|C| + |G|}. \tag{2.5}$$

The returned coefficient range is between 0 and 1. The higher the Dice, the better is the agreement.

Precision and recall metrics are robust detectors to over and under-segmentation errors, respectively. Over-segmentation produces a low precision value, while under-segmentation gives a low recall. A robust segmentation would yield a trade-off of both high precision and recall values.

Finally, the Receiver Operating Characteristic curve (ROC) indicates the robustness of an algorithm over different threshold values. More precisely it is useful for evaluating methods that does not bring a binary segmentation result but rather a probability-like result (such as random walks results), where different threshold values can be tested. A high value of the area under the ROC curve (AUC) indicates the robustness of the algorithm over different threshold values.

2.3 Tracking

Tracking is defined as identifying the location of a moving structure, such as coronary arteries, within a motion sequence (such as a video). Several techniques have been proposed for tracking

vascular structures from X-ray angiography. Instead of tracking the whole artery's lumen (the artery tube), these methods usually track the centerline of the artery (a thin line within the artery) and then extracts the artery's lumen if needed.

Polyline tracking method proposed by Dubuisson-Jolly *et al.* (1998) uses an adaptive method for tracking vessel's centerline represented by polylines in angiogram sequences. While the method return successful qualitative results, a pre-processing step involving a rigid registration is necessary to handle respiratory motion and to simplify the computations. Without such preprocessing, the computations of the method can be memory and time consuming as it needs to find the shortest path on a large graph representing all the possible segments that can be part of the centerline. Also, representing the artery by a polyline could lead to the loss of curvature information. Methods like Gao and Sundar (2012) define a motion model to track manually selected seeds. However, the authors mention that the model is limited to cardiac motion and additional steps may be necessary to handle respiratory motion to infer arteries displacements. Other methods propose to track landmarks of the blood vessels. Yumei (2011) proposed to automatically track blood vessels branches and junctions. The method shows good results in tracking the junctions in 2D X-ray sequences. However, as denoted by the authors, significant changes in the structure of the blood vessels, such as overlapping vessels, can limit the performance of the method.

Other works measure the 3D displacement of coronary arteries from 2D biplane angiograms. The work in Sundar (2015) presents a method for non-rigid registration of 3D CA with 2D fluoroscopic images. A global transformation model is then presented to get an initial alignment based on rigid and affine registration. The registration is further refined by non-rigid registration method defined by the authors. Hadida *et al.* (2012) modeled the coronary arteries' motion using a stochastic approach and based on a 2D angiographic sequences together with a 3D CTA model of the patient's arteries. In these cases, a 3D model of coronary arteries should be pre-acquired.

Another work presented by Compas *et al.* (2014) introduces a spatio-temporal approach to extract and track the coronary artery tree. While it shows robustness in tracking the vessels' centerline using multiscale optical flows, the vessel lumen is computed at each point in the centerline individually and does not compute a global optimum to extract the lumen. This computation may be sensitive to local deformation or noise. Moreover, the method tracks all the tube-like structures in the sequence and does not focus on tracking a specific vessel or part of the vessel.

Other methods focus on tracking other blood vessels such as cortical or retinal vessels. For instance, the work in Ding *et al.* (2011) tracks cortical vessels using intensity and vesselness information by searching in the actual frame along the orthogonal line to the vessels' centerline computed in the previous frame. This approach works well for cortical vessels which are subject to a rigid movement and where the vessel features are invariant in time. The work in Cao *et al.* (2011) tracks retinal vessels. Both cortical and retinal vessels do not undergo the same complex combination of respiratory and cardiac motions observed with coronary vessels. Indeed, in X-ray angiography, the coronary arteries are subject to rigid and non-rigid movement (cardiac and respiratory). These arteries' features may change in the angiography sequence due to the diffusion of the contrast agent (i.e., the intensity inside the vessel decreases as the contrast agent disappears).

Similar studies using spatio-temporal segmentation exist in the literature. These studies focus mostly on other modalities such as CT scans (Laguitton *et al.* (2007)) or MRI (Cousty *et al.* (2010)), which are not subject to the same constraints as 2D angiography sequences (projections, overlapping vessels, contrast diffusion, etc.).

To summarize, various methods have been proposed, to track coronary arteries in 2D angiography sequences. However, they are limited to tracking the centerline of the vessel (and not the lumen). Moreover, most of the works track the whole coronary tree and not one vessel in particular.

2.4 Quantification of vascular structures (distensibility)

Many measurements can be computed to evaluate the biophysical properties of arteries and assess the dynamics of the arteries in the cardiac cycle. Distensibility measure is one of the strongest indicators that evaluates arteries' dynamics and can predict a potential cardiovascular disease at an early stage (Cheung *et al.* (2002)). The measure evaluates the ability of an artery to expand and contract with cardiac contraction (systole) and relaxation (diastole) (Godia *et al.* (2007)) and computed as the following :

$$Distensibitliy = \frac{\left(\frac{Lumen\ diameter\ at\ end\ systole\ -\ Lumen\ diameter\ at\ end\ diastole}{Lumen\ diameter\ at\ end\ diastole}\right)}{blood\ pressure\ at\ end\ systole\ -\ blood\ pressure\ at\ end\ diastole} \qquad (2.6)$$

Distensibility measure is known to be higher in healthy patients and lower in patients with vascular disease (Kelle *et al.* (2011)). As shown in equation (2.6), distensibility relies mostly on the difference of the artery's diameter in systole and diastole. There have been different approaches for measuring arteries diameter in the cardiac cycle. Some methods would compute the diameter manually by an operator (a cardiologist or a clinical technician) from X-ray frames. However, this depends on the operator's experience and the measurements may not be precise. Other methods imply that the operator trace manually a centerline and a software computes the distance automatically to the borders of the vessel using edge detection techniques (Tomasello *et al.* (2011)). Nonetheless, such methods depend on the precision of traced centerline and the operator may not be precise, not to mention that this tracing can be time consuming.

On the other hand, an automatic quantitative evaluation makes the measurement more objective and independent from the clinician's experience. There are different commercialized systems to quantify arteries' diameter. As described by Tomasello *et al.* (2011), the two most commonly used systems are CAAS from PIEMedical and QAngio from Medis. However, to the best of our knowledge, these software compute the diameter from one image but does not evaluate the diameter changes in time from one segment of a vessel.

Besides, other works on distensibility involves studies on other imaging modalities: using MRI images (Kelle *et al.* (2011)); CT scans (Ahmadi *et al.* (2010)) (manually and automatically with Workstation AW 4.4; GE Medical Systems) ; using ultrasound (Maurice *et al.* (2014)) or using 3D reconstructed model from biplane views (Girasis *et al.* (2013)). Kelle *et al.* (2011) Evaluates the distensibility of coronary arteries from MRI images which have higher resolution than 2D X-rays. The method was evaluated on adult patients and showed accurate quantitative measurements. From our understanding, the artery's diameter is computed at systole and diastole without any tracking of the artery. Maurice *et al.* (2014) applies binary segmentation to measure the lumen of the carotid artery in ultrasound images. This may not be accurate in the case of 2D X-rays.

In conclusion, several methods exist to quantify the artery's diameter. Nonetheless, all these methods rely on computing the diameter one frame at a time and without an automatic tracking of the arterial structure in the moving sequence.

CHAPTER 3

CORONARY ARTERIES SEGMENTATION FROM 2D X-RAY ANGIOGRAPHY

3.1 Introduction

Percutaneous coronary interventions are used for the diagnosis and treatment of coronary arteries (CA) pathology, especially among newborns and young patients. These interventions are guided by real time 2D X-ray angiographies. Automatic segmentation of coronary arteries from angiograms is of clinical importance since it provides cardiologists with additional information, such as measuring different physiological properties of the patient's arteries. An
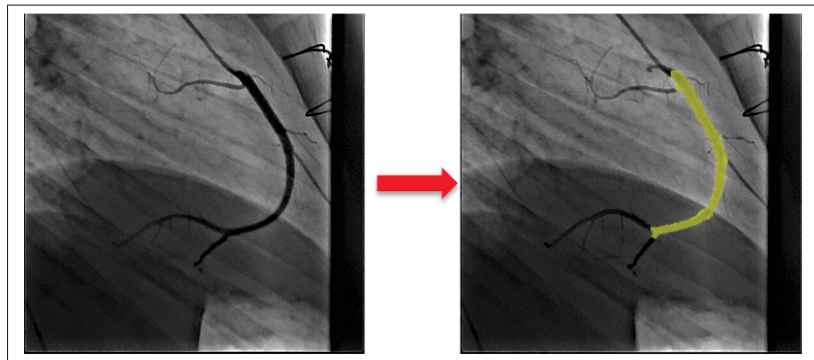
Figure 3.1   Overview of CA segmentation : (left) Original
image, (right) Segmentation result overlaid in yellow.

accurate and repeatable vessel segmentation from the 2D angiograms is a valuable tool to obtain both, an accurate delineation of anatomy with precise measurement of vessels and a good registration or reconstruction for navigation guidance Hadida *et al.* (2012); Rivest-Henault *et al.* (2012); Liao *et al.* (2010).

Segmenting CA from 2D angiograms can be challenging due to the complexity of their structure, the quality of the 2D X-ray image, and due to the presence of sternal sutures (as shown in Figure 3.2). Besides, angiograms are 2D projections of a 3D structure (the patient's thorax).

Thus, we can observe overlapping vessels that are in reality two vessels at different levels of depth.
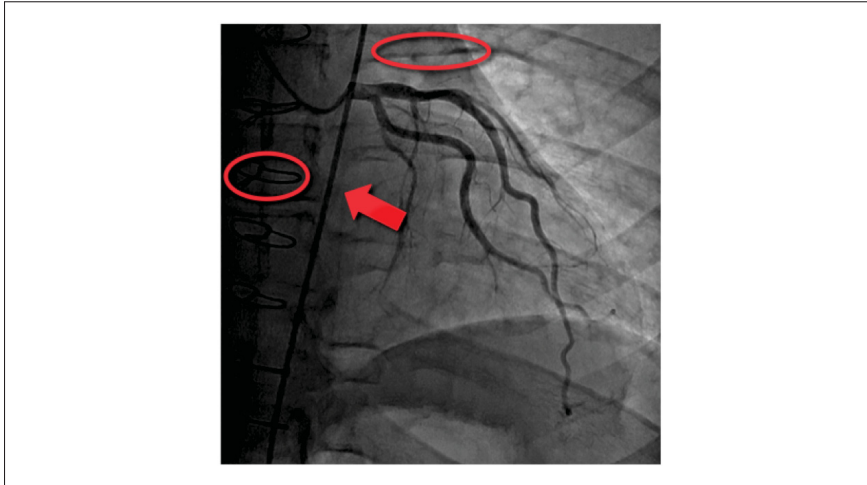
Figure 3.2   The presence of dark tubular regions that does not correspond to coronary arteries can be challenging for an automatic segmentation: Red circle on the left shows a stenal suture; red circle on the top shows a bone from the rib cage ; the arrow points to the catheter (the dark long tube crossing the image).

Two observations were considered to segment coronary arteries from 2D angiograms :

- Coronary arteries form connected regions with an intensity level different from the background;

- They constitute a set of different tubular segments where the intensity level varies mostly across the vessel.

As suggested by Lesage *et al.* (2009), the combination of a prior appearance information and existing segmentation models can enhance the result. In that matter, our work segmentation model adds prior information about intensity level and topological features. As described in section 2.2, recent works have considered similar combinations to segment arteries, like the

work of Hernández-Vela *et al.* (2012) or Freiman *et al.* (2009). However, the first work presented some limitations in extracting arteries' bifurcations and overlapping vessels, whereas the second work was applied on MSCT data using the Houndsfield values as prior, which does not apply to 2D X-ray angiographies. Another existing work is the random walks with prior (RWprior) presented by Grady (2005) and Andrews *et al.* (2010). Unlike the original RW formula, RWprior can rely on a prior model over pixels' intensity distribution or other feature computed from the processed image or other images. However, RWprior does not include any topological prior, which limits the performance for segmenting coronary arteries. Our work modifies the original random walks (RW) formulation of Grady *et al.* (2006a) by including a prior on intensity distribution. This chapter assesses the following hypothesis : *An automatic method to extract coronary arteries from 2D angiograms can be as accurate as an expert's manual segmentation* (Figure 3.1).

3.2 Proposed method : Vessel Walker for coronary artery segmentation

This section presents our main contribution: the Vessel Walker method. Firstly, an overview of our previous works, that led to the new proposed model, is presented. Following that, a description of the Vessel Walker model, is provided.

3.2.1 Preliminary works

The main contribution was preceded by two previous works : first an approach based on active contours (M'hiri *et al.* (2012b)) published in the International Conference on Information Science, Signal Processing and their Applications **ISSPA'12** and second a model using laplacian eigenmaps (M'hiri *et al.* (2012a)) presented in IEEE Computer Society Conference on Computer Vision and Pattern Recognition Workshops **CVPRW'12**.

Adaptive framework using active contours (M'hiri *et al.* (2012b))

We propose, at first, an adaptive segmentation framework of tubular structures in X-ray angiography, based on active contour method. The framework combines global and local active contours. It automatically computes the weights of local and global forces according to the image homogeneity using the approach from Cheng and Sun (2000) and it initializes the contour using vesselness filter by Frangi *et al.* (1998) . Experimental results have proved that the proposed framework overcomes the weaknesses of using global and local approaches individually. However, the adaptive active contour relies only on intensity information and does not use any topological information (besides the initialized contour) which results in the presence of false positives and of disconnected regions.

An alternative solution is to use graph-based approaches. These approaches have the advantage of preserving the neighbouring information, which solves the limitations of active contours. Moreover, graph-based methods usually guarantees the repeatability of the solution, unlike active contours.

Combining Laplacian eigenmaps and vesselness filters (M'hiri *et al.* (2012a))

We propose a segmentation method that aims at extracting CA, automatically. Our formulation incorporates vesselness features with connectivity information using a graph representation of the image, to segment structures with similar intensities and vesselness responses. The method succeeds in extracting vessels on synthetic and pediatric datasets despite the presence of local deformations. Nonetheless, computing eigenvectors can be time consuming, especially for images with big resolution and big neighbourhood size.

Based on these previous works on active contours and laplacian eigenmaps, we conclude that:

a. Graph-based methods are more accurate, in our case, and helps to preserve connectivity information

b. Using vesselness information within a segmentation model helps to extract thin, elongated structures

This leads us to our main contribution: the **Vessel Walker model**.

3.2.2 Vessel Walker : segmentation method combining Random walks and vesselness filters

Based on our work using the Laplacian eigenmaps (M'hiri *et al.* (2012a)), we explored the idea of combining graph-based method and vesselness features, further. Random walks method is well known to surpass other graph-based solutions by its fast computation to find a globally optimal solution and is less sensitive to the shrinking bias problem.

A new model is defined based on the random walks that adds vesselness information. This method, called Vessel Walker (VW), was first introduced in M'hiri *et al.* (2013). Vessel Walker extends the random walks formulation by adding a vesselness prior. Therefore, the method can preserve the connectivity information using the graph representation of the image. Moreover, it can extract only vessels given the vesselness features used in the formulation. Finally, the original random walks needs the specification of seed points to define foreground and background regions. The Vessel Walker can be solved automatically considering the vesselness features. Nonetheless, it can use manually selected seed points if we need to refine the segmentation of regions with low contrast or high level of noise.

Given an image $\mathscr{I}$ represented by a graph $G = \{N, E\}$, the VW method searches for a mapping $f : \mathscr{I} \to \{0, 1\}$, where, $f_i = 1$, if the pixel i belongs to the vessel, and $f_i = 0$, if i belongs to the background. Let $b_i \in [0, 1]$ be a value representing the vesselness of pixel i as computed using equation (2.1) by Frangi *et al.* (1998). This mapping minimizes the following energy equation:

$$E(f) = \frac{1}{2} \sum_{i=1}^{|\mathscr{I}|} \sum_{j=1}^{|\mathscr{I}|} w_{ij}(f_i - f_j)^2 + \alpha \sum_{i=1}^{|\mathscr{I}|} (1 - b_i) f_i^2$$
$$+ \beta \sum_{i=1}^{|\mathscr{I}|} b_i (f_i - 1)^2. \tag{3.1}$$

The first term of the energy formulation minimizes the total weight of edges in the graph, which connects background and foreground regions (w_{ij} computed using equation (2.2)). Parameters $\alpha, \beta \geq 0$ are used to control the trade-off between minimizing the vesselness of background pixels and maximizing the vesselness of foreground pixels. Since the equation in 3.1 is based on an extension of the random walks formula using not only intensity but also vesselness information, the method is called Vessel Walker.

To express this formulation in a matrix form, let L be the Laplacian matrix derived using the adjacency matrix presented in Equation (2.2). We denote by b the vector of vesselness values b_i, and let B be a diagonal matrix such that $[B]_{ii} = b_i$. The energy function can be rewritten as:

$$
\begin{aligned}
E(f) &= f^\top \left(L + \alpha I + (\beta - \alpha)B\right)f - 2\beta b^\top f + \beta b^\top \mathbf{1} \qquad (3.2)\\
&= f^\top M f - 2\beta b^\top f + \beta b^\top \mathbf{1}. \qquad (3.3)
\end{aligned}
$$

with I representing the identity matrix and $\mathbf{1}$ representing a vector of ones.

The proposed model can be solved automatically or semi-automatically using a set of selected seeds.

3.2.2.1 Semi-automatic formulation

To refine the segmentation of smaller vessels or noisy regions, manually selected seeds are needed . Given a set of seeds $\mathscr{S}$, the pixels of $\mathscr{I}$ are reordered in two groups containing labelled and unlabelled pixels. We denote by f_U the mapping of unlabelled pixels and by f_L the mapping of labelled ones. We can then rewrite Equation (3.2) as:

$$
\begin{aligned}
E(f) = \left[\; f_U^\top \;\middle|\; f_L^\top \;\right]
\left[\begin{array}{c|c}
M_{UU} & M_{UL} \\
\hline
M_{UL}^\top & M_{LL}
\end{array}\right]
\left[\begin{array}{c}
f_U \\
\hline
f_L
\end{array}\right] \\
- 2\beta \left[\; b_U^\top \;\middle|\; b_L^\top \;\right]
\left[\begin{array}{c}
f_U \\
\hline
f_L
\end{array}\right] + \beta b^\top \mathbf{1}.
\end{aligned}
\qquad (3.4)
$$

Expanding this equation gives:

$$E(f) = f_U^\top M_{UU} f_U + 2 f_U^\top M_{UL} f_L + f_L^\top M_{LL} f_L - 2\beta f_U^\top b_U - 2\beta f_L^\top b_L + \beta b^\top \mathbf{1}. \quad (3.5)$$

To find the optimal solution, we relax the integer constraint on f, derive the function with respect to the variable f_U, and set the result to zero:

$$\frac{\partial E}{\partial f_U} = 2 M_{UU} f_U + 2 M_{UL} f_L - 2\beta b_U = 0. \quad (3.6)$$

This yields the following solution:

$$f_U = M_{UU}^{-1} \left(\beta b_U - M_{UL} f_L \right). \quad (3.7)$$

Once the solution for f_U is computed, a threshold θ value is estimated automatically using Otsu's algorithm Otsu (1979) to obtain a binary segmentation result. We can then compute the binary segmentation of image $\mathscr{I}$ with the given θ:

$$\mathscr{I}_F = \{ i \in \mathscr{I} \mid f_i \geq \theta \}, \quad (3.8)$$

$$\mathscr{I}_B = \{ i \in \mathscr{I} \mid f_i < \theta \}. \quad (3.9)$$

where $\mathscr{I}_F$ is the set of pixels belonging to the foreground in the VW solution and $\mathscr{I}_B$ is the set of background pixels.

While seeds can be used to refine the segmentation in regions where the vesselness response is unreliable, the proposed method can also be used without any seeds.

3.2.2.2 Automatic formulation

In this fully automatic approach, the solution can be obtained by relaxing the integer constraints on f and deriving equation (3.2) with respect to variables f and setting the result to zero. This

gives the following solution:

$$f = \beta (M)^{-1} b. \tag{3.10}$$

We then apply the threshold θ on vector f, as described in the previous subsection 3.2.2.1, to obtain a binary segmentation mask. Otsu's algorithm can be used to fix the value of θ.

3.3   Experimental results

This section evaluates if the proposed segmentation method generates results as accurately as manual segmentation. First, we start by presenting the data acquisition protocol. Then, we list the different metrics used for evaluating the segmentation. The following section, assesses the influence of the VW parameters and the seed numbers. Finally, a comparative study shows the results of the proposed method with other existing methods in the literature.

3.3.1   Data Acquisition

The proposed method was tested on nine 2D X-ray images presenting left and right coronary arteries acquired from adult patients during coronary catheterization. Each image has the size of 256×256 pixels. The groundtruth of the images was computed using frangi's vesselness filter with manual post-processing to eliminate false positives.

3.3.2   Influence of parameters α, β and r

Different parameters, in the presented work, have their influence on the accuracy of the final result. In this section, we present the effect of the Vessel walker most influential parameters: α, β and the neighbourhood size r (in Equation (2.2)). These parameters control, respectively, the influence of background and foreground information and the sparsity of the adjacency matrix. Therefore, the selection of their values depends on each dataset.

A k-fold cross-validation step was applied to select the right parameter values in terms of α, β and r, where, the number of folds is equal to the number of the sequences, $k = 9$. The following

figures (3.3, 3.4 and 3.5) show the mean values over all the dataset in terms of Dice, recall and precision depending on each of these parameters.

This section evaluates if the proposed segmentation method generates results as accurately as manual segmentation. First, we start by presenting the data acquisition protocol. Then, we list the different metrics used for evaluating the segmentation. The following section, assesses the influence of the VW parameters and the seed numbers. Finally, a comparative study shows the results of the proposed method with other existing methods in the literature.

Parameter α has a high influence on the number of false positives. As shown in the last curve in Figure 3.3, the higher the value of α, the higher the mean precision value, which makes the parameter have fewer false positive errors. On the other hand, as α gets a higher value, the recall does not change until after $\alpha = 2$, where the value of recall drops to 0.2. This can be explained by the fact that the more α controls the precision, the less true positives we may get. In conclusion, α minimizes the vesselness of background pixels: from Eq. (3.1), the lower the vesselness value of b_i, the lower the probability for the corresponding pixel p_i to belong to the foreground: As α gets bigger value, this probability gets lower.   As shown in Figure 3.4, parameter β as a greater influence on the recall values than on the precision. The higher the β value is, the more true positives we get. This proves that if a pixel p_i has a high vesselness value b_i, parameter β maximizes the probability for that pixel to belong to the foreground. We can also notice that β influences precision values. However, these values change from 0.63 to 0.73, which is not a big influence compared to its effect on recall values. Whereas, as β grows from 0.002 to 20, recall grows from 0.4 to 0.75.

An optimal choice between α and β is necessary to obtain both high recall and precision values. The values of these parameters have to be defined depending on the contrast level in the image. The k-fold cross validation returned an optimal value for $\alpha = 2$ and $\beta = 20$.

The size of the neighbourhood radius r can be critical in computing the segmentation. The value should be large enough to facilitate the diffusion of information across noisy pixels but small enough so that we can keep the sparsity of the Laplacian matrix, thus, keeping a moderate
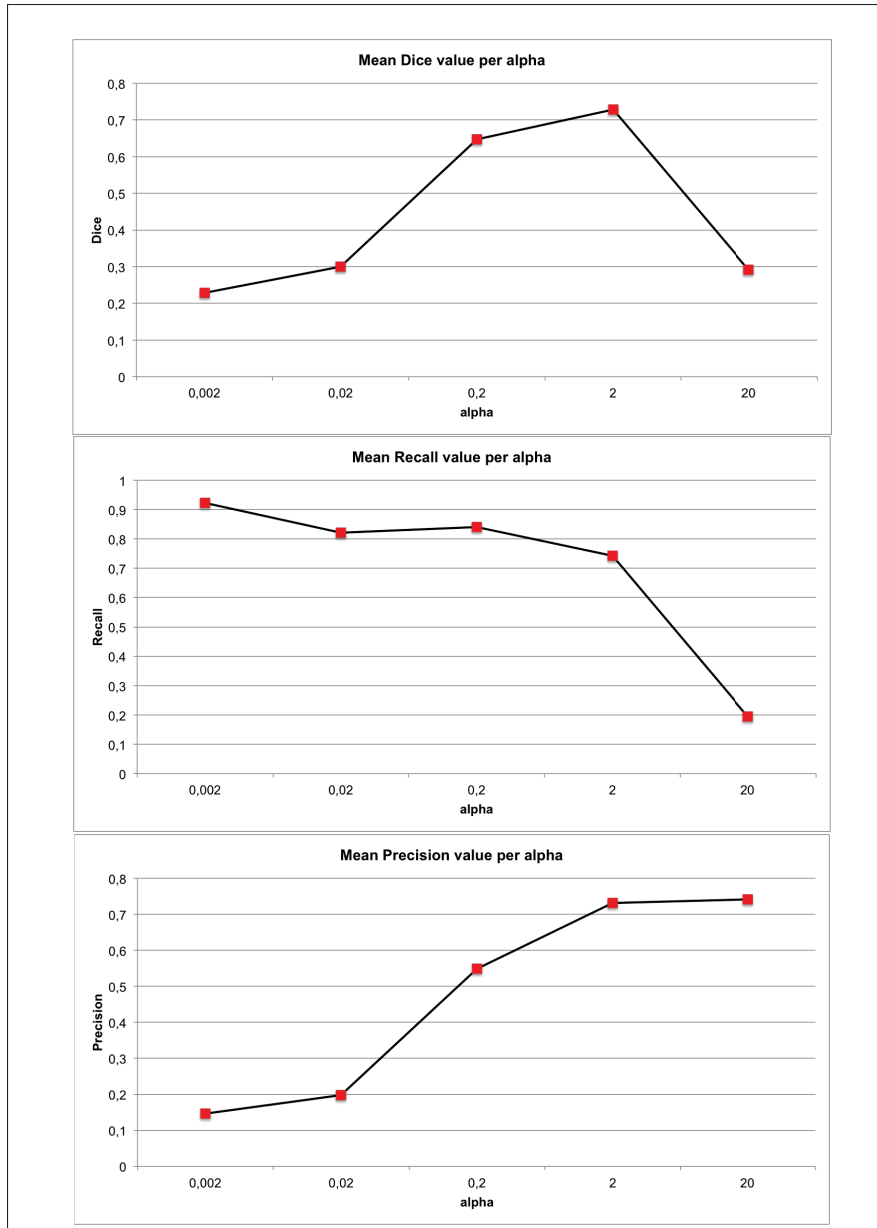
Figure 3.3   Influence of parameter α on Dice, Recall and
Precision values (respectively from top to bottom).

computation time and memory requirements. As shown in Figure 3.5, the radius r has a greater
influence on recall values (from recall= 0.49 at $r = 1$ to 0.74 at $r = 5$). The larger the radius
size, the more true positives are added to the segmentation result. This influence is reversed
in the case of precision values. Indeed, the radius r is inversely proportional to the robustness
of the method to false positives. Finally, as r gets higher, Dice value increases until $r = 5$
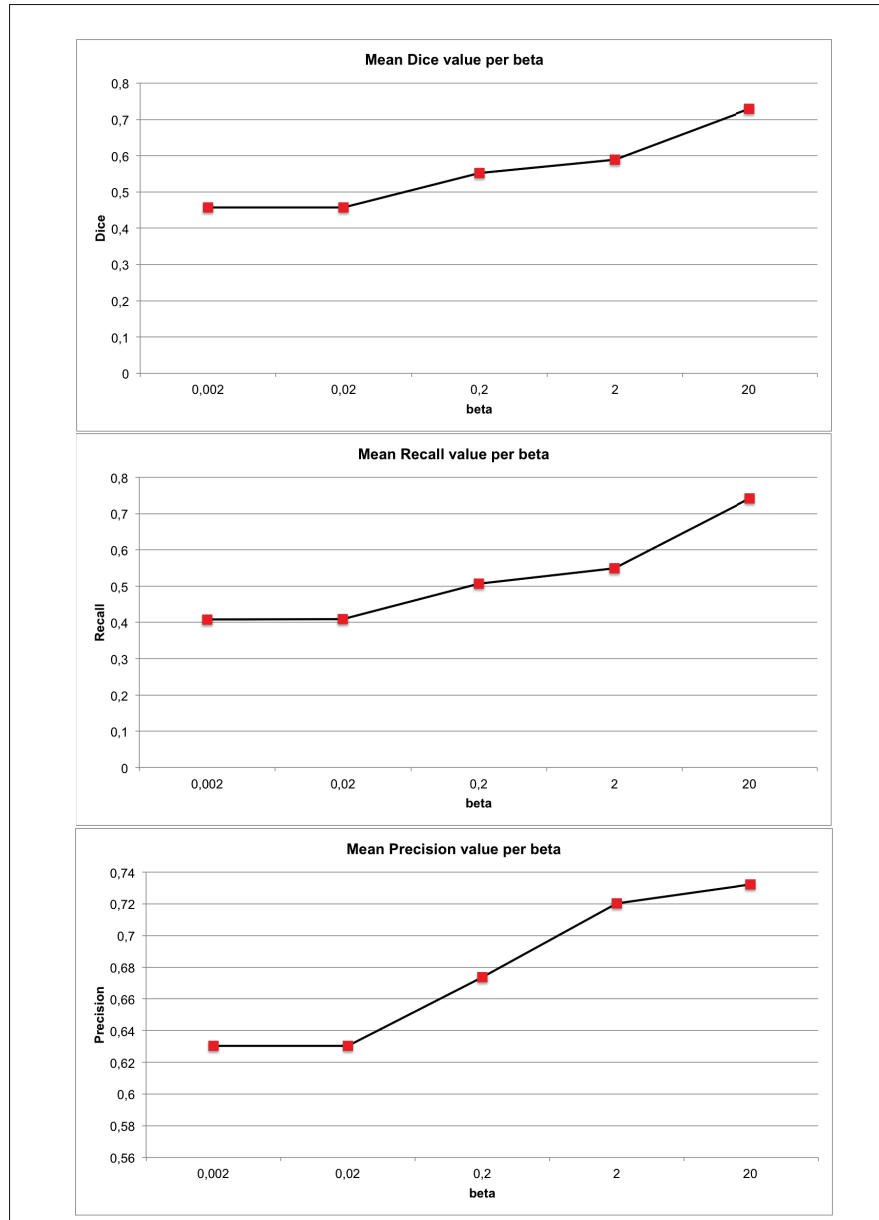
Figure 3.4   Influence of parameter β on Dice, Recall and
Precision values (respectively from top to bottom).

where it levels out around a Dice value of 0.73. The neighbourhood size r has a large influence on the computation of the Laplacian matrix L that expresses the similarity measure between pixels. If r value is low, similar pixels that are in the vicinity of each other might not have the same label in the segmentation result. On the other hand, if the value of r is high, the Laplacian matrix becomes less sparse and finding the right segmentation result would involve
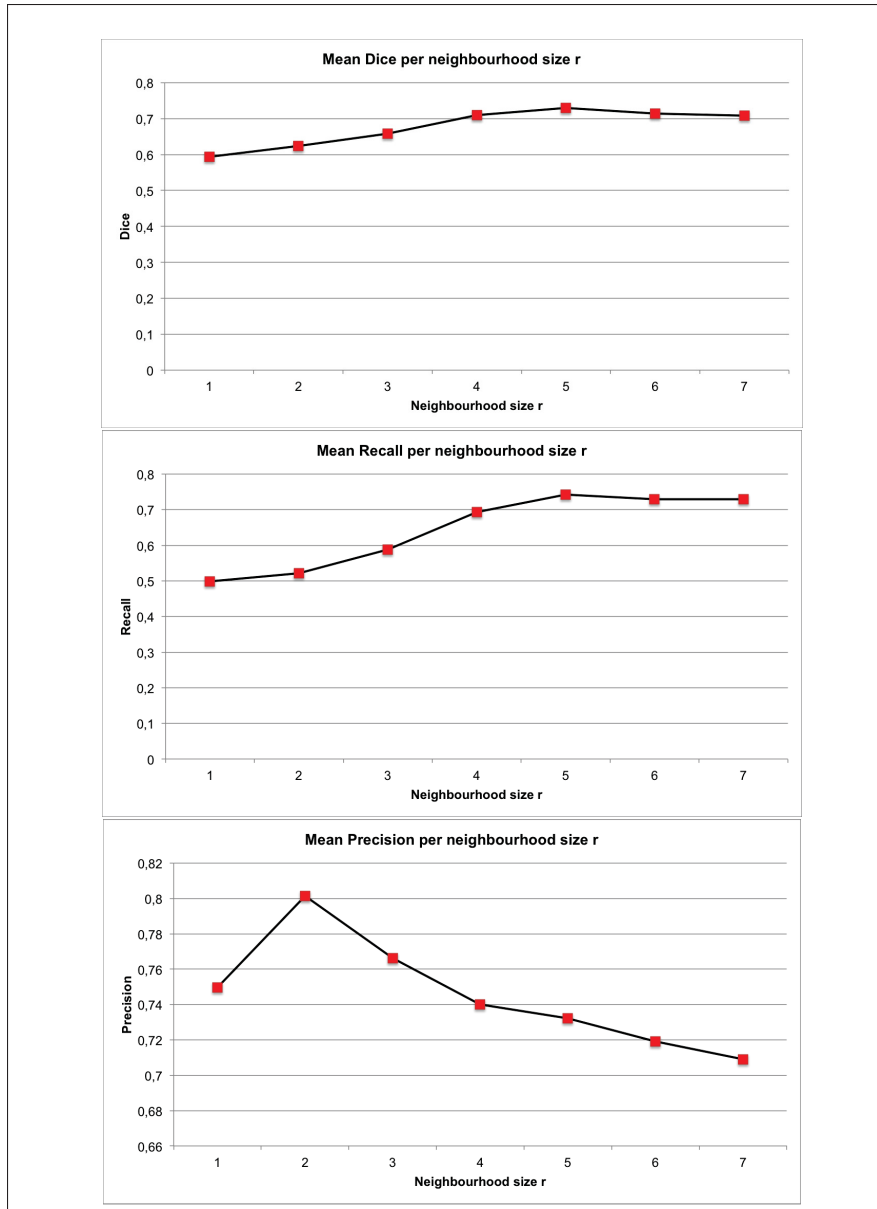
Figure 3.5 Influence of the neighbourhood radius *r* on Dice, Recall and Precision values (respectively from top to bottom).

complex computations and pixels that are not necessarily similar to each other would share the same label. The k-fold cross validation returned an optimal value for the neighbourhood radius $r = 5$.

3.3.3 Influence of seed points number

Specifying seeds can be useful, especially around regions with low contrast and noisy regions (e.g. in the case of small vessels with low contrast agent to depict them). To evaluate their influence on the VW performance, we randomly selected foreground and background seeds using the ground truth masks. At the beginning, we started without any specified seeds, then we seeded from 1% of foreground pixels and 1% of background pixels to 90% of each, foreground and background pixels. Figure 3.6 shows the seeded pixels on the image at different percentages of the image's pixels: starting at 0%, then 5% of foreground and background regions are seeded (respectively in red and blue) until 70% of seeded pixels. The bottom row displays the corresponding segmentation result to each percentage of seed used. As the number of seeds grows, we can notice that fewer errors are made and more true positives are detected.

a) 0% seeded pixels	b) 5% seeded pixels	c) 20% seeded pixels	d) 70% seeded pixels
e) Segmentation with 0% seeded pixels	f) Segmentation with 5% seeded pixels	g) Segmentation with 20% seeded pixels	h) Segmentation with 70% seeded pixels
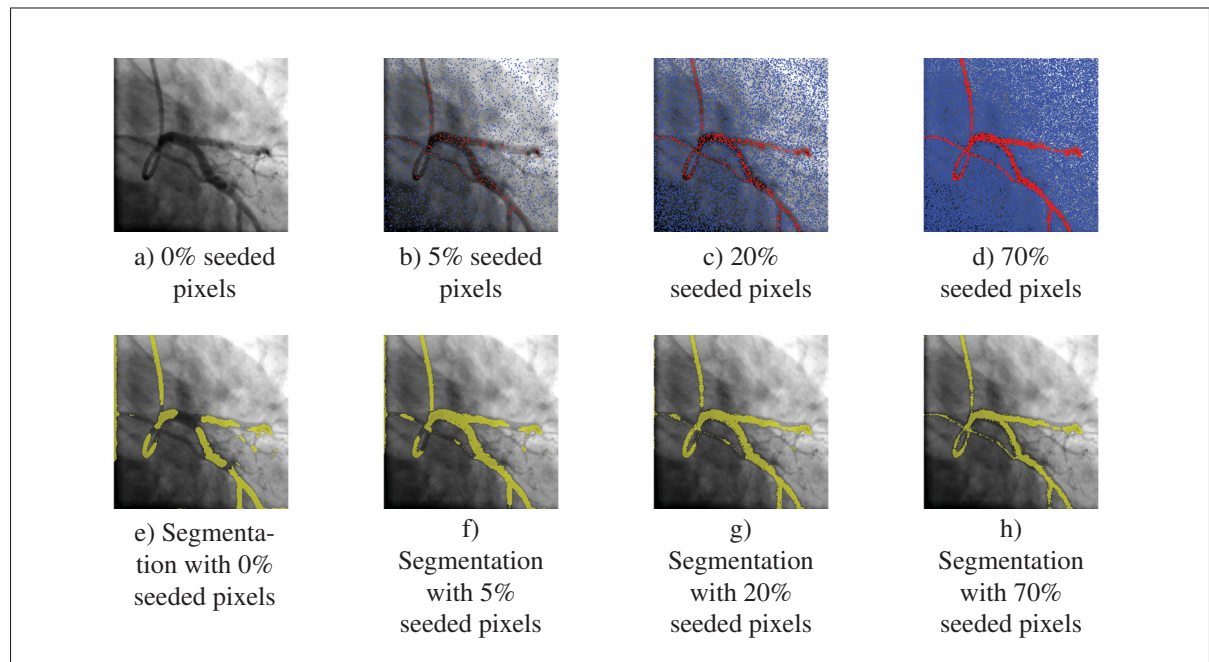
Figure 3.6 The influence of the percentage of seeded pixels on the segmentation results. Top: Original X-rays with different percentage of seeded pixels (blue pixels for background seeds, red pixels for foreground seeds). Bottom: Corresponding segmentation masks in yellow overlaid on the X-rays.

Figure 3.7 evaluates the influence of the percentage of seeded pixels in the dataset on the performance of the vessel walker method. In the four graphics, the results show that as the number of seeds in the images grows from 0% to 90% of the pixels, the performance of the VW enhances as well. We notice that the automatic VW (with a number of seeds $= 0$) performs with $AUC = 0.96$ which shows the robustness of the method even when no seeds are selected. Moreover, this automatic formulation performs better in terms of Recall $= 0.73$ than Precision $= 0.66$. This explains that the VW has the tendency to highlight pixels with even low vesselness values. The AUC evolution curve, shows that as the percentage of seeded pixels in background and foreground grows from 0% to 10%, the AUC value "jumps" from 0.96 to 0.99.

3.3.4   Vessel walker compared to existing methods

Table 3.1   Average performance on the 9 angiograms, obtained by Frangi's filter (VF), the active contour method (AC), the random walks algorithm (RW) and our proposed method (both in the automatic (VW-A) and semi-automatic (VW-SA) formulations)

	VF	AC	RW	VW-A	VW-SA
Precision	0.77	0.68	0.54	0.66	0.63
Recall	0.35	0.54	0.76	0.73	0.82
Dice	0.46	0.58	0.62	0.68	0.70
AUC	0.94	0.93	0.93	0.96	0.97

The Vessel Walker method (both with the automatic (VW-A) and semi-automatic formulations (VW-SA)) was evaluated on the presented dataset. Moreover, the method is compared to the vesselness filter (VF) by Frangi *et al.* (1998), the random walks algorithm (RW) by Grady *et al.* (2006a) and our previous work on active-contour method (AC) (M'hiri *et al.* (2012b)). To get a binary segmentation, the prescribed threshold of 0.5 was used for RW result, while Frangi and our VW method used Otsu's Otsu (1979) thresholding technique. For the VW parameters, the optimal values used were $\alpha = 2$; $\beta = 20$ and $r = 5$ with Frangi's vesselness filter computed within the scales $[1,3]$. The adjacency matrix (Eq. (2.2)) parameter was fixed to $\gamma = 850$.
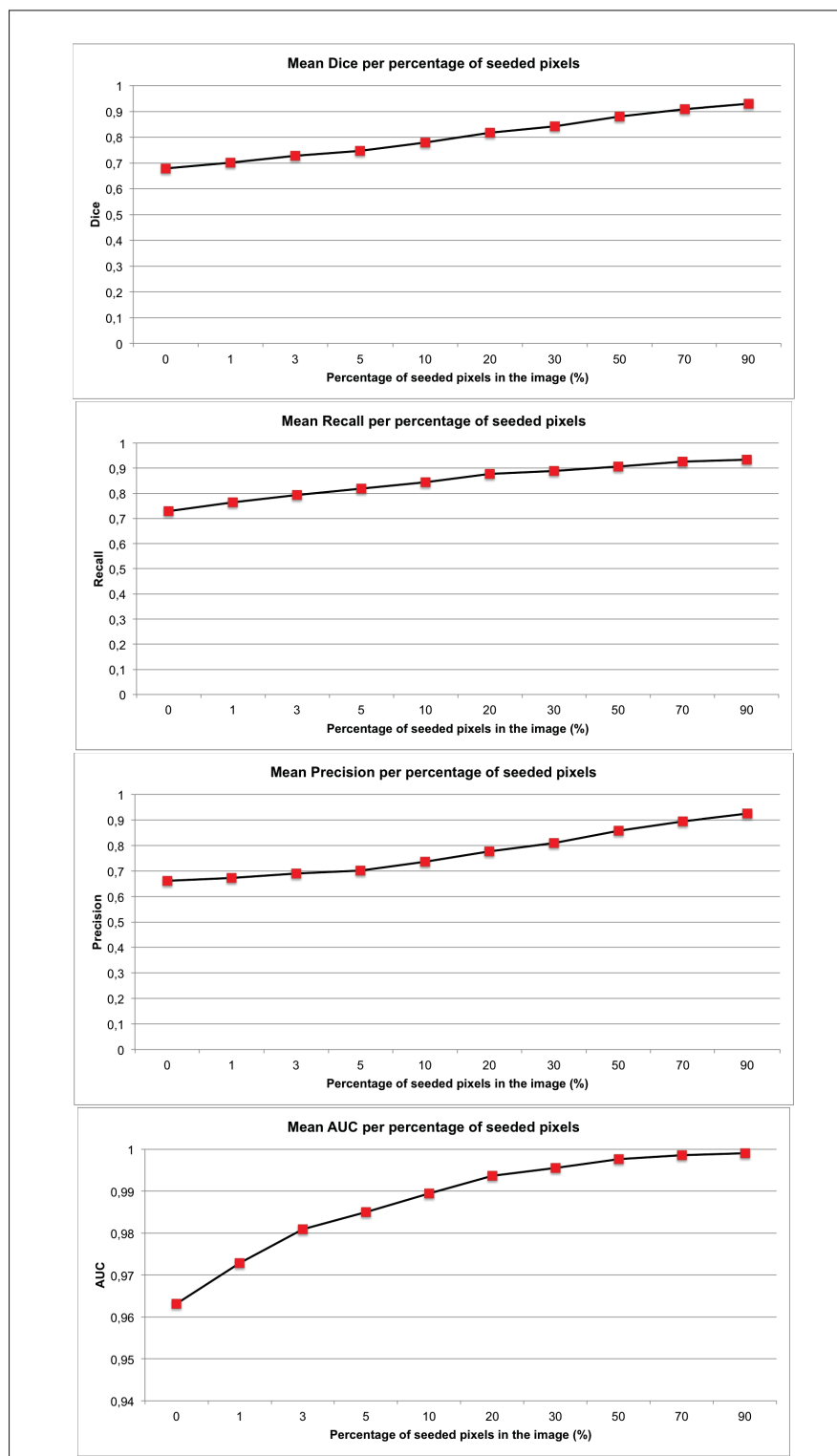
Figure 3.7   Influence of the percentage of seed number in the image on the performance in terms of Dice coefficient, Recall and Precision and AUC values.

Regarding the RW and the semi-automatic formulation, we used the same set of seed points representing 0.2% of pixels seeded with background and foreground seeds.
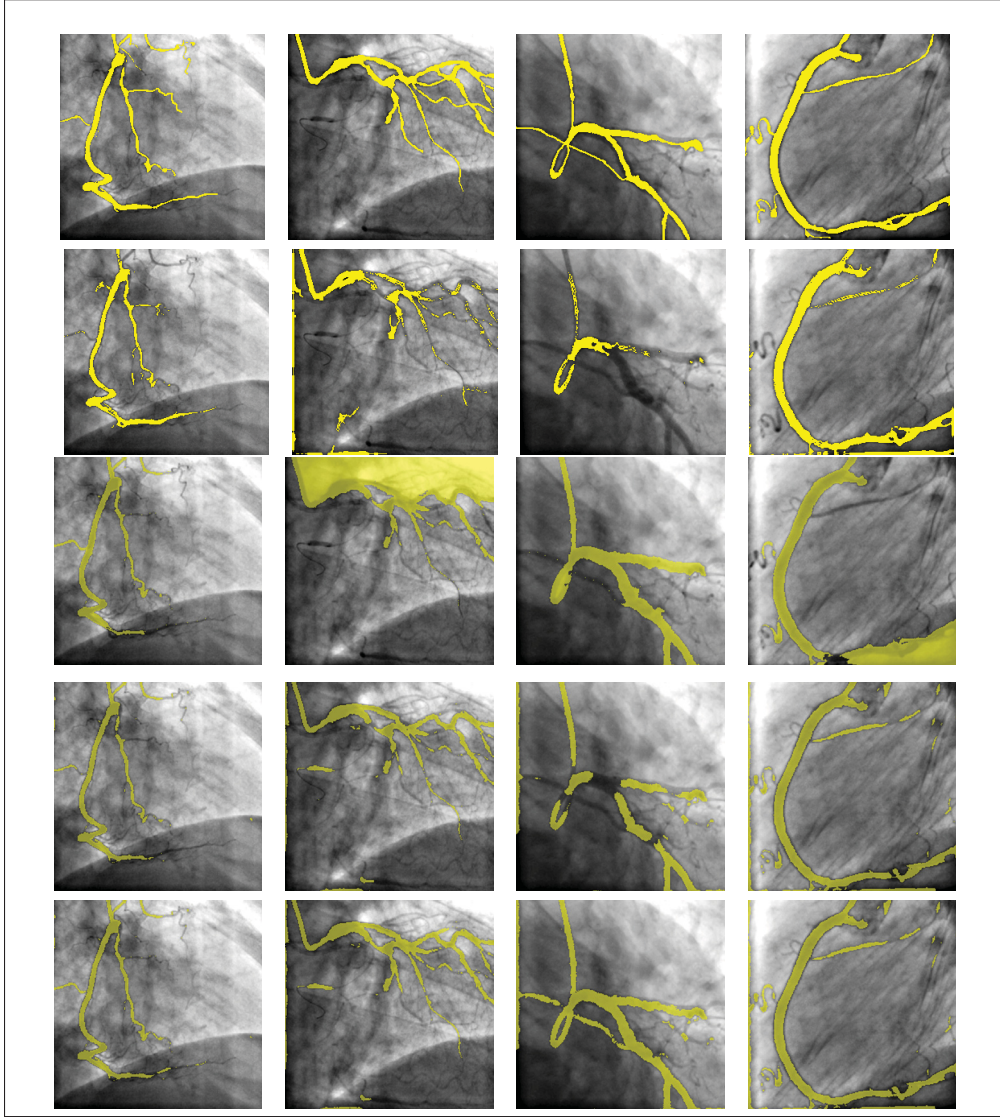
Figure 3.8   Segmentation results obtained with automatic thresholding. From top to bottom: Groundtruth, Active contours results, random walks results and our proposed method using the fully automated and the semi-automatic formulations.

Table 3.1 shows the mean performance of our proposed method and the other methods on the dataset in terms of precision, recall, Dice coefficient and the area under the ROC curve

(AUC). ROC curves were computed by varying the threshold (parameter θ defined in section 3.2.2.1) from 0 to 1. The result in table 3.1 shows that the proposed method has a good tradeoff between the precision and recall values in both automatic and semi-automatic formulations. The semi-automatic method shows the best Dice value of 0.70. Besides, both of our automatic and semi-automatic methods achieved the best performance, in terms of AUC value of 96% and 97% respectively. This proves the robustness of the proposed method to the potential bias of threshold selection.

Figure 3.8 shows four angiograms and their corresponding segmentation (overlaid in yellow), obtained with the Active Contour method, the random walks algorithm, and our Vessel Walker approach (using the automatic and semi-automatic formulations). The qualitative results show how both of the automatic and semi-automatic methods succeed in extracting vessels. Thanks to the vesselness features, the method extracts both large and small vessels with low contrast. The VW-A brings satisfactory results in comparison with the RW and AC. However, the VW-A can be limited in regions with low contrast which can disconnect parts of the coronary arteries (e.g. Fig. 3.8, third column and fourth row). In such cases, the automatic result can be enhanced with specifying seeds and the VW-SA can correct the limitations of the VW-A in the most challenging cases.

Both RW and VW-SA, as shown in Figure 3.9, used the same seed points to compute the results. While, we can see that RW failed in extracting the coronary artery due to leakage problems, our method avoids this limitation by using the vesselness features. Finally, both of the proposed formulations bring fewer false negative results than the Active Contour method. Despite the fact that the original contour of the AC method was initialized using vesselness results, the method relies only on intensity homogeneity to deform the contour, which can make it more sensitive to low contrast regions.

Finally, Figure 3.10 shows Fangi's vesselness values and our VW f non-thresholded result. The figure shows the probability value per-pixel of belonging to the foreground regions. Values from 0 to 1 are colour-coded such that the lowest possible foreground probability is dark blue
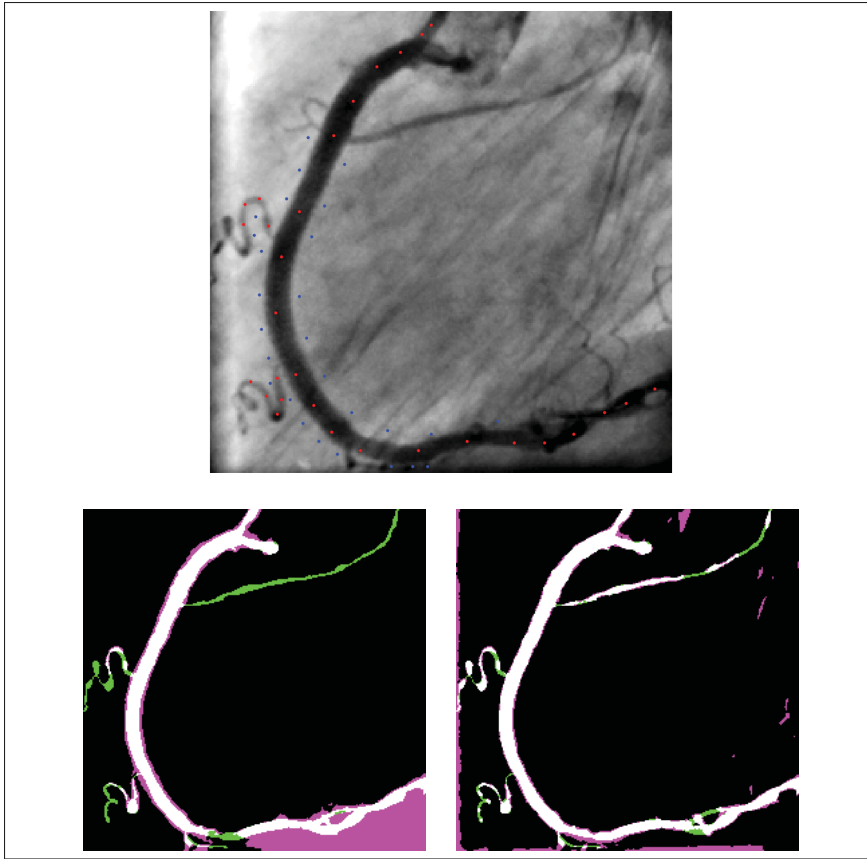
Figure 3.9   Top figure : manually selected seeds for image
number 6 (blue dots are background seeds ; red dots are
foreground seeds) Bottom row : From left to right : segmentation
masks of RW and VW-SA methods overlaid on the groundtruth
mask : White color shows perfect overlap ; green color shows
false negatives and pink color shows false positives in the
segmentation results

and the highest one is red. Our proposed method emphasizes the coronary arteries and their
bifurcations more accurately than the vesselness filter alone.Figure 3.8 shows that all methods
extract part of the catheter with the coronary artery. While the structure does not belong in
the coronary arteries, it is shown in the images as part of the vessels since it is connected to
them and shares the same tubular features. Further work would add a post-processing step
to suppress the catheter from the coronary arteries. Overall, our proposed method succeeded
in extracting all the dark tubular structures in the images. To summarize, the Vessel Walker
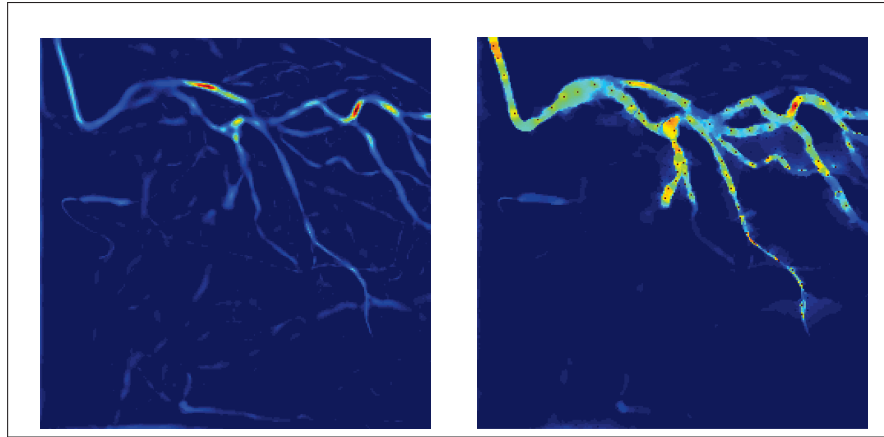
Figure 3.10   Foreground class probabilities obtained by Frangi's
filter (*left*) and our proposed method (*right*).

extends both of Frangi's vesselness filter and random walks, combining the advantages of both these approaches.

3.3.5   Limitations of the method

The VW method in both automatic and semi-automatic formulations has shown successful segmentation results. However, some limitations of the method were noticed and should be considered to further improve the VW:

- **Threshold θ selection** : Despite the fact that VW shows robustness across various θ values, as shown with the high AUC (96% and 97% from Table 3.1), using Otsu's thresholding solution does not seem to give the best binary result (which explains the relatively low Dice coefficient). We considered using different thersholding techniques such as K-means or fixing the threshold at 0.5. However, these results are not conclusive enough. We might consider exploring other thresholding techniques. Another solution would be to have an additional prior to the VW formulation, such as the vessel direction, to better distinguishes between background and foreground pixels.

- **Automatic versus semi-automatic formulations** : Semi-automatic formulation can be helpful in some challenging cases. However, our focus will be on how we can enhance the VW formulation to make the automatic method more accurate and robust in these cases.

- **Image contrast**: The dataset used for VW evaluation was challenging, especially for the low image quality. In this case, we may consider adding a preprocessing step (such as applying the anisotropic filter by Weickert (1998)) to enhance the quality of the image and the contrast of small vessels before applying the VW method.

3.4   Conclusion

This chapter presented our first contribution which is a new segmentation method to extract coronary arteries from 2D X-ray angiograms. The method, called Vessel Walker (VW), combines a graph-based method with vesselness prior. The method modifies the Random walks model to include vesselness information. Vessel walker was compared to the Random walks and other methods and has shown better quantitative results with a Dice of 0.70.

Future works

While our method presents an AUC higher than 97%, using Otsu's method does not seem accurate enough to get a binary segmentation between the foreground and background pixels. Further investigation has to be done to find a suitable thresholding method for the VW. Moreover, other priors can be included in the model, such as the direction and scale of the vessel computed with the vesselness filter (Frangi *et al.* (1998)).

CHAPTER 4

TEMPORAL SEGMENTATION OF CORONARY ARTERIES IN ANGIOGRAPHIC SEQUENCES (2D+T)

4.1 Introduction

Two-dimensional X-ray moving sequences (called angiograms) are used in percutaneous coronary interventions (PCI). They are a valuable tool to diagnose and treat coronary artery (CA) pathologies in newborns and young patients. The accurate and repeatable vessel segmentation and tracking in 2D angiograms (as illustrated in Figure 4.1) are essential for the assessment of the biophysical measurements of coronary arteries to predict cardiovascular diseases. These measurements include computing the vessel segment length (Tomkowiak *et al.* (2014)) or detecting stenosis (Janssen *et al.* (2010)) or estimating the severity of a stenosis by measuring the vessel's diameter (Compas *et al.* (2014)). Segmenting and tracking the artery along the moving angiography sequence is a key step for measuring the artery and assessing its dynamic change in the cardiac cycle.
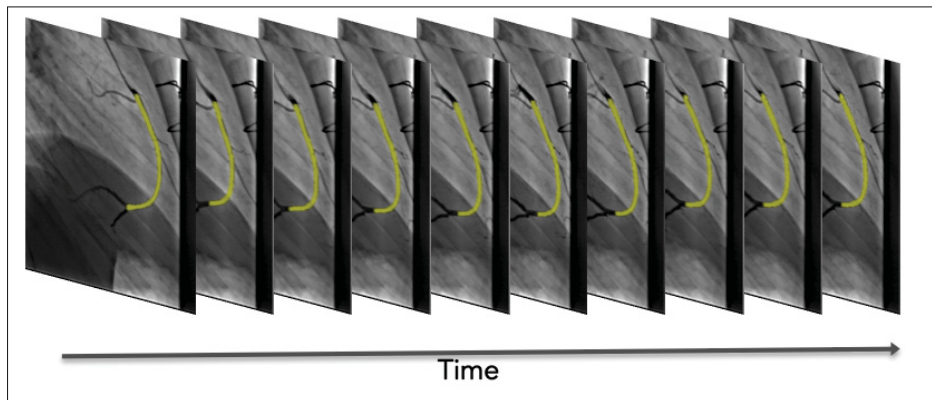
Figure 4.1   Overview of the segmentation of a coronary artery in
2D+time: Segmenting and tracking the RCA lumen (highlighted
in yellow) in an angiographic motion sequence

Vessel segmentation from a 2D moving sequence is a challenging task. First, the visualization of coronary arteries in X-rays depends on the diffusion of the contrast agent in the blood flow.

The faster the diffusion of the contrast agent, the harder it is to outline the artery. This is the case for pediatric patients, where the heart rate can be as high as 160 beats per min (twice that of an adult). Therefore, an entire vessel tree cannot be depicted in one single image, but gradually in the angiography sequence at a typical frame rate of 15 or 30 frames/s. Moreover, the displacements of coronary arteries are influenced by both the respiratory and the cardiac motions. For these reasons, it is difficult to track coronary arteries automatically with these motions. To address this problem, temporal coherence should be preserved, while segmenting the artery in all the frames in the sequence. This coherence will guarantee that the method is tracking the specific artery despite the respiratory and cardiac motions. The tracking result is crucial in order to evaluate the artery's function and elasticity.

In addition, using new image features to define homogeneous groups of pixels can enhance the segmentation accuracy. Superpixels have been used to define image primitives for image segmentation (Ren and Malik (2003)). They can help by preserving the essential information while simplifying the spatio-temporal segmentation. Instead of extracting pixels independently, the method would extract a group of connected pixels that share the same properties.

Our objective is to design a spatio-temporal segmentation algorithm that can be coherent both spatially and temporally for pediatric interventional cardiology. The spatial coherence guarantees that the method segments one particular vessel from the background, while the temporal coherence tracks the segmented vessel in the motion sequence. The results obtained will guide cardiologists after PCI interventions in evaluating the dynamics and the measurements of the vessel of interest (VOI) during the cardiac cycle.

This chapter evaluates the following hypothesis: *Using temporal information in 2D X-ray moving sequence helps segmenting and tracking coronary arteries* (Figure 4.1).

The contribution of this chapter is the development of an algorithm for segmenting a specific coronary artery in a moving X-ray sequence, while preserving a spatio-temporal coherence. Figure 4.1 illustrates the results of the proposed work, where a specific coronary artery is

segmented and tracked in a moving X-ray sequence. The contribution is divided into three parts:

a. Enhancing the vessel walker method by incorporating superpixels (Ren and Malik (2003)) instead of pixels.

b. Adding a temporal prior to the vessel walker method to segment and track in time: the Temporal Vessel Walker.

c. Proposing a pipeline where a clinician can specify by two clicks a vessel of interest. This vessel is segmented and tracked automatically during the angiographic sequence.

The findings are expected tp significantly contribute to the field of segmentation and tracking in 2D X-ray sequences. Most importantly, the findings may lead to the development of new protocols for assessing and evaluating coronary artery dynamics directly from monoplane 2D X-ray sequences.

4.2   Literature review

Different approaches have been proposed in literature for segmenting coronary arteries. A complete review of segmentation methods can be found in Lesage *et al.* (2009). However, most segmentation methods deal with the segmentation of a single image, and not a moving angiogram sequence. To consider the movement of a CA, other studies have proposed a solution for tracking the same structure in time. The polyline tracking method that was proposed by Dubuisson-Jolly *et al.* (1998) extracts and tracks a CA's centerline in 2D angiographic sequences. The CA's centerline is represented by a set of lines or *polylines*, and each line is retrieved in the sequence. The polyline tracking method is a reference work in the literature (Gao and Sundar (2012)), and shows successful qualitative results. Moreover, the method is formulated as a minimization problem on a constructed graph, similar to our method. However, to handle respiratory motion and simplify the computations, polyline tracking is applied after a

pre-processing step. Otherwise, the computations can be memory intensive and time consuming because the solution relies on finding the shortest path within a large graph in which each node represents a possible line segment of the centerline. Moreover, the polyline representation of a vessel may lead to the loss of curvature information.

Gao and Sundar (2012) proposed a motion model to track seeds that belong to the CA during the angiography sequence. Nonetheless, their model considers only cardiac motion, and not both cardiac and respiratory displacements.

More recently, Compas *et al.* (2014) presents a spatio-temporal approach to extract and track the coronary artery tree. However, the method tracks the entire tree, and not only one artery in particular. It is accepted that tracking one artery is more challenging because all of the arteries in the sequence will share similar features, and it is difficult to automatically distinguishes one from the others, while dealing with the artery's motion in time. Besides, in Compas *et al.* (2014), the vessel lumen is extracted at each point in the centerline individually and does not compute a global optimum.

Finally, while other studies have used spatio-temporal segmentation to track and segment arteries, they either focus on other types of arteries, which do not have the same motion as CA (such as cortical vessels in Ding *et al.* (2011)), or they work on other imaging modalities such as 3D CT scans in Laguitton *et al.* (2007), where the artery's displacements are not depicted in the same manner as in 2D X-ray angiograms.

To the best of our knowledge, this work is the first to undertake a spatio-temporal segmentation method, where the method tracks the lumen of one specific artery, while being robust to both respiratory and cardiac motions from a monoplane 2D X-ray sequence.

4.2.1 Superpixel Method

To enhance the segmentation process, one effective pre-processing step for image representation is superpixel extraction. First introduced by Ren and Malik (2003), the method organizes
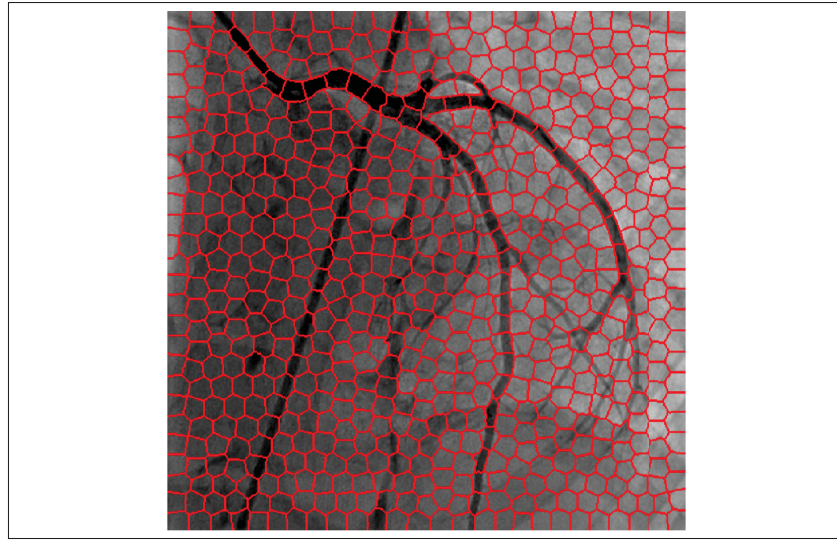
Figure 4.2   X-ray frame oversegmented with superpixels (red
lines are the borders of superpixels)

an image into small groups of pixels sharing the same features with low contour energy in-side the group.The use of superpixels, on the other hand, preserves the important information needed for segmentation, while simplifying the representation of the image and reducing the model's search space. One of the most efficient methods for superpixel computations is the simple linear iterative clustering (SLIC) by Achanta *et al.* (2012). The method performs a local clustering of pixels using their colour values and spatial locations. Figure 4.2 shows an X-ray frame segmented using the SLIC superpixel algorithm [1].

Superpixels have been used within graph-based methods. For instance Çiğla and Alatan (2010) used them within a normalized cut segmentation approach. Another work, presented by Desrosiers (2015), used superpixels with the random walks method to enhance the segmentation. Super-pixels simplifies the graph size and the retrieval of the optimal solution, where each node represents one superpixel instead of one pixel in the image.

---

[1]We used the implementation of SLIC from the VLFeat package : http://www.vlfeat.org/api/slic.htm

4.3 Proposed method : Temporal segmentation of CA in 2D X-ray moving sequences

This section presents our main contribution for a spatio-temporal algorithm to segment and track coronary arteries. Before presenting the main method, we start by introducing our preliminary works on the subject that lead us to the main contribution.

4.3.1 Preliminary works

To find the right solution to our spatio-temporal segmentation challenge, we started by first defining the **Temporal Vessel Walker** method (TVW). The method extends the original Vessel Walker formulation, presented in Chapter 3, by adding temporal prior to preserve the structure of interest. This work has been presented at the International Conference on Image Processing (ICIP2015).

4.3.1.1 Temporal Vessel Walker

In a multiple-frame sequence where we observe the same vessel of interest, we want to segment the vessel from a new frame $\mathscr{I}^t$ at time t, knowing the segmentation result in its previous frame $\mathscr{I}^{t-1}$.

The proposed idea is as follows: If we have a pixel p_i^{t-1} at location i in $\mathscr{I}^{t-1}$ and p_j^t at the same location in $\mathscr{I}^t$, and if p_i^t or one of its neighbors shares the same features as p_i^{t-1}, then pixel p_j^t or one of its neighbors has a high probability of having the same label (i.e., background or foreground label) as p_i^{t-1}. To guarantee this temporal similarity, we define graph G_τ, which connects by edges each pixel p_i^{t-1} in $\mathscr{I}^{t-1}$ to pixel p_j^t and its neighbors within a radius r_τ from $\mathscr{I}^t$, as shown in Figure 4.3. Each edge has a weight $w_{\tau ij}$ expressing the similarity between p_i^{t-1} and p_j^t using the following formulation:

$$w_{\tau ij} = \begin{cases} \exp\left\{-\gamma_\tau \left(I_i^{t-1} - I_j^t\right)^2\right\}, & \text{if } i = j \\ & \qquad \text{or } \mathrm{dist}(i, j) \leq r_\tau \\ 0, & \text{otherwise.} \end{cases} \tag{4.1}$$
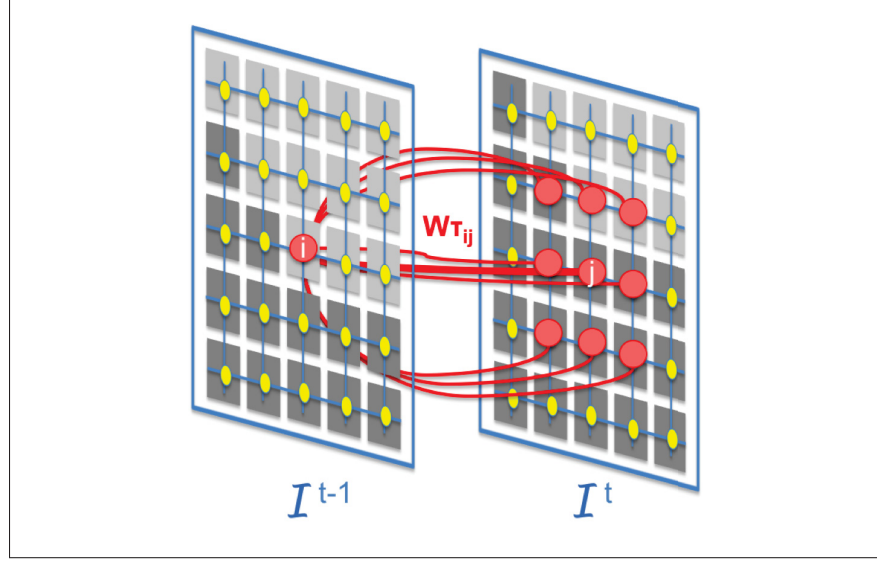
Figure 4.3   Representation of the temporal graph G_τ: Node i from image $\mathscr{I}^{t-1}$ is connected to the node having the same location as $\mathscr{I}^t$ and its surrounding 8-neighbours. We compute the temporal similarity measures between i and all the connected nodes (j and its neighbors).
source: M'hiri *et al.* (2015).

I_i^{t-1} is the intensity value at pixel p_i^{t-1} and γ_τ a parameter controlling the effect of the intensity differences on the weight.

We define the new Temporal Vessel Walker (TVW) following a Bayesian approach. The proposed method looks for a mapping f that maximizes the posterior probability of the Markov random field (MRF) associated with the label map:

$$f = \arg\max_f p(f\,|\,Y, f^{t-1}) \tag{4.2}$$

$$\propto p(f)p(Y\,|\,f)p(f^{t-1}\,|\,f). \tag{4.3}$$

The maximization problem is equivalent to the minimization of the energy function:

$$E(f) = \log(p(f)) + \log(p(Y\,|\,f)) + \log(p(f^{t-1}\,|\,f)) . \tag{4.4}$$

where each term is defined as follows, and the first term:

$$\log(p(f)) = -\sum_{i=1}^{|\mathscr{I}|}\sum_{j=1}^{|\mathscr{I}|} w_{ij}(f_i - f_j)^2. \tag{4.5}$$

the second term:

$$\log(p(Y\,|\,f)) = f_i^2 \log(p(y_i\,|\,f_i = 1)) + (1 - f_i)^2 \log(p(y_i\,|\,f_i = 0)). \tag{4.6}$$

with

$$p(y_i\,|\,f_i = 1) = \mathscr{N}(1, \alpha^{-1}) \tag{4.7}$$

$$p(y_i\,|\,f_i = 0) = \mathscr{N}(0, \beta^{-1}) \tag{4.8}$$

the third term expresses the temporal prior:

$$\log(p(f^{t-1}\,|\,f)) = \sum_{i=1}^{N}\sum_{j=1}^{N} w_{\tau ij}(f_j - f_i^{t-1})^2. \tag{4.9}$$

Combining these terms leads to the final formulation of the energy function:

$$\begin{aligned}
E(f) &= \frac{1}{2}\sum_{i=1}^{|\mathscr{I}|}\sum_{j=1}^{|\mathscr{I}|} w_{ij}(f_i - f_j)^2 + \alpha \sum_{i=1}^{|\mathscr{I}|}(1 - b_i)f_i^2 \\
&+ \beta \sum_{i=1}^{|\mathscr{I}|} b_i(f_i - 1)^2 + \mu \sum_{i=1}^{|\mathscr{I}|}\sum_{j=1}^{|\mathscr{I}|} w_{\tau ij}(f_j - f_i^{t-1})^2.
\end{aligned} \tag{4.10}$$

The last term in the equation conserves temporal coherence, where the formulation tries to obtain the segmentation result f in the actual frame similar to the segmentation result f^{t-1} obtained from the previous frame $\mathscr{I}^{t-1}$. Parameter $\mu > 0$ is a parameter controlling the weight of the temporal prior in the overall TVW formulation. Representing equation (5.1) in a matrix form yields :

$$E(f) = f^{\top}Mf - 2\beta b^{\top}f + \beta b^{\top}1 + \mu T. \tag{4.11}$$

With

$$M = (D - W) + \alpha I + (\beta - \alpha)B. \tag{4.12}$$

and

$$T = f^\top D_\tau f - 2f^\top W_\tau f^{t-1} + f^{t-1\top} D_\tau^{t-1} f^{t-1}. \tag{4.13}$$

I is the identity matrix and $B \in \mathbb{R}^{(n \times n)^2}$ is a diagonal matrix with $[B]_{ii} = b_i$ the vesselness value for each pixel. $D - W$ represents the Laplacian matrix (as defined in Eq. (2.2)) computed at $\mathscr{I}^t$, W_τ is the temporal adjaceny matrix using Eq. (4.1) and D_τ and D_τ^{t-1} are the degree matrices computed using W_τ.

Relaxing the binarity constraint on f and deriving the function with respect to f yields to the following:

$$\frac{\partial E}{\partial f} = 2Mf - 2\beta b + 2\mu D_\tau f - 2\mu W_\tau f^{t-1} = 0. \tag{4.14}$$

The solution of the equation gives :

$$f = (M + \mu D_\tau)^{-1}(\beta b + \mu W_\tau f^{t-1}). \tag{4.15}$$

The resulting f vector describes the probability that each pixel belongs to the foreground. To obtain a binary segmentation, a threshold has to be selected or computed. In our implementation, we chose the thresholding algorithm by Otsu (1979) to find a final binary segmentation of f. This well-performing method computes the threshold that minimizes the weighted within-class variance.

The TVW method extracts the vessel in $\mathscr{I}^t$ having the result f^{t-1} from $\mathscr{I}^{t-1}$. However, in the context of coronary arteries displayed in angiographic sequences, the shape and the position of the vessel can change dramatically due to the respiratory and cardiac motions and to the diffusion of the contrast over time. Applying TVW alone, while connecting pixels between two images, may succeed in extracting parts of the coronary artery and tracking it in the sequence.

However, it can also amplify the effect of background noise especially around the borders of the vessel when the contrast can be limited (as it is discussed in the result section 4.4). Consequently, additional steps are necessary to enhance the result of VWT in the context of coronary arteries segmentation in angiographic sequences.

4.3.1.2 Multiscale Temporal Vessel walker (M'hiri *et al.* (2015))
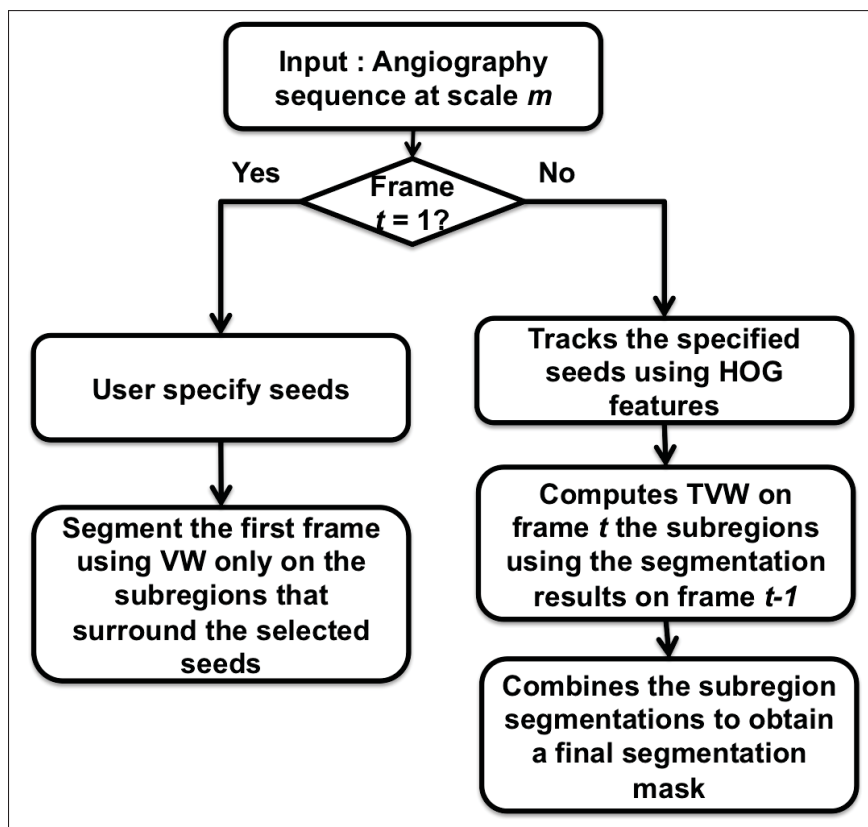
Figure 4.4   Multiscale hierarchical angiography segmentation at
a single scale.
source : M'hiri *et al.* (2015)

To capture cardiac and respiratory motions, using the Temporal Vessel Walker alone for segmentation and tracking is not sufficient. For this reason, the method is used within a hierarchical framework to track the structure accurately with the use of Histogram of Oriented Gradient (HOG) features. As presented in Figure 4.4, at the beginning of the sequence, the method asks

the user (i.e, a clinician) to select seeds defining the artery or part of the artery to track. Those seeds are used by the Vessel Walker method (from Chapter 3) to compute the segmentation at the first frame. Then, for the rest of the sequence, the seeds are retrieved using the Histogram of Oriented Gradient (HOG) features. These features were introduced by Dalal and Triggs (2005) and are known to be robust to illumination changes. To simplify the computations and limit noise effect, a frame is partitioned into subregions where each seed is the center of one subregion. The TVW Eq. (5.1) is computed for each subregion. The results for all subregions are then combined to find the segmentation for one frame at one scale m_i. These steps are reapplied on the sequence at different scales $m_i = [1, m]$. Finally, the segmentation results at different sizes are rescaled to their original size. The final mask is computed using weighted combinations of these results. Finally, shape matching technique, by Ling and Jacobs (2007), is applied between the segmentation results of frames $\mathscr{I}^t$ and $\mathscr{I}^{t-1}$ to ensure the coherence between both results.

Using TVW within a multiscale framework gives encouraging results by keeping track of the specified artery in the sequence. However, the results are still limited especially in the case of overlapping vessels, where it is more difficult to distinguish the vessel of interest from the overlapping vessel. Moreover, the use of TVW in a pixelwise fashion can show some limitations, since each pixel is treated independently from the rest of the image. Indeed, computing temporal similarity between pixels without considering the global context in the image can limit the performance. This is even more challenging when segmenting overlapping vessels or when the contrast is limited.

A new proposition is to enhance the TVW performance by computing similarities between groups of pixels. Superpixel grouping method can be a good alternative. Instead of computing temporal similarities between pixels independently, we compute similarities between superpixels which are a more meaningful entity to segment and to track. Moreover, using TVW within a multiscale approach can enhance the result but it is not sufficient especially with cardiac and respiratory motions. Besides, part of the information in the frame can be lost, when the frame's size is too small. In that context, superpixels can also be an interesting solution where the

VWT is applied at different sizes of superpixel to capture large and thinner parts of the same artery, while dealing with the artery's motion.

The following section presents the proposed algorithm for spatio-temporal tracking using the TVW with superpixels to segment and track a coronary artery in 2D X-ray sequence.

4.3.2   Temporal Vessel Walker with superpixels
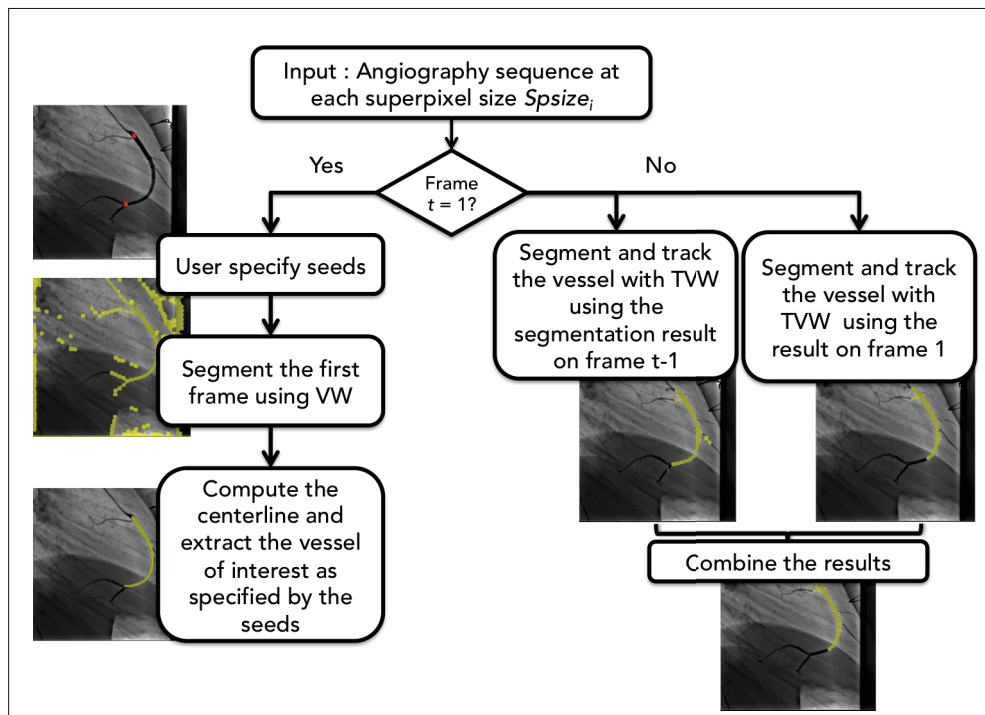
Figure 4.5   Proposed pipeline for spatio-temporal segmentation
of an artery in 2D X-ray angiogram

The proposed algorithm uses the TVW method, with the incorporation of superpixels , to segment and track the vessel lumen. Figure 4.5 summarizes the proposed algorithm: At the beginning of the sequence, the clinician defines the vessel of interest by specifying -using a simple click- the limits of the vessel. The vessel walker method with superpixels is applied to segment all the vessels in the image. This result is further refined to extract only the lumen of interest based on the seeds specified by the clinician, as described in section 4.3.2.1. For the

rest of the sequence, the Temporal Vessel Walker with superpixels is applied, as described in section 4.3.2.2. To track and segment the vessel, the method uses the segmentation result at the first frame of the sequence and the segmentation result at the previous frame as prior. The steps presented in Figure 4.5 are applied using different superpixel sizes to capture thick and thin parts of the same artery. The results obtained at different superpixel sizes are merged using a weighted combination to get a final segmentation result. All these steps are summarized in the algorithm 4.1 at section 4.3.2.3.

4.3.2.1 Segmentation of the first frame : Vessel Walker method using superpixels
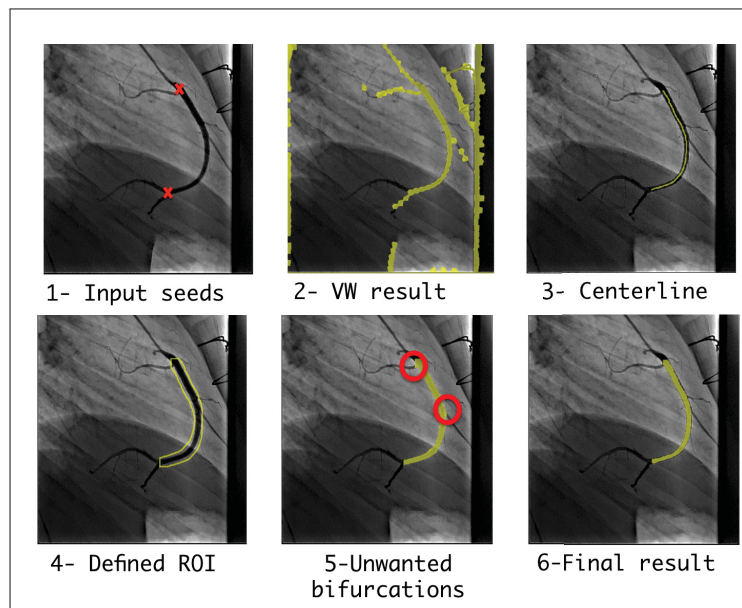
Figure 4.6   The steps for segmentation of the first frame

At the beginning of the X-ray sequence, and because we do not have an initial prior, the method starts by asking the operator to specify two seed points. These seeds corresponds to the beginning and the end of the vessel of interest, as shown in the first image in Figure 4.6. More than two seeds can be defined in the case when the contrast in the image is limited, or if there is vessel overlap or many bifurcations. Using the Vessel Walker and the specified seeds, the method extracts the vessel of interest as described in the following subsections. It is important

to perfectly extract the lumen of the first frame in the sequence, which is why different steps are used (as shown in Figure 4.6):

a. **Extending the Vessel Walker method using superpixels :** The Vessel walker automatic method, described in Chapter 3, is applied by using superpixel information instead of pixels. Image $\mathscr{I}$ is undersegmented to a number N_{sp} of superpixels $sp_i, i = 1..N_{sp}$. The image is then represented by an undirected graph $G = (V, E)$. V is the node set where each superpixel sp_i from $\mathscr{I}$ is represented by node v_i from V ($|V| = N_{sp}$). E is the edge set that connects two neighbouring nodes to each other. The weight w_{ij} of each edge e_{ij} describes mean intensity similarity between two neighbouring superpixels v_i to v_j:

$$
w_{ij} = \begin{cases} \exp\left\{ -\gamma(\mathscr{I}_{sp_i} - \mathscr{I}_{sp_j})^2 \right\}, & \text{if } \mathrm{dist}(sp_i, sp_j) \leq r \\ & \text{and } i \neq j \\ 0, & \text{otherwise.} \end{cases}
\tag{4.16}
$$

Where $\mathscr{I}_{sp_i}$ corresponds to the mean intensity in the superpixel sp_i and γ is a parameter controlling the effect of intensity's differences on the weight. The same equation defined at (3.2) in Chapter 3 is applied, where instead of pixels we simplify the computations of VW by using superpixels. The result (second image in Figure 4.6) extracts all the vessel-like structures in a frame. To extract only the vessel of interest (VOI) as specified by the clinician, the following step is needed.

b. **Extracting the vessel of interest using VW result :** To extract the vessel of interest, first, the centerline of the vessel is computed, then its corresponding lumen is segmented.

- Computing the centerline of the vessel: The centerline can be represented as the shortest path that connects the endpoints of the vessel (i.e., selected seeds) passing by pixels with similar features to them. Using the VW result, a first centerline is retrieved by the Hamilton-Jacobi Skeleton (Bouix *et al.* (2005)). Since the clinician can select a seed a little far from the actual centerline and these seeds are hard contraint in our pipeline, their location should be as accurate as possible. For this reason, the seeds location is

enhanced by moving them to the closest centerline point (for more accurate result). Then, the adjacency matrix is computed using the geodesic distance map (using the work of Sundar *et al.* (2006)) and using other features such as intensity similarity between seeds and all the pixels of the image and their orientation, we compute the new adjacency matrix as described in Freiman *et al.* (2012). Dijikstra's shortest path algorithm (Dijkstra (1959)) computes the centerline of the vessel based on the computed matrix and seed locations. The method allows the user to initialize more than two points along the vessel of interest (VOI), when necessary. The centerline will then be computed iteratively, where two consecutive seed points are connected using the shortest path algorithms. The resulting centerline is then constructed one segment at a time. The result is shown in the third image at Figure 4.6.

- Computing the lumen of the vessel: Once the centerline is extracted from the first
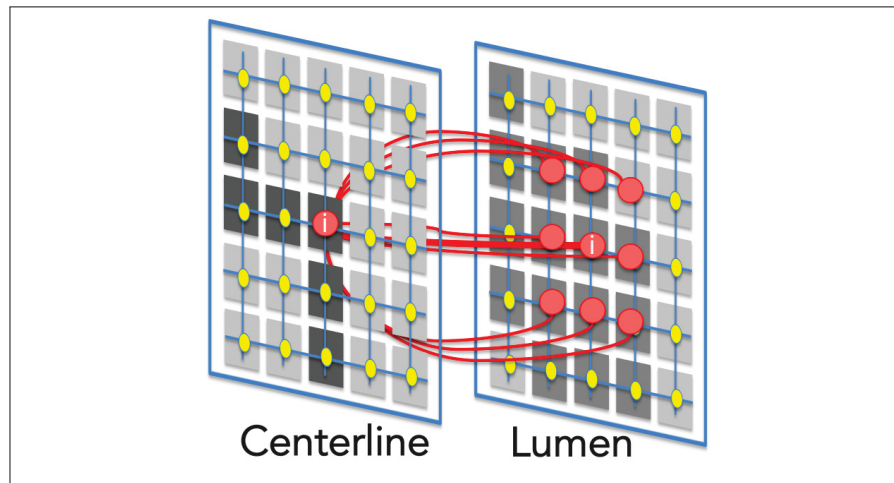
Figure 4.7   3D adjacency matrix connecting the centerline result and the extracted lumen and computing the similarity between the pixels on the centerline and the pixels belonging to the extracted lumen.

frame, a region surrounding the centerline is defined (the radius of the region is selected empirically depending on the dataset) and the lumen within that region is extracted (fourth image in Figure 4.6). However, this result can include some bifurca-

tions of the VOI that are not interesting for the clinicians (third image in Figure 4.6). Those small erroneous bifurcations are detected by computing the 3D adjacency matrix between the centerline and the lumen, keeping only pixels that are similar to the ones in the centerline as shown in Fig. 4.7. This is motivated by the fact that around a specific neighbourhood, the centerline and the lumen must share the same Vessel Walker probability value. If there is any bifurcation or vessel's crossover, the similarity value is low between the centerline and these regions. We apply Otsu (1979) threshold to remove the regions that have low similarity values in the 3D adjacency matrix to get the final segmented vessel. The result is shown in the last image in Figure 4.6.

While computing the lumen at the first frame may seem to be demanding in terms of the number of steps and computations, the complete computation takes a mean time value of 20 s per frame (running non-optimized Matlab code on an Intel Core i7 3.1 GHz).

4.3.2.2 Segmentation and tracking : Temporal Vessel Walker using superpixels

| Segmentation result at I^{t-1} | Defined ROI around the Segmentation result at I^{t-1} | The same ROI is used at I^t |
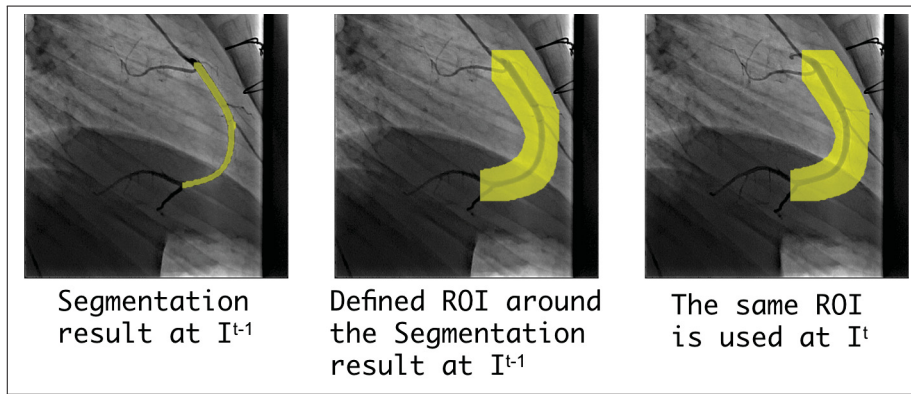
Figure 4.8   The defined region of interest (ROI) for sink nodes selection.

The Temporal Vessel Walker (TVW) in equation (5.1) is extended using superpixels. These groups of pixels increase the accuracy of the retrieval of similar groups from one frame to

the next. The temporal adjacency matrix W_τ (defined in Eq.(4.1) is modified to use superpixels instead of pixels. The source nodes are the superpixels belonging to frame $\mathscr{I}^{t-1}$ and sink nodes are the ones that belong to $\mathscr{I}^t$. The value of $w_{\tau ij}$ expresses the similarity of the mean intensity value of two neighbouring superpixels[2]. Because the motion from $\mathscr{I}^{t-1}$ to $\mathscr{I}^t$ is located
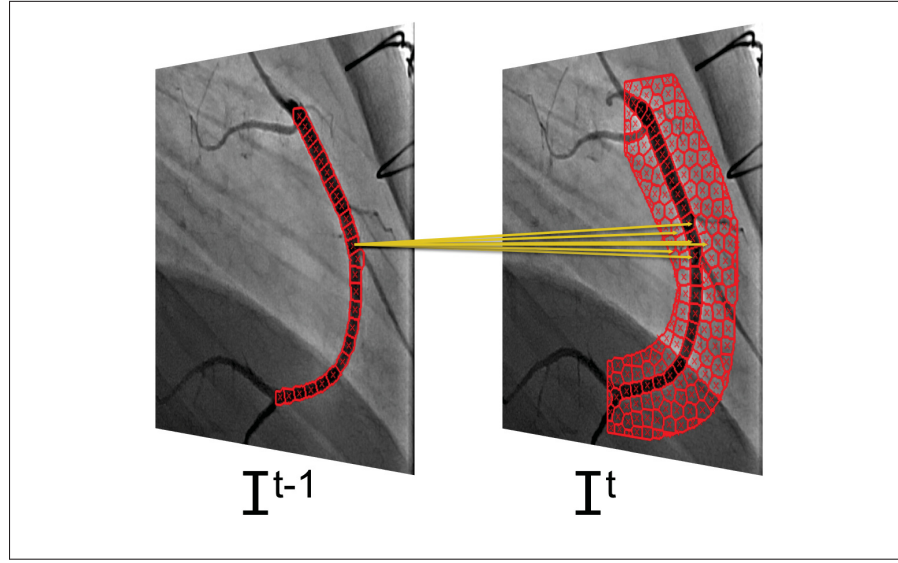
Figure 4.9 Temporal connections between selected source nodes and sink nodes

around a specific region, we simplify the computations in the equation (4.1) by selecting only the superpixels in $\mathscr{I}^{t-1}$ and $\mathscr{I}^t$ within a specific region (instead of using all the superpixels in $\mathscr{I}^{t-1}$ and $\mathscr{I}^t$). Therefore, the selected source nodes are only the superpixels belonging to the foreground segmentation result in $\mathscr{I}^{t-1}$, and the sink nodes in frame $\mathscr{I}^t$ are those belonging to a specific region of interest ROI_τ (as shown in the last image in Figure 4.8), which is the region surrounding the foreground result at $\mathscr{I}^{t-1}$, where the radius of the ROI_τ is selected based on the maximum displacement of arteries from one frame to the next. The temporal adjacency matrix is computed using the selected source and sink nodes, as defined in Figure 4.9. Considering only these specific nodes gives a sparse adjacency matrix, which speeds up the computations and limits the background noise.

---

[2]This computation was done using the code for the region adjacency graph, source : http://www.mathworks.com/matlabcentral/fileexchange/16938-region-adjacency-graph–rag-

4.3.2.3 Proposed algorithm

Algorithm 4.1 summarizes the proposed pipeline (as illustrated in Figure 4.5) for a spatio-temporal segmentation of 2D X-ray angiography sequence.

Data: Input 2D X-ray sequence of $frame_i$; $i = 1...nbFrm$

The weights corresponding to each superpixel size $weight_j$

Result: Segmentation result TVW_i^* of the sequence ; i = 1 ... nbFrm

1   **for** *each* $frame_i$ *i* ← 1 *to nbFrm* **do**

2   **if** $frame_i = 1$ **then**

3   Ask operator to select seeds (limits of the vessel) ;

4   Apply Vessel Walker with superpixel (VW) ;

5   Compute the centerline and lumen using the VW result ;

6   **else**

7   **for** $SPsize_j$ ← 1 *to* $SPsize_{Max}$ **do**

8   Compute TVW using $frame_{i-1} => TVW_{(i,i-1)}$;

9   Compute TVW using $frame_1 => TVW_{(i,1)}$;

10               $TVWsize_j = TVW_{(i,i-1)} + 2 \times TVW_{(i,1)}$;

11               $TVW_i = TVW_i + weight_j \times TVWsize_j$;

12   **end**

13   Threshold the result : $TVW_i^* = TVW_i > mean(TVW_i)$;

14   **end**

15   **end**

Algorithm 4.1: Proposed algorithm for tracking and segmenting coronary arteries in 2D X-ray sequences

At the first frame ($frame_i = 1$), the operator (the cardiologist) specifies the artery to be tracked. The centerline of the artery is computed and then its lumen is segmented using the vessel walker method. Then, for the rest of the sequence, the algorithm applies the temporal vessel walker
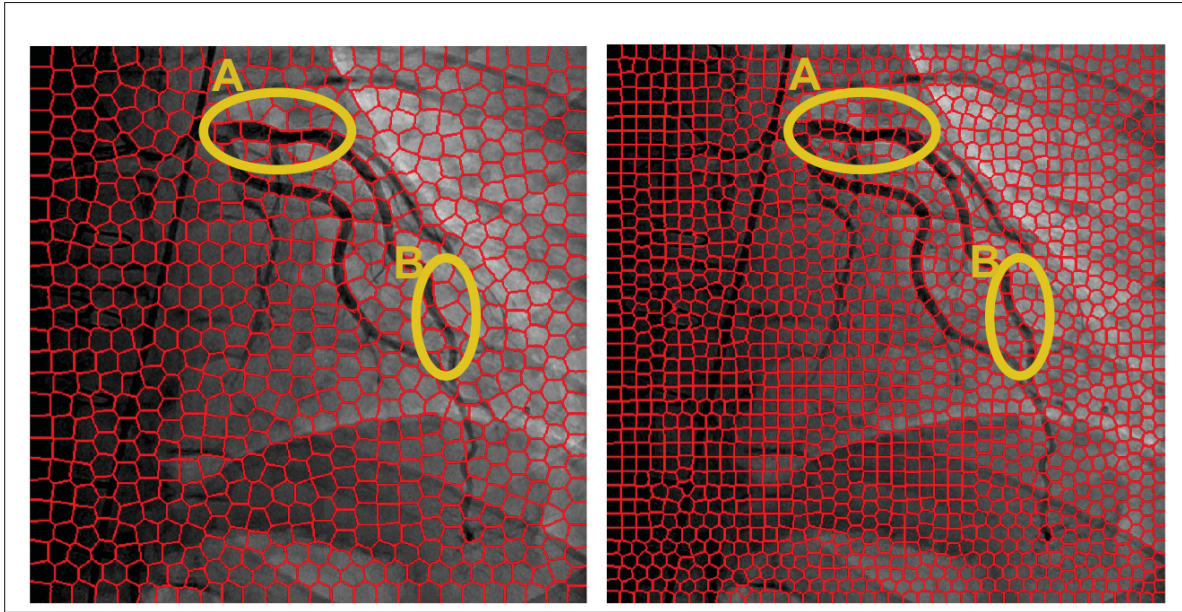
Figure 4.10   Computing superpixels at different sizes : left
SPsize = 20 ; right : SPsize = 13

at different superpixel sizes (where $SPsize_j = [1...SPsize_{Max}]$) to track and segment the same artery in the angiographic sequence.

For each frame i, and at each superpixel size $SPsize_j$, the algorithm computes the temporal vessel walker, using the segmentation result obtained from the previous frame ($TVW_{(i,i-1)}$) and again using the result at the first frame ($TVW_{(i,1)}$). The computations use the segmentation mask of the previous frame because the changes from the previous to the actual frame are less dramatic. Besides, the changes in intensity from consecutive frames are less important. However, during segmentation in the moving sequence, the result of the previous frame may contain some errors (such as overlapping vessels or missing parts of the vessel of interest). Therefore, in addition to the previous frame, the SP-TVW is applied using the first-frame segmentation mask as prior, because this prior was computed accurately. Consequently, both SP-TVW results (i.e., using the previous frame and first frame) are combined to determine the final segmentation result $TVWsize_j$, computed at a specific superpixel size.

Because the CA's thickness changes from the proximal to the distal parts of the artery, the result is applied at different superpixel sizes ($SPsize_j = 1..SPsize_{Max}$). Figure 4.10 shows the superpixels computed at different sizes. We notice that a large SPsize captures the proximal and thick parts of the artery (highlighted region A in Figure 4.10), which have a high contrast with the background. On the other hand, a smaller SPsize captures the distal thinner parts of the artery, where the contrast level is limited (highlighted region B in Figure 4.10). For this reason, the segmentation result $VWTsize_j$ is computed at different superpixel sizes.

The results for the same frame at different superpixel sizes are weighted and combined to obtain a final segmentation result VWT_i at frame i: as the SPsize value decreases, more weight is given to the corresponding TVW result (i.e., the value of k_j gets higher). To obtain a binary segmentation mask, TVW_i is thresholded (as shown in the last line in algorithm 4.1). Once the segmentation mask TVW_i^* is obtained, the method uses it to compute the segmentation result VWT_{i+1} in the next frame in the sequence, until the end of the sequence.

4.4 Experimental results

4.4.1 Data Acquisition

To evaluate the proposed work, we used a dataset of 12 angiographic sequences of coronary catheterization. The sequences were acquired from six young patients with congenital heart disease from the Sainte-Justine's Hospital (Montreal, Canada). These data were saved and anonymized into the DICOM format, and were recorded after approval by Sainte-Justine's Institutional Ethics Review Board. The angiograms were acquired by a C-arm Infinix-CFI BP by Toshiba profiling : six angiograms of right coronary arteries (RCA), three angiograms of the left anterior descending artery (LAD) and three others of the circumflex branch (Cx). Each sequence comprised nine frames (± 2) having a size of 512×512 pixels, and each of which represents a single cardiac cycle selected as the one that best delineates the anatomy from among the full angiographic acquisition. Different challenges are observed in the dataset: The frame-rate is low (15 fps), which makes the motion from one frame to the following more

pronounced. In addition, some sequences depict sternal sutures (when the patient has been previously operated on), which are dark tubular regions that can alter the segmentation result.

Because it can be complex and time-consuming to manually segment all of the sequence's frames, one segmentation expert has manually segmented 4 key frames for each sequence. Each key frame represents a different stage of the cardiac cycle: at the beginning (0%), at 20%, at 40%, and at the end of the cycle (100%). Using these frames, it is sufficient to evaluate the performance of the segmentation method, since each frame represents different motion changes along the sequence. We assume that, based on these key-frames, we can estimate the performance of the segmentation method. Only the main vessels were segmented (i.e. RCA, LCA and Cx). The manual segmentation is delimited at a terminal bifurcation or when the vessel would measure half of its original diameter. This ground-truth data has been subject to a double correction and validation by two cardiologists (the 4th and 5th authors).

Vessel lumen's segmentation is evaluated using the ROC curve's AUC, precision, recall, and Dice metrics. To evaluate the centerline extraction and tracking, we modified the classical computations of precision and recall metrics. PrecisionCL, RecallCL and the distance error were computed as proposed in Hernández-Vela *et al.* (2012): for each pixel in the ground truth, we checked within its neighbourhood of radius 5 if there is a corresponding point from the computed centerline. Finally, we computed the location error between the ground truth and the computed result to evaluate the accuracy of the centerline location.

4.4.2 Comparing the proposed method to polyline tracking

Our algorithm was evaluated in comparison with the polyline tracking method by Dubuisson-Jolly *et al.* (1998). The polyline tracking is a well-performing method that is still cited in the literature as a reference work for tracking CA in moving sequences (Gao and Sundar (2012)). Besides, the method is formulated as a minimization problem on a constructed graph, similarly to the proposed method.

Because the polyline tracking follows only the centerline of the vessel, and that our work tracks the lumen of the vessel, the evaluation of both methods is in terms of centerline tracking and not lumen tracking. To do so, we applied the Hamilton-Jacobi Skeleton (Bouix *et al.* (2005)) method is used to extract the centerline from the SP-TVW lumen. The Hamilton-Jacobi method analyzes the normalized flux of the gradient vector field to detect the skeletal points (or centerline points). It has been proven to be computationally efficient and robust to boundary noise. Both the polyline and the proposed methods were initialized using the same centerline computed from the first frame (as described in section 4.3.2.1).

Table 4.1 displays the performance of the polyline tracking and our algorithm on the dataset. The results are evaluated in terms of the centerline precision (PrecisionCL), and recall (RecallCL), and distance error. The proposed method has a higher trade-off than polyline tracking in terms of PrecisionCL and RecallCL. Moreover, its corresponding distance error of $0.23mm$ is lower than that obtained using polyline tracking, which returns a mean distance error of $0.94mm$.

Table 4.1   Average performance of the polyline tracking method (Dubuisson-Jolly *et al.* (1998)) versus our proposed algorithm on the dataset

	PolyTrack	TVW
PrecisionCL	0.78	0.81
RecallCL	0.75	0.78
Distance error	0.94	0.23

Figure 4.11 shows the centerline extraction performance using the proposed method and the polyline tracking method on sequence 8 of our dataset displaying a left anterior descending artery. Polyline tracking preserves the general shape of the initialized artery. This is explained by the fact that the neighborhood search using the polyline tracking is small. However, as the artery expands because of the cardiac work, the polyline tracking cannot capture some parts of the artery. Indeed, the images in the first row in Fig.4.11 displays green coloured pixels that
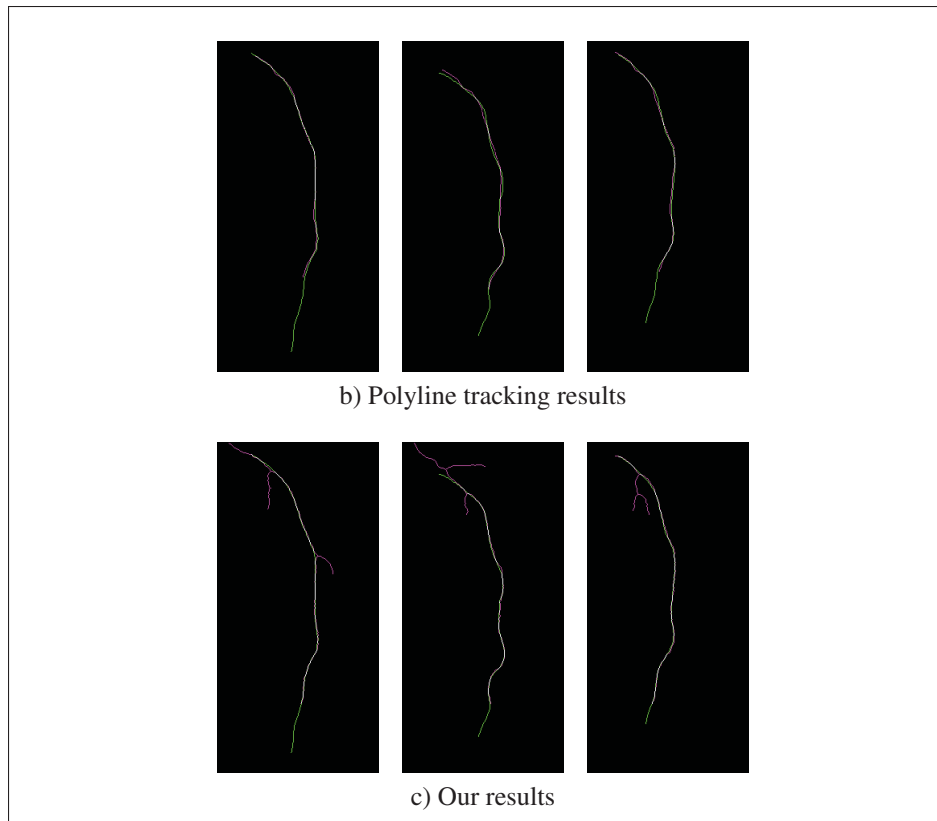
Figure 4.11   Computed centerline at different frames (left to
right : frame 2, 4 and 9) on sequence 8 and their overlap on the
groundtruth centerline. Top row: PolyTrack results. Bottom row:
Our results. Green colored pixels show false negative; pink
colored pixels show false positives and white colored pixels are
for true positives (i.e. overlap)

exhibit false negatives. We believe that this is caused by the length constraint in the polyline

method. The constraint ensures that the length of the artery does not change from one frame to

the following. The proposed algorithm gives more accurate results and retrieves the coronary

artery in the rest of the sequence with fewer false negatives, as shown in the second row of

Fig.4.11. Moreover, despite the presence of false positives in the proposed result (pink pixels),

the proposed method overlaps more with the ground-truth compared to the polyline method. As

a matter of fact, the location of the computed centerline is well aligned with the ground-truth

data. This is illustrated by the presence of more white pixels in the proposed results than the

polyline result in Fig.4.11. Indeed, the proposed method combines the prior information from

the previous frame but it also relies on the actual frame's information in terms of vesselness and intensity values. Therefore, the method is able to extract the centerline and to track it accurately in the sequence.

4.4.3 Extending the TVW model using superpixels : contribution of the proposed algorithm

Table 4.2 displays the mean results on four angiographic sequences of our database using the temporal vessel walker (TVW) with superpixels in comparison to using TVW pixelwise and to the TVW within the multiscale approach as introduced in M'hiri *et al.* (2015).

Table 4.2   Average performance (Precision, Recall and
Dice coefficient) on the first four angiographic
sequences of our dataset

	VWT	VWT(multiscale)	VWT(SP)
Precision	58.75%	85%	79.75 %
Recall	82%	52.75%	73.5 %
Dice	63.25%	63.5%	75.5 %

Using the TVW method pixelwise, while we have a better recall value, there is limited precision. The TVW within the multiscale approach returns the highest precision result, but it yields low recall values. In this approach, TVW is applied on subregions of the image, which limits the effect of noise. However, in the multiscale framework, TVW is computed at different scales of each frame, which can lead to the loss of contrast (especially at small scales) making the final segmentation result limited with low recall. On the other hand, TVW with superpixels returns the highest trade-off between recall and precision values, and the highest Dice value of 75.5%. Indeed, adding superpixels helps retrieving similar groups of pixels from one frame to the next more accurately than applying TVW in a pixelwise fashion. Besides, the use of superpixels improves the size of the adjacency matrix (the size of the matrix gets smaller), which makes the computations straightforward. Finally, TVW with superpixels limits the effect of noise propagation noticed with the TVW pixelwise.
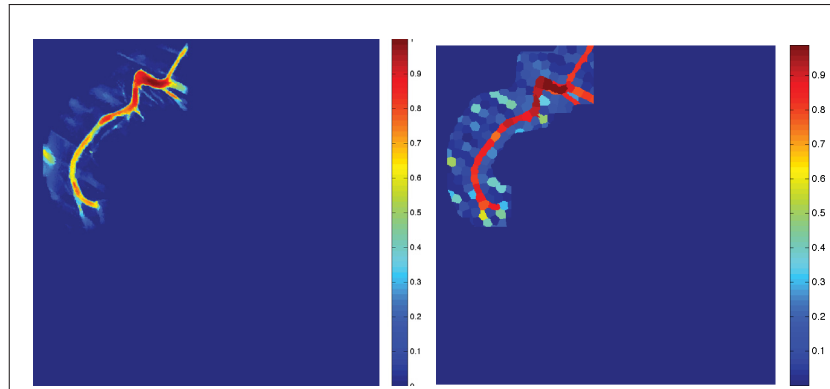
Figure 4.12   Results showing per-pixel probability values to
belong to the foreground as computed with the TVW alone (left)
and with superpixels (right)

Figure 4.12 illustrates the computed probabilities of pixels belonging to the foreground (i.e.,
the non-thresholded results computed using Eq. (5.1)), using the temporal vessel walker for-
mulation with and without superpixels. The colors in the images show the probability values;
the red pixels correspond to probability that it belongs to the foreground close to 1, while the
blue pixels correspond to a probability of 0. The use of superpixels better highlights the dif-
ference between the foreground and background regions, whereas the result computed without
superpixels has some limitations in terms of extracting parts of the vessels. This is observed
particularly in the yellow region at the end of the vessel where the probability values are around
0.6 and 0.5.

Figure 4.13 shows the ground-truth and the segmentation results using the three approaches
in sequence 3 of our dataset at frame 4. In the left image of the second row, the use of TVW
pixelwise displays false positives in its segmentation mask, where sternal sutures belonging
to the background is highlighted as part of the artery. SP-TVW and the multiscale approach
exhibit more precise results in the extraction of the artery. Nonetheless, the multiscale approach
is less precise around the borders of the vessels, where its segmentation mask oversteps the
edges of the vessel.
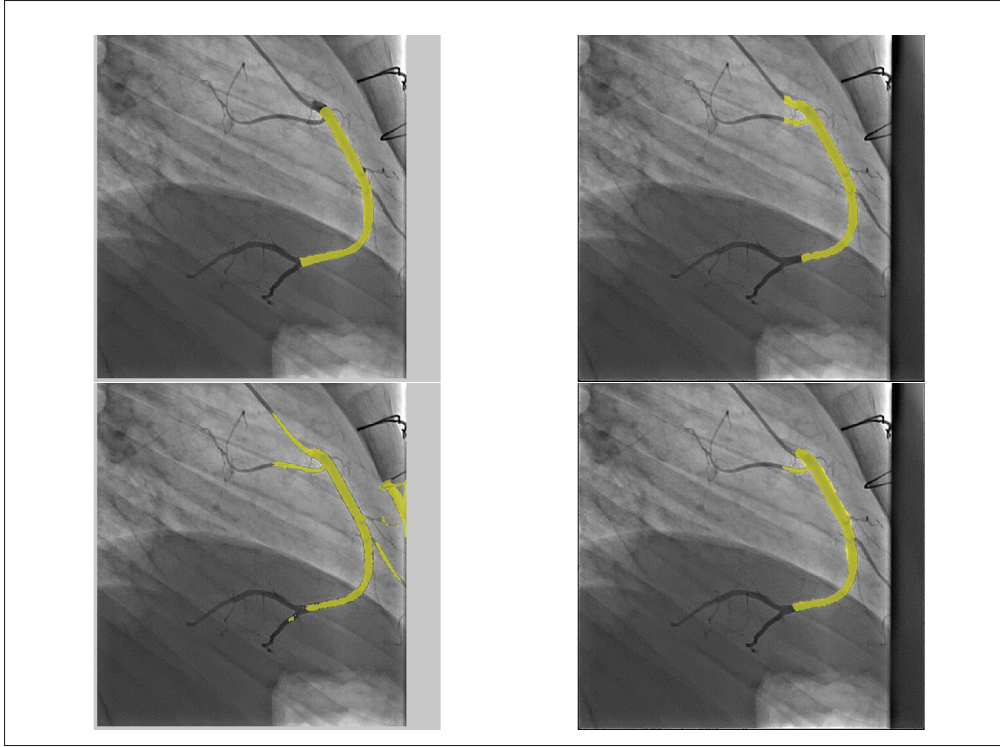
Figure 4.13   Segmentation overlaid on the original frame 4 of the
RCA sequence 3 of our dataset. Top row: the groundtruth (left)
and the TVW with superpixels result (right). Bottom row: TVW
method pixelwise (left) and TVW within the multiscale approach
(right).

4.4.4   Parameter's influence

This section evaluates the influence of the algorithm's parameters on the overall performance.
Different parameters are tested : superpixel size, μ, α and β.

4.4.4.1   Superpixel size

In this section, we evaluate the effect of the superpixel size (SPsize) on the mean performance
in terms of Dice, precision and recall values, as illustrated in Figure 4.14. The values were
computed on the first three sequences of the dataset. Each sequence represents a different type
of coronary arteries : LAD, Cx, RCA. When the SPsize becomes too large, each superpixel will
regroup pixels that are less similar to each other. Therefore, pixels belonging to the vessels and
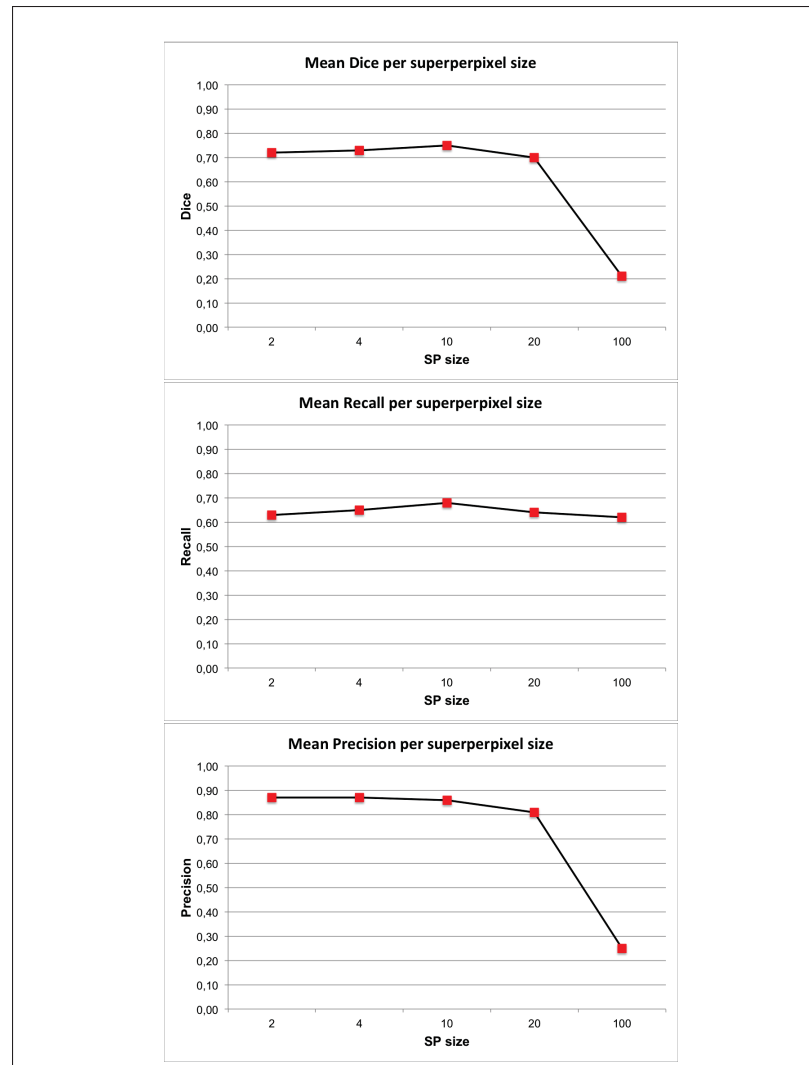
Figure 4.14   Influence of the superpixel size on Dice , Recall and
Precision using our proposed work

to the background will get grouped in the same superpixel and if the segmentation result makes this superpixel as part of the foreground it will include the background pixels that are within this superpixel. This explains the sensitivity of the precision curve when the superpixel size becomes larger than 10. On the other hand, recall value increases as the SPsize is increased, until it reaches the value of SPsize= 10 pixels. Indeed, superpixels creates groups of similar pixels, making a high rate of true positives. This shows the importance of selecting the appropriate SPsize, especially in the case of thin long structures like coronary arteries. When the SPsize is too small (around 4 pixels), the algorithm has a high precision, making fewer false positive

errors. On the other hand, at the same SPsize value, the recall is lower than when using a higher SPsize (= 10). Finally, Dice index, affected by both precision and recall curves, increases until SP size = 10.
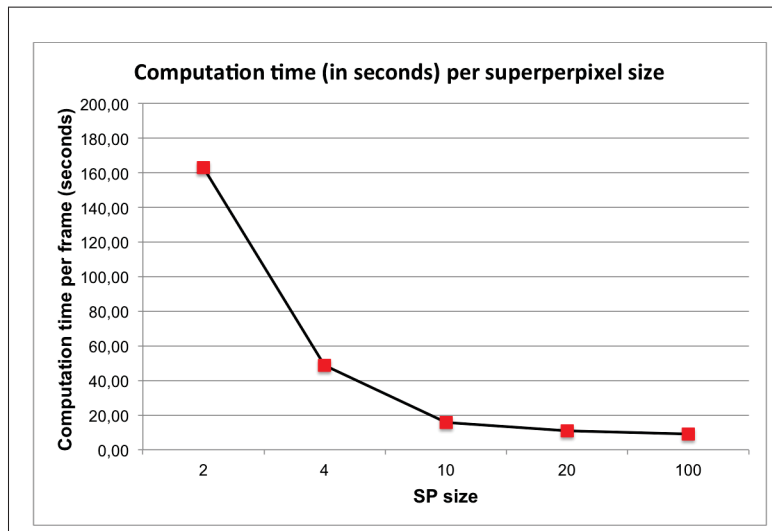
Figure 4.15   Influence of the superpixel on the computation
times per frame

Figure 4.15 shows the impact of the size of superpixels on the computation times. Note that as the SP size increases the computation times are faster. As the SP size becomes bigger, the number of nodes in the adjacency and temporal adjacency graphs decreases, making the matrices computation lighter.

Finally, Figure 4.17 displays the impact of different superpixel sizes (from the largest 100 to the smallest 4) on the segmentation result. We can see that as the SPsize gets smaller, fewer errors are made. However, when the SP size is the smallest, there is some difficulty highlighting the border of the vessel.

Selecting the right SPsize is important to keep a balance between high recall and precision values. However, one coronary artery may have thick diameter, at the proximal part of the artery and a thinner diameter at the distal part of the artery (as shown in Fig.4.10). That is
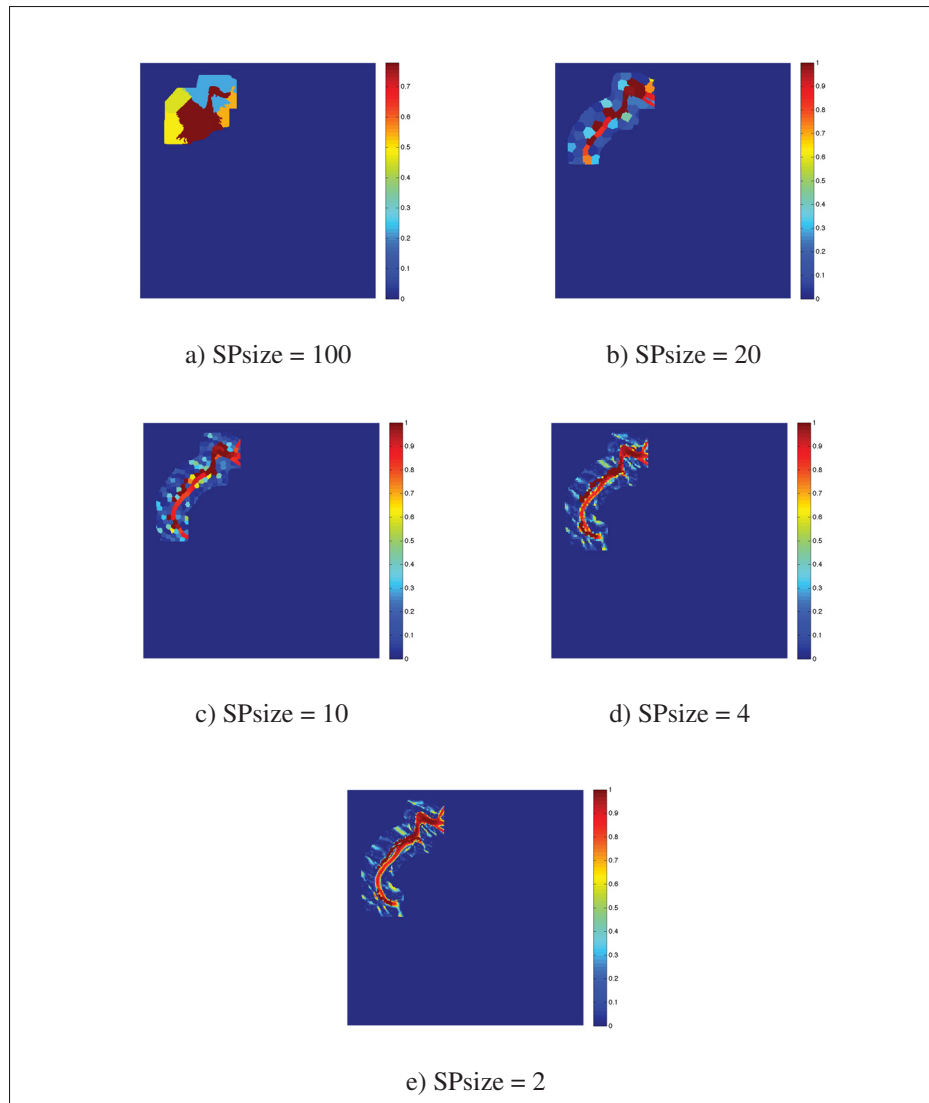
Figure 4.16   Influence of the superpixel using the TVW with superpixels model at different superpixel sizes on the probability values

why the proposed method computes the SP-TVW at different superpixel sizes to optimize the trade-off between precision and recall, which guarantee a better performance.

4.4.4.2   Tracking parameter μ

Figure 4.18 shows the influence of the temporal parameter μ on our method. We tested the temporal vessel walker using the previous segmentation frame as a prior and at a fixed optimal
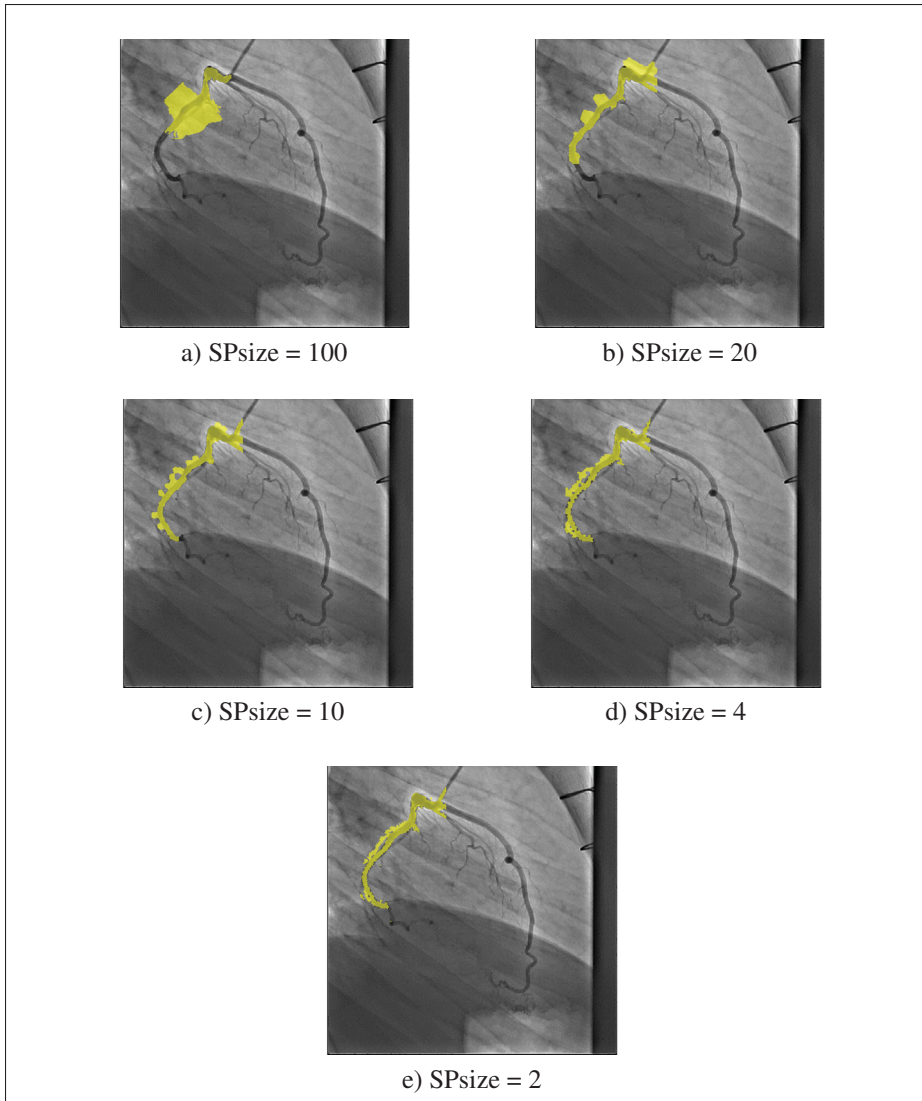
Figure 4.17   Influence of the superpixel using the VWT with
superpixels model at different superpixel sizes on the
segmentation result

superpixel size. These tests were done on the first three sequences of the dataset. The first curve

in Figure 4.18 displays the performance in terms of the Dice values as μ increases.When the μ

value is between 0.1 and 1, the Dice curve increases and reach a peak at $\mu = 1$. Once $\mu > 1$,

the performance drops dramatically. Optimal values for the temporal parameter μ are within

the interval $[0.1, 1]$. This temporal parameter can have a critical impact on the performance

because it helps to ensure that the vessel of interest is tracked along the angiography sequence.
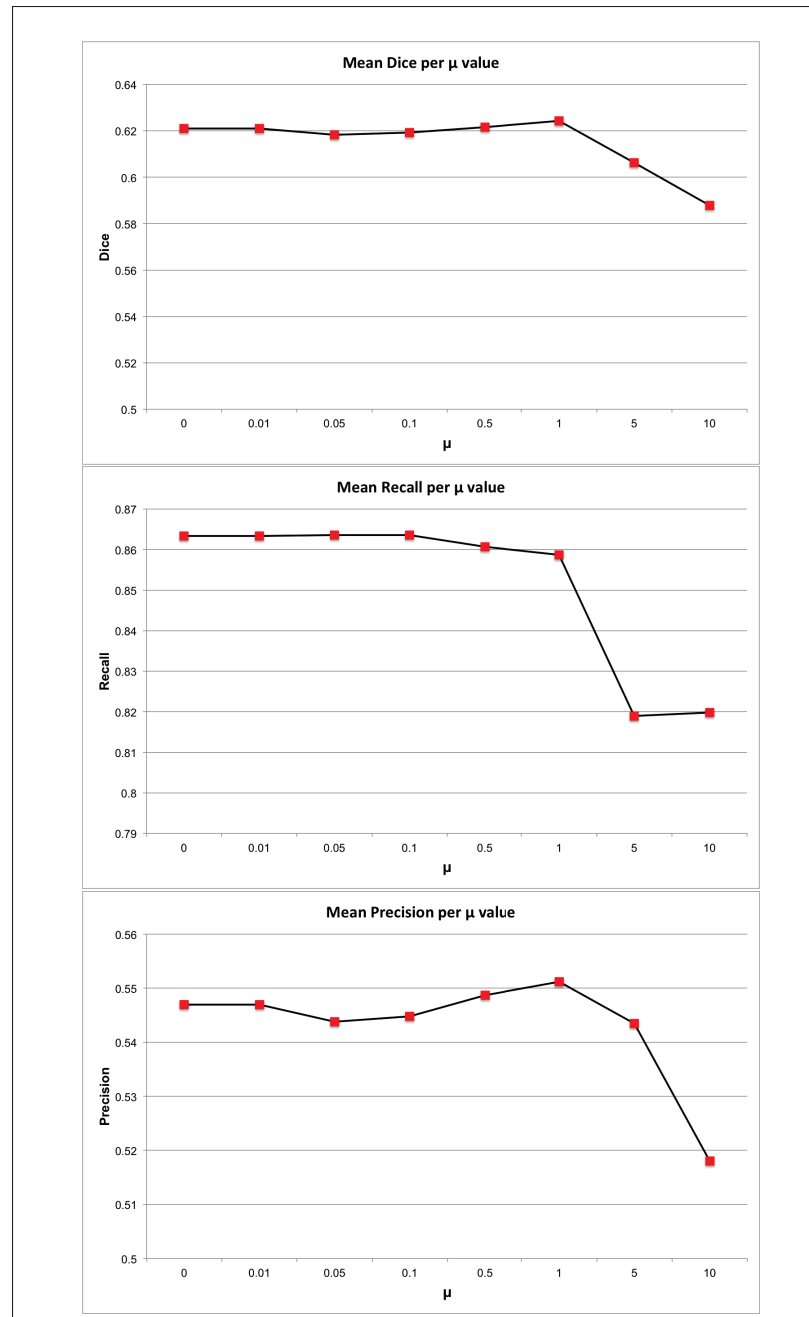
Figure 4.18   Influence of the μ values on Dice , Recall and
Precision using the TVW with superpixels

Parameter μ has the same effect on the precision curve where the optimal value of μ is within

the interval $[0.5, 1]$. However, the parameter does not affect the recall values (as shown in the

second curve in Figure 4.18). Having a temporal prior may limit the rate of false positives,

but it can also limit the true positive rate; hence, μ increases the precision level but can also at certain values limits the recall value.
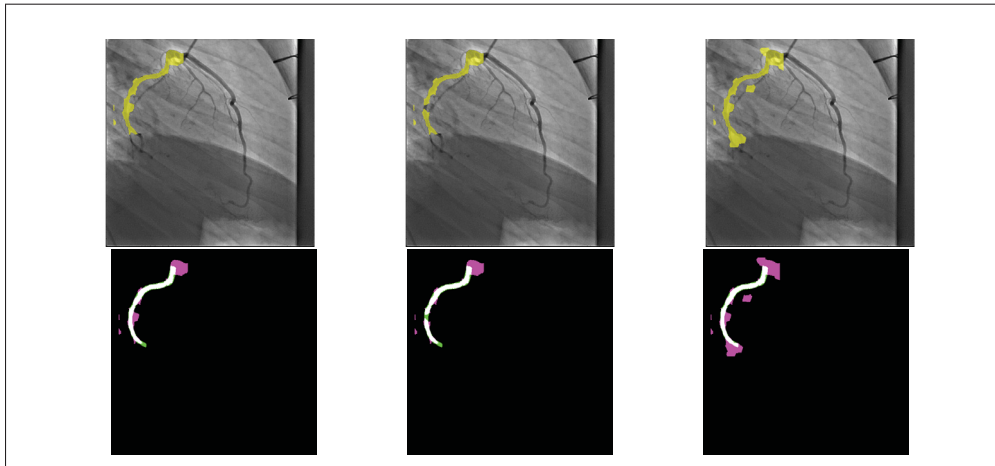
Figure 4.19   Influence of the μ values on the TVW results: first row : segmentation masks overlaid in yellow on original frames. Bottom row : Segmentation mask displaying true positives (white), false positives (pink), false negatives (green) . From left to right : results at $\mu = 0$, 1 and 10

Figure 4.19 displays the proposed method's results on the second frame of sequence 2 in the dataset. Each column shows the result for $\mu = 0$, 1 and $\mu = 10$. The top row shows the effect of μ on the segmentation masks. There is an improvement between $\mu = 0$ and $\mu = 1$, where the background noise around the end of the vessel is limited to $\mu = 1$. However, when μ gets a higher value, more background noise is added because the SP-TVW highlights the connection between the previous segmentation result and the actual frame.

These findings are highlighted further in the second row in Figure 4.19, where there is some overlap between the segmentation mask and the ground-truth, where false positive pixels are coloured in pink, false negatives in green and true positives are in white. When parameter $\mu = 1$, false positives are limited compared to the result at $\mu = 0$. On the other hand, when $\mu = 10$, the true positive rate increases and more pixels are coloured in white. However, the method becomes less robust to the background noise. The results in Figure 4.19 proves that

having a μ value close to 1 helps the method in tracking the structure of interest, while being more robust to background noise.

4.4.4.3   Influence of parameters α and β
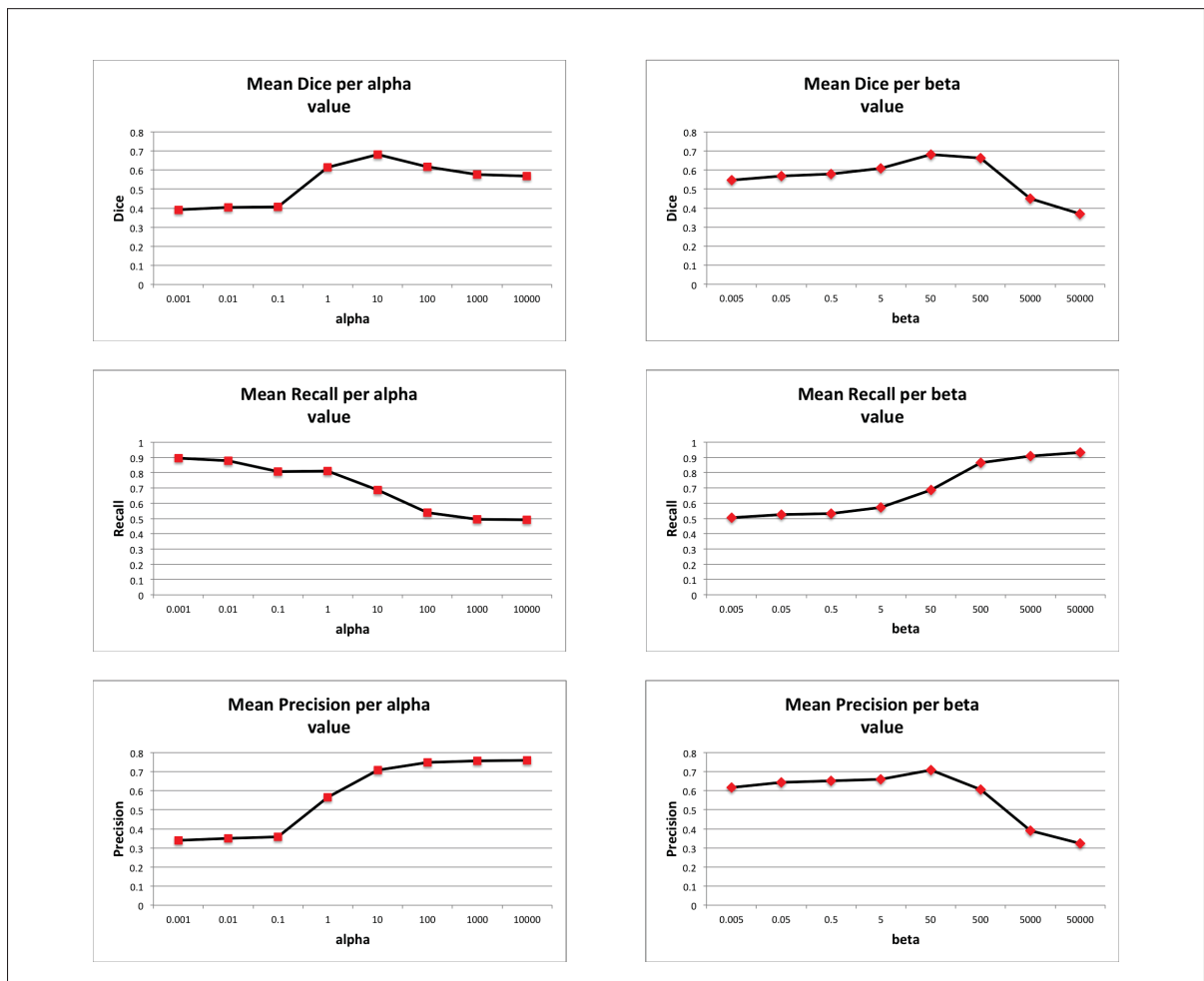
Figure 4.20   Influence of α (left column) and β (right column)
parameters on the overall performance using the proposed method.

The impact of parameters α and β, from equation (5.1), is presented in Figure 4.20. Parameter α influences the weight of the foreground pixels. As the value of α increases, the more robust becomes the result to the background noise, increasing the precision value. On the other hand, when α is greater than 10, the method will discriminate not only background noise, but also the

pixels belonging to the vessels, which explains the low recall values. The value of α should be optimally selected to preserve a trade-off between precision and recall. The Dice curve shows that an optimal value of $\alpha = 10$ leads to this trade-off.

The parameter β affects the weight of the background pixels. Unlike parameter α, higher β values result in a higher recall. However, background pixels that have an important vesselness value will be considered as part of the foreground. This limits the precision of the method. The Dice curve shows that at $\beta = 50$, the method gives the optimal segmentation result.

An optimal choice between α and β values will respect a good trade-off between recall and precision. That's why their values have to be selected depending on the nature of the dataset.

4.4.5 Performance depending on the nature of the vessel : RCA , LAD or Cx

The parameters' values were empirically selected following a K-fold cross validation on our 9 angiography dataset. Optimal values used were $\alpha = 50$, $\beta = 1000$, and temporal parameter $\mu = 0.05$. Superpixel sizes for the SLIC Achanta *et al.* (2012) implementation are 20 and 10 (with a regularizer value 0.01). Frangi's vesselness scales are within the range $[1,8]$. Finally, $\gamma = 4000$ and $r = 1$ were selected for the adjacency matrix, and $\gamma_\tau = 50$ and $r_\tau = 1$ for the temporal adjacency matrix.

The performance of the proposed framework is assessed in tracking and extracting the vessel's lumen during the angiographic sequence. Because the motion range depends on the nature of the coronary artery, we evaluated the dataset according to each category of coronary arteries (RCA, LAD or LCX). Figure 4.21 shows the dependence of the performance depending on the nature of the artery in terms of dice, precision, and recall values. Figure 4.22 shows the segmentation results at different frames in different sequences displaying from top to bottom : LAD, Cx and RCA arteries. The method gives the best performance when tracking RCA, with a dice close to 0.8. The RCA is one of the arteries that have a large motion range under the cardiac work. Despite the motion, the method is able to track and extract the artery accurately. Segmenting and tracking Cx arteries is more challenging, but there is still gives a good trade-
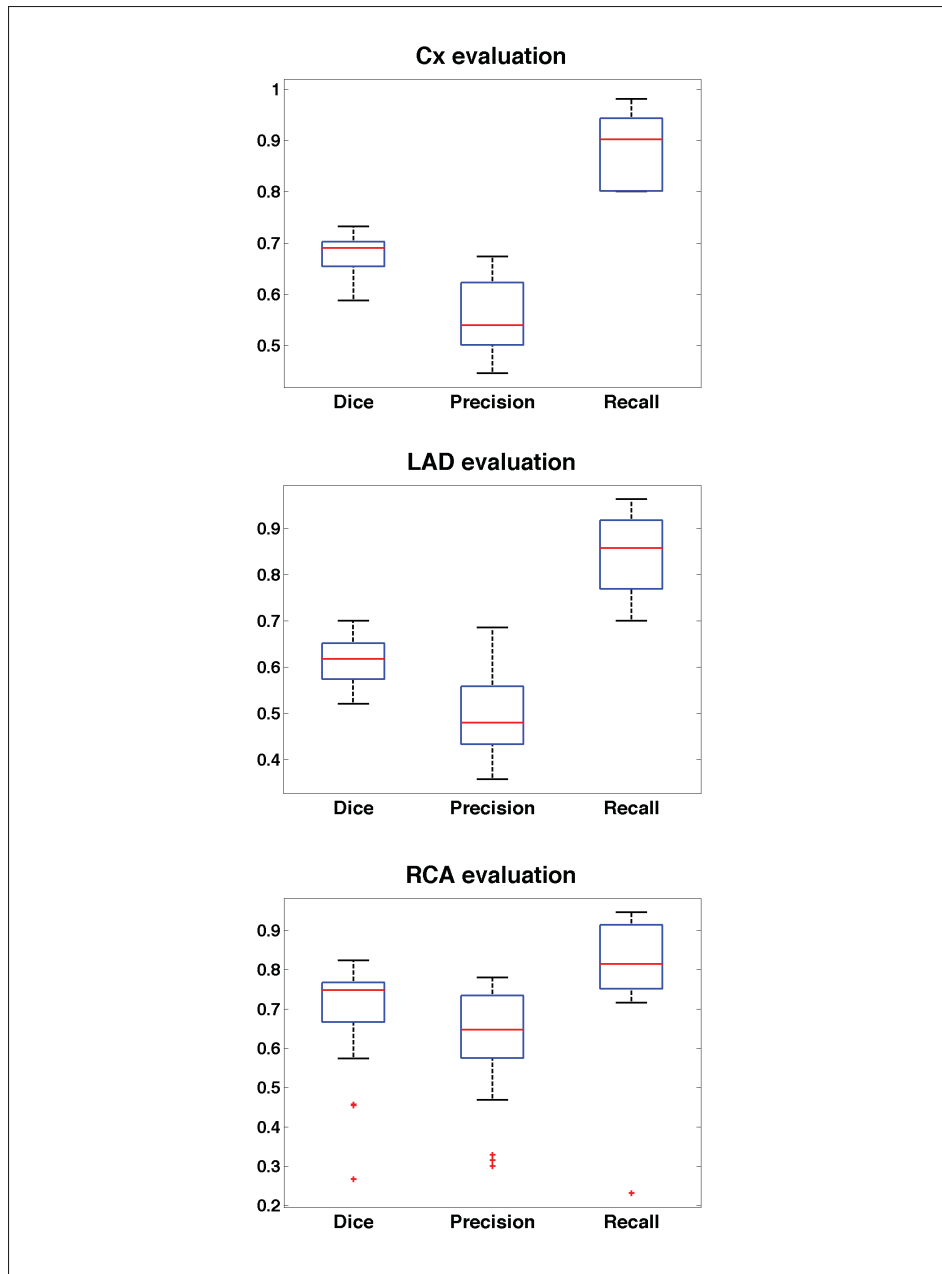
Figure 4.21   Performance of the proposed pipeline depending on
the nature of the coronary arteries. Top to bottom : Circumflex
artery (Cx), Left anterior desending artery LAD) and Right
coronary artery (RCA).

off between the precision and recall with a mean Dice of 0.7. LAD arteries are the most

challenging cases, because of their nature in terms of their shape and motion. Indeed, in all

the sequence displaying LAD, there is a vessel overlap or vessels that bifurcate from the main

artery and the tracking gets more challenging as it is difficult to distinguish between the arteries. Therefore, more features must be added to enhance the method in such cases.

Overall, the method shows a high recall value with all the types of vessels. However, the method seems to be more sensitive to the background noise in some sequences. This can be explained by different factors : the presence of overlapping vessels, the decrease of contrast level in the sequence and the low frame rate that leads to a large motion range from one frame to the following. The results are encouraging in terms of tracking the right structure of interest and extracting it from the background. More work has to be conducted in order to enhance the precision of the method by adding new features, such as the vessel's orientation.
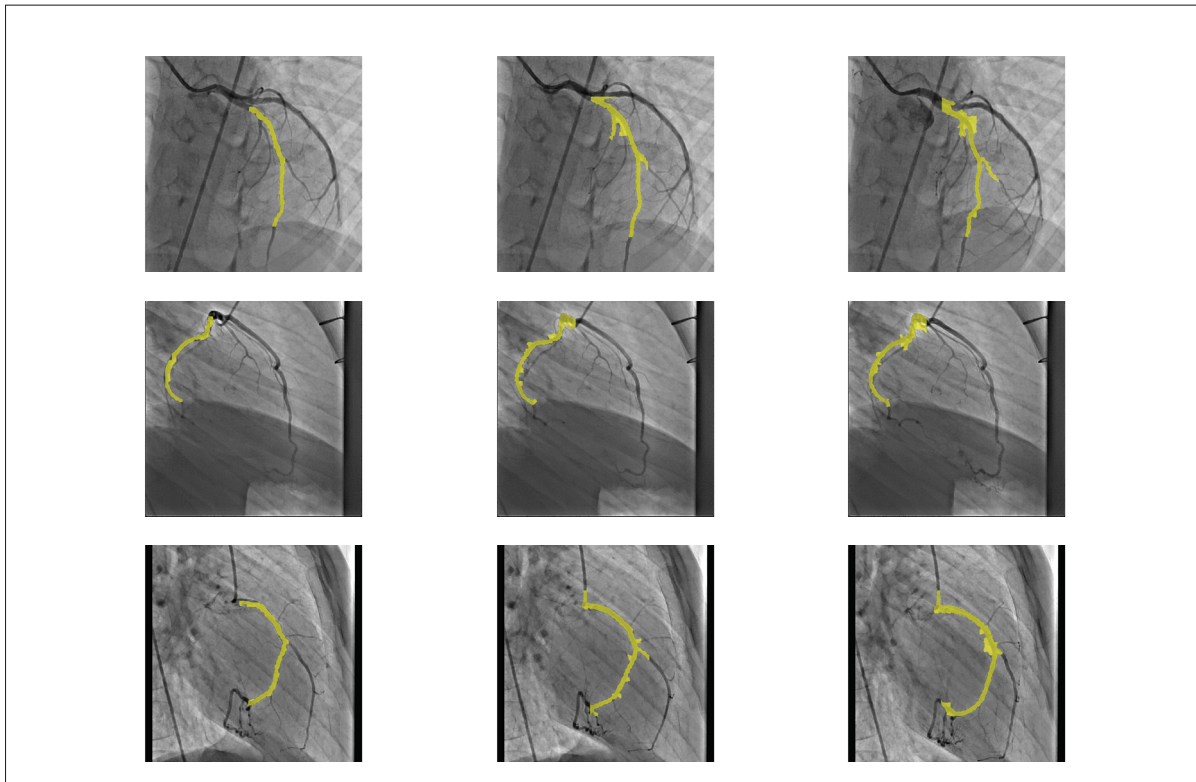
Figure 4.22   Segmentation mask overlaid in yellow on the original frames
of three sequences at different times. Top row: result on LAD artery.
Second row: result on a Cx artery. Third row: result on an RCA artery.

4.5   Discussion and conclusion

This work presents a spatio-temporal algorithm for simultaneous segmenting and tracking of a coronary artery in a 2D X-ray moving sequence based on the "Temporal Vessel Walker" (TVW) and superpixels. The model is defined as the combination of a temporal prior and intensity and topological features. The superpixels method regroup similar pixels, which leads to the accurate extraction of thinner and thicker parts of the same artery and fewer computations. Besides, combining different superpixel sizes leads to an optimal precision/recall trade-off and a better extraction of thinner and thicker parts of the same artery.

The chapter presented different iterations that were proposed to enhance the TVW result. Since tracking a vessel accurately while dealing with respiratory and cardiac motions is challenging. The best solution was to use the VWT with superpixel grouping at different superpixel sizes, making the tracking of a specific artery in the sequence accurate.

Experimental tests on a dataset for young patients show the efficiency and robustness of the proposed algorithm, while dealing with respiratory and cardiac motions. Moreover, the algorithm gives better performance than the polyline tracking method, which is a reference work on vessel tracking. Results of the proposed pipeline prove that it is possible to track and segment a vessel simultaneously without any pre-processing step to deal with the respiratory motion or cardiac motion alone. The ability to accurately track a specific artery (or part of an artery) may be crucial for measuring the properties of the vessel during the cardiac cycle as well as helping with the detection of pathologies.

Future Works

Future work includes the development of an adaptive formulation to automatically select the parameters of the proposed method depending on the contrast level in the X-ray sequence. Moreover, additional features are needed, such as the vessel's direction, to solve the challenge of overlapping vessels. Finally, more tests with longer sequences at different cardiac cycles will help to evaluate the repeatability of the proposed method.

CHAPTER 5

AUTOMATICALLY MEASURING VESSEL'S DISTENSIBILTY FROM 2D X-RAY SEQUENCES

5.1 Introduction

Early detection of blood vessel anomalies can improve the treatment of cardiovascular pathologies such as Kawasaki disease or arteriosclerotic vascular disease. Such pathologies affect the elasticity of coronary arteries (CAs) as mentioned by Vaujois *et al.* (2013). The elasticity of coronary arteries during the cardiac cycle is used to assess vascular function, for diagnosis and treatment. Distensibility measure is one of the most accurate indicator of elasticity and of any potential cardiovascular disease at an early stage (Cheung *et al.* (2002)). This measure computes the correlation between vessel's diameter changes in systole and diastole, with the variations in blood pressure. A healthy artery displays differences between its diameter during the cardiac cycle, resulting in a high distensibility measure.
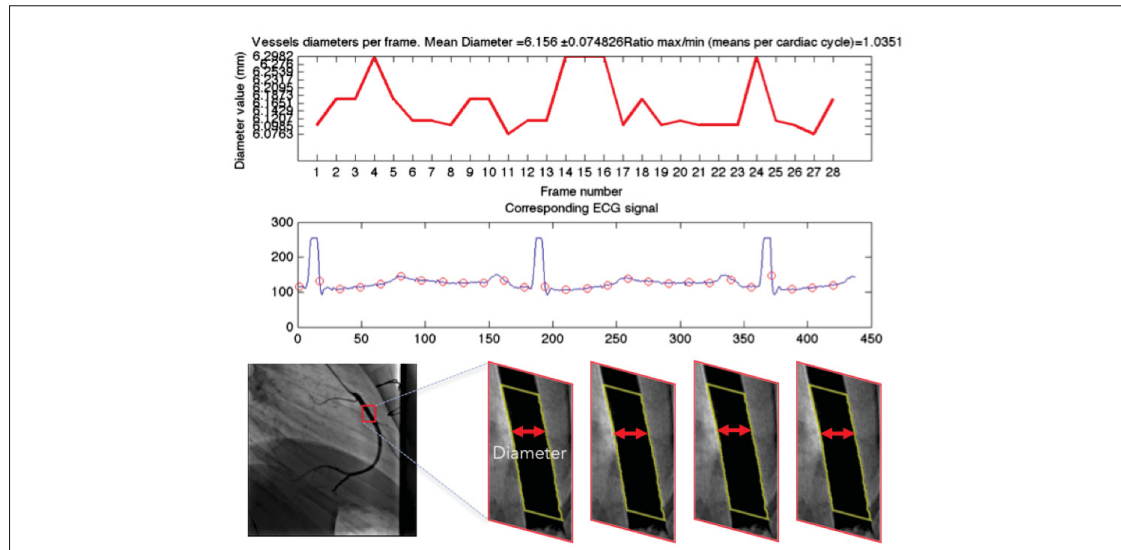
Figure 5.1   Segmenting and tracking part of vessel in a motion
sequence to measure its diameter and compute distensibility
measure

An accurate measurement of the blood vessel's diameter from 2D X-ray angiograms is critical to compute distensibility. An optimal solution to guide cardiologists is to: 1) Segment the section of the vessel of interest. 2) Track the same vessel's section in the moving sequence. 3) Compute its diameter at each frame. All these steps should be held automatically as illustrated in Figure 5.1.

Extracting, tracking and measuring the diameter of arteries from moving sequences is a challenging task. First, segmenting arteries can be dependent on the nature of the artery and the imaging modality. An exhaustive litterature review on the subject can be found Lesage *et al.* (2009). Different approaches have been proposed to address the challenge of segmenting blood vessels. They are either based on variational approaches such as the levelsets (Zhao *et al.* (2015a)) or graph-based methods such as graphcuts (Shahzad *et al.* (2013)) or random walks (Zhu and Chung (2013)). In this work, we used our Vessel Walker method, described in chapter 3, that extends the random walks method by Grady *et al.* (2006b) to segment blood vessels. Secondly, vessels like coronary arteries are subject to a combination of cardiac and respiratory motions, which are challenging to model as noticed by Shechter *et al.* (2004). Also, clinicians need to evaluate a specific part of the artery. Existing solutions, such as the work of Compas *et al.* (2014) track the entire coronary tree in the angiogram sequences. This is used to detect the presence of stenosis but not to evaluate the elasticity of a specific segment of an artery. In this chapter, we focus on tracking and evaluating a segment of the artery within a specific region of interest defined by a cardiologist. This can be challenging, since this segment is a dark tubular structure similar to all the arteries displayed in the sequence. Third, diameter changes in the cardiac cycle can be very small (less than 1mm for coronary arteries). Therefore, a precise measurement tool to capture small diameter changes is needed.
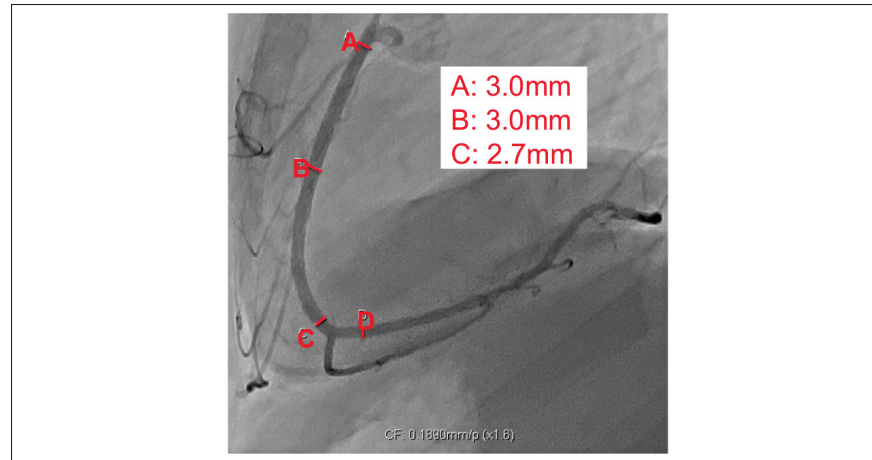
Figure 5.2   Manual measurements of coronary artery's diameter
at different parts of the vessel.

Computing distensibility usually involves manual diameter measurements at specific locations in one or two frames in the angiographic sequence, as displayed in Figure 5.2. However, such procedure can be time consuming and can lead to important interobserver and intraobserver variability as noticed by Tomasello *et al.* (2011). Other measurement techniques are proposed in the literature or in existing software (Gronenschild *et al.* (1994); PIEMedical; Medis) to semi automatically segment part of a vessel from a single frame. To the best of our knowledge, these methods do not include a temporal analysis of the diameter variation; neither do they track the vessel in the moving sequence. In addition, existing works that evaluate distensibility measure are applied on other imaging modalities, such as ultrasound images (Maurice *et al.* (2014)), CT images (Ahmadi *et al.* (2010)) or MRI (Kelle *et al.* (2011)). Studies on quantifying arterial structures based on 2D X-ray angiograms do not present fully automatic tracking of the diameter of a specific part of an artery in the cardiac sequence. Besides, some of these works usually use a 3D reconstructed model from biplane views to evaluate the vessel's width, as described in Girasis *et al.* (2013).

Few groups have studied the correlation between the assessment of CA distensibility from 2D angiography sequences and the detection of pathologies, using automatic centerline extraction and diameter estimation (Benovoy *et al.* (2016, 2015)). The present research is enrolled in

the line of these studies and explores the automatic computation of blood vessel's diameter variation from monplane 2D X-ray sequences.

The present research explores, the possibility of computing distensibility measures, of a specific segment of a coronary artery during the cardiac sequence, **automatically** and based on **monoplane 2D X-ray angiographic sequence**. This chapter evaluates the following hypothesis: *Distensibility measure can be computed directly from monoplane 2D X-ray angiograms* (Figure 5.1).

5.2 Proposed Method : Using VWT for vessel's diameter measurement in 2D X-ray sequences

Figure 5.3 describes the steps of the proposed method. First, a region of interest (ROI) surrounding a section of an artery is selected (first image in Fig.5.3). Then the artery within the ROI is segmented and tracked, using our proposed method described in the following section. Finally, the diameter of the extracted artery is computed at each frame, and is described in section in 5.2.2.

5.2.1 Temporal vessel walker method to track part of a vessel

Manually selected ROI   Segmentation and tracking in Time
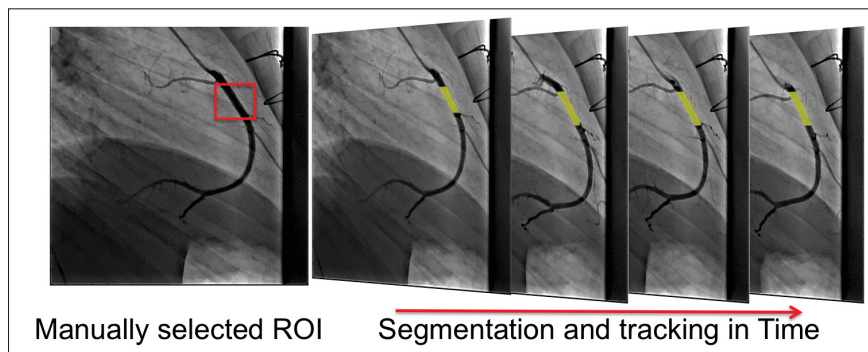
Figure 5.3   Segmentation and tracking of a section of a CA as defined by the manually selected ROI

The proposed algorithm uses the temporal vessel walker for segmenting and tracking a segment of a coronary artery in a moving X-ray sequence. To specify the segment of interest, the algorithm asks the clinician to specify a region of interest (ROI) surrounding the segment, in the first frame of the sequence (as shown in the first image in 5.3). The Vessel Walker method is applied to segment the vessel within the ROI. Then, for the rest of the sequence, the Temporal Vessel Walker (TVW) is applied to segment and track the vessel of interest. The results of these stages are illustrated in Figure 5.3. The TVW segmentation method is defined as the minimization problem. Having the segmentation result f^{t-1} from the previous frame at time $(t-1)$, the method computes the segmentation result f at the current frame at time t. The optimal solution f is a mapping $f : \mathscr{I} \rightarrow \{0,1\}$, where $f_i = 1$, if the pixel i belongs to the vessel, and $f_i = 0$, if i belongs to the background. The method is defined as the following energy equation:

$$
\begin{aligned}
E(f) \; = \; & \frac{1}{2}\sum_{i=1}^{|\mathscr{I}|}\sum_{j=1}^{|\mathscr{I}|} w_{ij}(f_i - f_j)^2 \; + \; \alpha\sum_{i=1}^{|\mathscr{I}|}(1-b_i)f_i^2 \\
& + \; \beta\sum_{i=1}^{|\mathscr{I}|} b_i(f_i-1)^2 \; + \mu\sum_{i=1}^{N}\sum_{j=1}^{N} w_{\tau ij}(f_j - f_i^{t-1})^2.
\end{aligned}
\tag{5.1}
$$

Where frame $\mathscr{I}$ is represented by a graph $G = \{N,E\}$, with a node set N representing all pixels in the image. Each pair of neighbour nodes is connected by an edge with a weight w_{ij} expressing the intensity similarity between the nodes (i.e. between pixels). The vesselness of pixel i is expressed with $b_i \in [0,1]$ and is computed using the method by Frangi $et\ al.$ (1998). Parameters $\alpha, \beta \geq 0$ are used to control the trade-off between minimizing the vesselness of background pixels and maximizing the vesselness of foreground pixels. Parameter μ controls the weight of temporal prior information in the final segmentation result. Since the temporal vessel walker model does not have a fixed term to validate that the extracted vessel-segment length is similar to the segment extracted in the first frame, a rigid registration step is added. Finally, for each segmented frame and to limit the background noise, a postprocessing step is applied to get only the biggest connected component as a segmentation result.

5.2.2   Measuring vessel's diameter

The diameter of the segmented vessel is computed at each frame. The proposed method starts by extracting the centerline of the vessel using the Hamilton-Jacobi Skeleton as defined by Bouix *et al.* (2005) and shown in the first image in Figure 5.4. The Hamilton-Jacobi method is well known for its accuracy in extracting skeletons (or centerlines) homotopic to the original objects. The method analyzes the normalized flux of the gradient vector field to detect the skeletal points. It has been proved to be computationally efficient and robust to boundary noise.
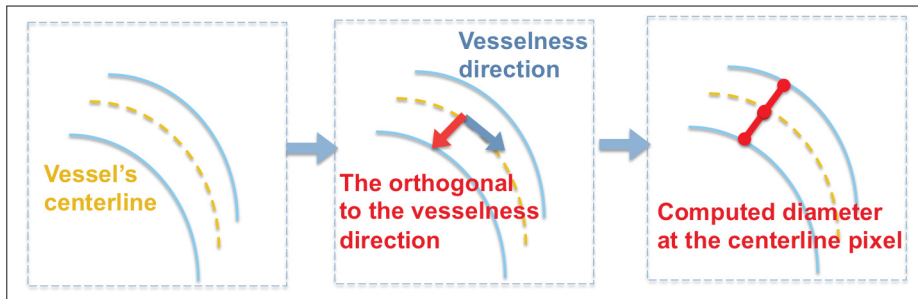
Figure 5.4   The different steps to compute vessel's diameter

To measure the diameter, the vesselness vector for each centerline point is computed using the method by Frangi *et al.* (1998). This vector indicates, at each point of the centerline, the direction of the vessel. Then, for each centerline point, the method looks for the boundary pixels on either side of the centerline, following the direction normal to the vesselness vector at that centerline point (as illustrated in the second image in Fig.5.4). The diameter of the vessel at each point is computed as the distance between each centerline point and its corresponding boundary pixel. The diameter of the vessel is computed as the sum of the distances between each centerline point and its corresponding boundary pixel from two sides of the centerline (Last image in Figure 5.4).

The method computes the diameter at each point of the vessel's centerline. Such information can be valuable for identifying deformation within the vessel such as stenosis (if the vessel di-

ameter decreases drastically). If the objective is to detect local deformations within the vessel, then each diameter at each centerline point would be evaluated independently. However, in the context of this work, we consider the mean diameter value of the segment of interest.

The proposed approach is a modification of the method presented in Compas *et al.* (2014) to compute vessel's stenosis.

5.3 Experimental results

5.3.1 Data acquisition

To evaluate the proposed method, three dataset have been selected :

a. **Simulated data:** One simulated X-ray sequence displaying the CA tree. The sequence was acquired with the XCAT phantom, developed by The Carl E. Ravin Advanced Imaging Laboratories (Segars and Tsui (2009)). The XCAT provides a realistic view of CAs in 2D X-ray angiography. The sequence displays in 69 frames, right and left coronary arteries moving under respiratory and cardiac motions. Ground truth segmentation mask of the artery is provided using the XCAT system, this is used to evaluate the segmentation accuracy of the proposed TVW method.

b. **Patient's data:** Seven 2D X-ray sequences of young patients were acquired from Sainte-Justine Hospital (Montreal, Canada). The data were saved and anonymized into the DICOM format, and were recorded after approval by the Sainte-Justine's Institutional Ethics Review Board. The angiograms were acquired by a C-arm Infinix-CFI BP by Toshiba and display coronary arteries and the ascending aorta:

   a. Four 2D X-ray sequences of young patients displaying coronary arteries. Groundtruth segmentation masks are not provided. However, two X-ray sequences have corresponding manual diameter measured by one clinical expert at one frame.

b. Three X-ray sequences displaying the ascending aorta of three young patients. To evaluate the diameter computations of the proposed method, the width of the ascending aorta was manually measured by an experienced user, at each frame. Knowing that the aorta can be much larger than a coronary artery, the degree of manual measurement error can be smaller. Therefore, these manual measurements are used to validate the diameter computations.

Our final results are compared to manual measurements and to the work of Mirzaalian and Hamarneh (2010). This work involves graph based method and Markov Random Field to assess blood vessel's scale. The following experiments evaluate the segmentation, the tracking and the width measurements of coronary arteries and the aorta on simulated and patient's X-ray sequences.

5.3.2   Results on simulated coronary arteries sequence

The proposed method is evaluated on the simulated X-ray sequence. The objective is to evaluate the accuracy of the method in segmenting, tracking and measuring a section of a right coronary artery. We used the Dice index to assess the overlap of our results with the groundtruth mask provided using the XCAT system. The mean performance of the method has a high Dice value of 0.98 with a precision result of 1 and recall of 0.96. Such results confirm the accuracy and robustness of the proposed method in segmenting and tracking a section of an artery in all the 96 frames of the sequence.

Figure 5.5 shows the results of tracking and segmenting a selected part of a right coronary artery (RCA) on the simulated XCAT sequence. Some parts of the vessel can be missed. However, the level of false positives in very low (limited pink regions in the images on the bottom row), which highlights the precision of the method. Overall, the method gives a good tradeoff between precision and recall leading to encouraging Dice value. Moreover, the method successfully tracks the artery despite its large motion.
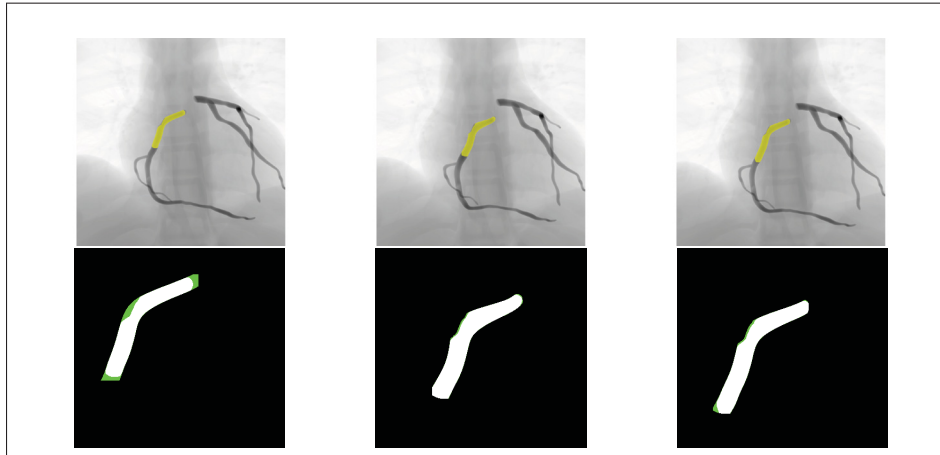
Figure 5.5 Top row : Segmented section (in yellow) of a right coronary artery overlaid on different frames in the synthetic sequence. Bottom row : our results and their overlap on the groundtruth mask. Green colored pixels show false negative; pink colored pixels show false positives and white colored pixels are for true positives (i.e. overlap).
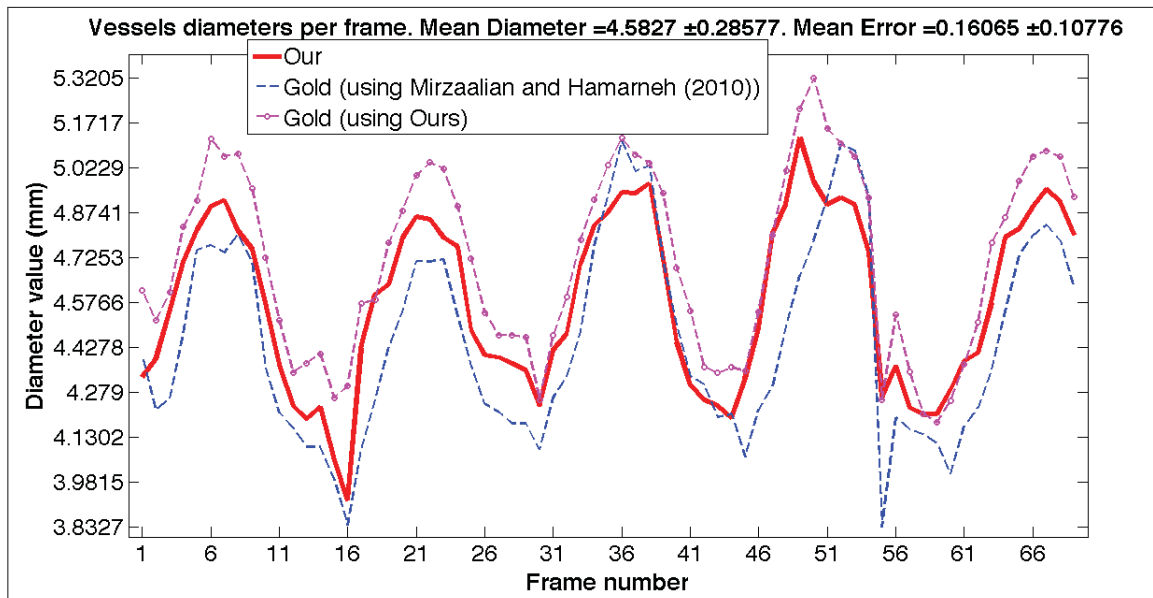
Figure 5.6 Diameter measurements of the targeted section of the vessel at each of the 96 frames of the simulated sequence. Red curve : TVW segmentation result with our proposed diameter measurements. Pink curve : Diameter measured using our diameter computation method on the groudtruth segmentation masks provided by the XCAT system. Blue curve : Diameter measured using Mirzaalian and Hamarneh (2010) method on the groudtruth segmentation masks.

Since the ground-truth results in terms of vessel's diameter in the sequence were not available, the vessel's width from the ground-truth masks were computed using our diameter approach and using the method proposed by Mirzaalian and Hamarneh (2010). We compared these measurements to our proposed TVW method. Figure 5.6 shows the different diameter measurements of the section of RCA in the simulated sequence. The three curves have a similar pattern with values of diameter close to each other. Our computed mean diameter is 4.58 ± 0.29mm. Comparing our results (red curve) with the ground truth measurements using Mirzaalian's method (blue dashed curve) gives a mean squared error is 0.16 ± 0.11mm. Comparing our results with the ground truth measurements using our measurement approach (pink dotted curve) brings a MSE $= 0.18 \pm 0.31$mm. Both errors are relatively low and our method succeed in measuring the diameter while capturing the small diameter changes.

Despite the differences of diameter measurements between the 3 curves, they all have the same pattern repeated 5 times. This pattern corresponds to 5 cardiac cycles simulated by the sequence. The three curves capture the same diameter changes in systole and diastole which confirms the hypothesis that it is possible to capture the small changes in an artery's diameter from 2D X-ray sequences. More tests should be made in order to assess the precision of our diameter measurements. The following section evaluates this precision.

5.3.3 Results using patients sequences

5.3.3.1 Results using aorta dataset

The proposed method was tested on three sequences displaying the aorta. The aorta is a large blood vessel, with large diameter variations in the cardiac cycle. Sequences showing the ascending aorta were selected and their corresponding diameter were manually computed. Unlike coronary arteries and since they have a larger diameter, the degree of manual measurement error can be smaller.

The sequences displaying the aorta have low contrast, compared to CAs sequences. Therefore, the intensity level is inhomogeneous in the aorta and the contrast with the image's background is low. To enhance the contrast level in the frame, the anisotropic filter introduced by Weickert (1998) and further developed by Kroon *et al.* (2010) is applied in order to enhance the homogeneity within the aorta, while limiting noise level. It has the quality of smoothing the image in the homogeneous regions, while preserving the edges of these regions. The anisotropic filter was then applied to the sequences of the ascending aorta to enhance the homogeneity within the aorta region, as displayed in Figure 5.7.

a) Original frame   b) Filtered frame
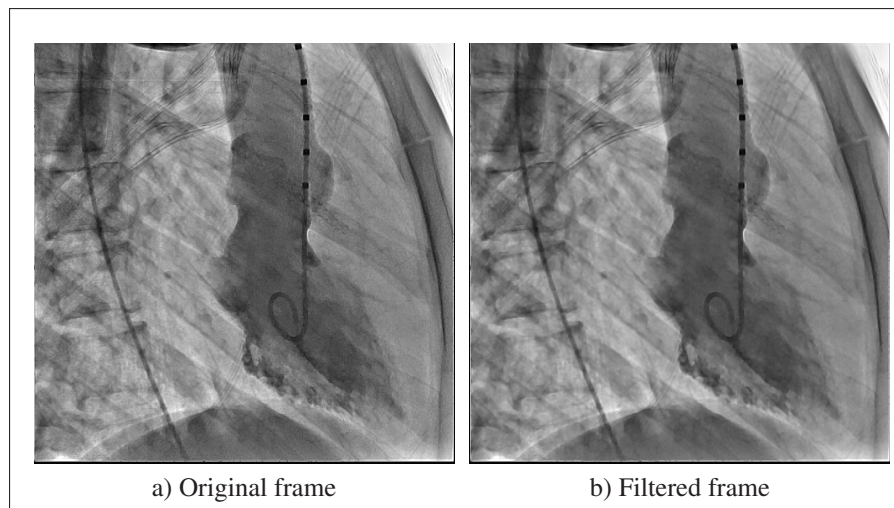
Figure 5.7   Original X-ray frame displaying the ascending aorta
(left) and the same X-ray after applying Weickert (1998) filter
(right)

Moreover, superpixel computation by Achanta *et al.* (2012) have been added as a pre-processing step to simplify the segmentation and tracking step. Superpixels method defines small groups of similar pixels. It is an oversegmenation method that ensures that similar pixels stay connected together, while respecting object's boundaries. Since the contrast in these images can be limited and the intensity level inside the aorta can be inhomogeneous, superpixels helps creating large groups of similar connected pixels. This makes the segmentation and tracking more accurate. Moreover, using superpixels simplifies the design of the graph G used in equation

(5.1) by considering each superpixel as one node of the graph (instead of considering each pixel as a node in the graph G). Additionally, the registration step is skipped because the motion of the aorta is not as large as CAs' motion.

Figure 5.8b displays the selected ROI in the second sequence of our dataset. Figure 5.8a shows the probabilities assigned by the Vessel Walker method to each pixel in the frame. We notice that the method highlights accurately the aorta (red colored regions showing high probabilities to belong to the aorta) from the background (blue colored regions showing low probabilities). Using this result, the segmentation mask is computed on the part of the aorta within the specified ROI. The result on the first frame is displayed in yellow on Fig. 5.8c. The segmentation and tracking results on the other frames (Fig. 5.8d and 5.8e) using TVW and superpixels show that the method succeeds in extracting and tracking the specified part of the ascending aorta.

a) Frame 1: VW result

b) ROI on Frame 1   c) Frame 1

d) Frame 8   e) Frame 16
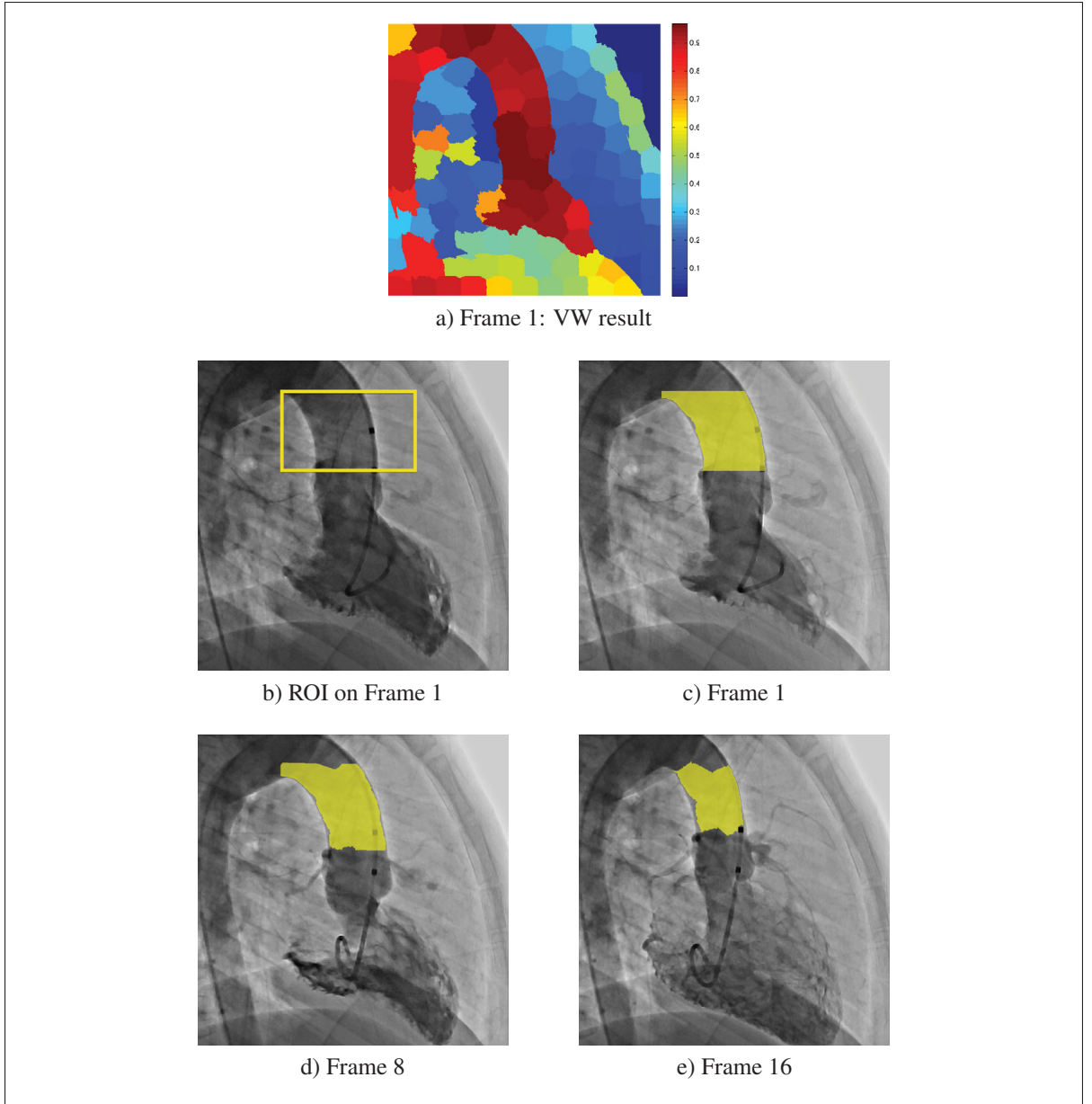
Figure 5.8   Results on the sequence 2 of our dataset. Top: The defined region of interest (ROI) in the first frame of the second sequence displaying the ascending aorta. Second row: Results of the VW method on the first frame, the method assigns a probability value to each pixel to belong to the foreground (left). Segmentation result of the VW within the ROI. Bottom: Segmentation results of the TVW at frame 8 and 16 of the sequence.

Figure 5.9 shows the mean diameter of the ascending aorta computed at each frame of the sequence. It displays the diameter variation curve using our approach (red curve) compared

to ground-truth manual measurements (blue dashed curve) and the diameter computed using the approach by Mirzaalian and Hamarneh (2010) (pink dotted curve). Our measurements are close to the ground truth. Indeed, the computed mean squared error is 0.7 ± 0.6 mm. The proposed diameter measurement performs better than the approach by Mirzaalian.
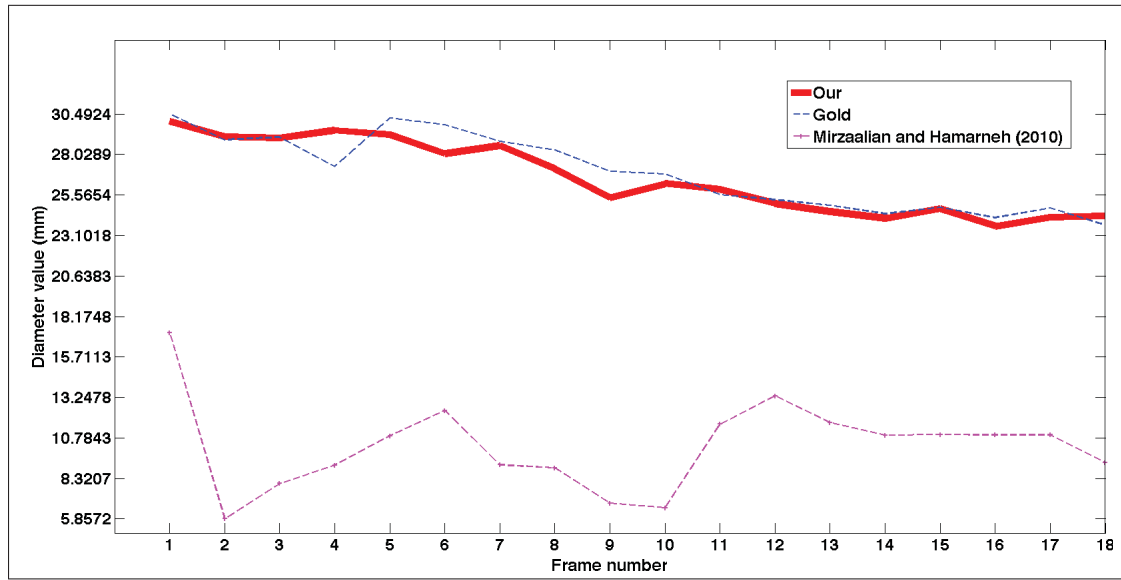
Figure 5.9   Diameter values of the second sequence displaying
the ascending aorta using the proposed approach and Mirzaalian
approach, compared to groundtruth values.

Table 5.1 shows the mean diameter result over each sequence of the aorta data set. The first and second columns of the table exhibit the diameter computed using our method and Mirzaalian's. Third and fourth columns show the corresponding mean squared error (MSE) between our measurements and the manual ground-truth and between Mirzaalian's result and the ground-truth. The results indicate that the proposed method returns better performance with a mean MSE= 1.5mm compared to Mirzaalian approach, which has a mean MSE= 18.1mm. This is explained by the fact that their method works accurately on thin vessels and is not adapted to compute the scale of large vessels like the aorta. Our method on the other hand can compute accurately the scales of both thin and large vessels.

Table 5.1   Mean diameter measurement (in mm) using the proposed method and Mirzaalian's method, with the corresponding mean squared error computed on each sequence of the aorta dataset

Seq.	Diameter (TVW)	Diameter using Mirzaalian's work	MSE (TVW)	MSE Mirzaalian's work
1	41.6± 2.6	12.3 ±2.7	2.1± 2.2	27.4± 1.6
2	26.6± 2.2	10.3 ±2.7	0.7 ± 0.6	16.7 ± 3.5
3	26.5± 2.0	14.7 ±2.6	1.7± 1.8	10.1± 2.9
Mean	31.6	12.4	1.5	18.1

5.3.3.2   Results using coronary arteries dataset
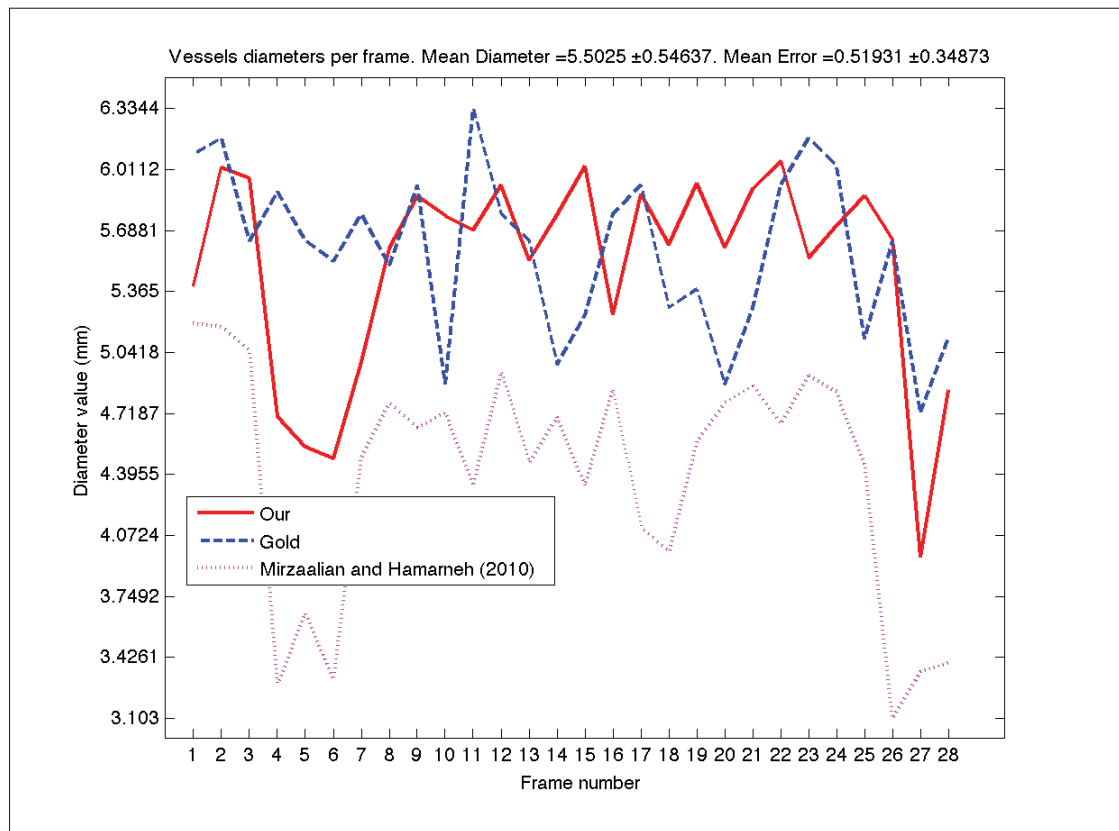
Figure 5.10   Diameter values per frame using the proposed approach and Mirzaalian approach compared to groundtruth values on sequence 1.

The proposed approach is tested on 4 angiographic sequences displaying coronary arteries. For the first sequence, the diameter was manually measured. It is true that these manual measurements may be not as precise as the ones on the aorta. However, it can be used as a general indicator of the performance of the proposed method.

Figure 5.10 shows the computed diameter values per each frame of sequence 1. The curves from the ground-truth (blue dashed curve) and the proposed method (red curve) are close to each other and have measurements in common (for example at frames : 9 and 26). This is further shown by an MSE of 0.52 ± 0.35mm. Moreover, the proposed diameter measurement method performs better than the method by Mirzaalian and Hamarneh (2010), where its curve is far below the ground truth results with MSE= 1.19 ± 0.67mm.

Manual measurement by a clinician was provided on one frame from sequences 2 and 4. Fig. 5.11a shows the manual measurements of the artery made by a clinician on sequence 4 of the dataset. The rest of the images in Fig. 5.11 show the manually specified region of interest in the first frame of sequence 4 of our dataset with the computed segmentation results overlaid in yellow on four different frames of the sequence. The segmentation results are encouraging since they track accurately the specified section of the vessel despite the presence of cardiac and respiratory motions. Moreover, the computed mean diameter using our method is 3.08 ± 0.2mm which is close to the diameter measured around region B in Image 5.11a with a measurement of 3mm, indicating again the accuracy of the proposed method.

a) Manual measurements of the RCA

b) frame 1 with ROI (white box)

c) frame 5

d) frame 15

e) frame 25

f) frame 50
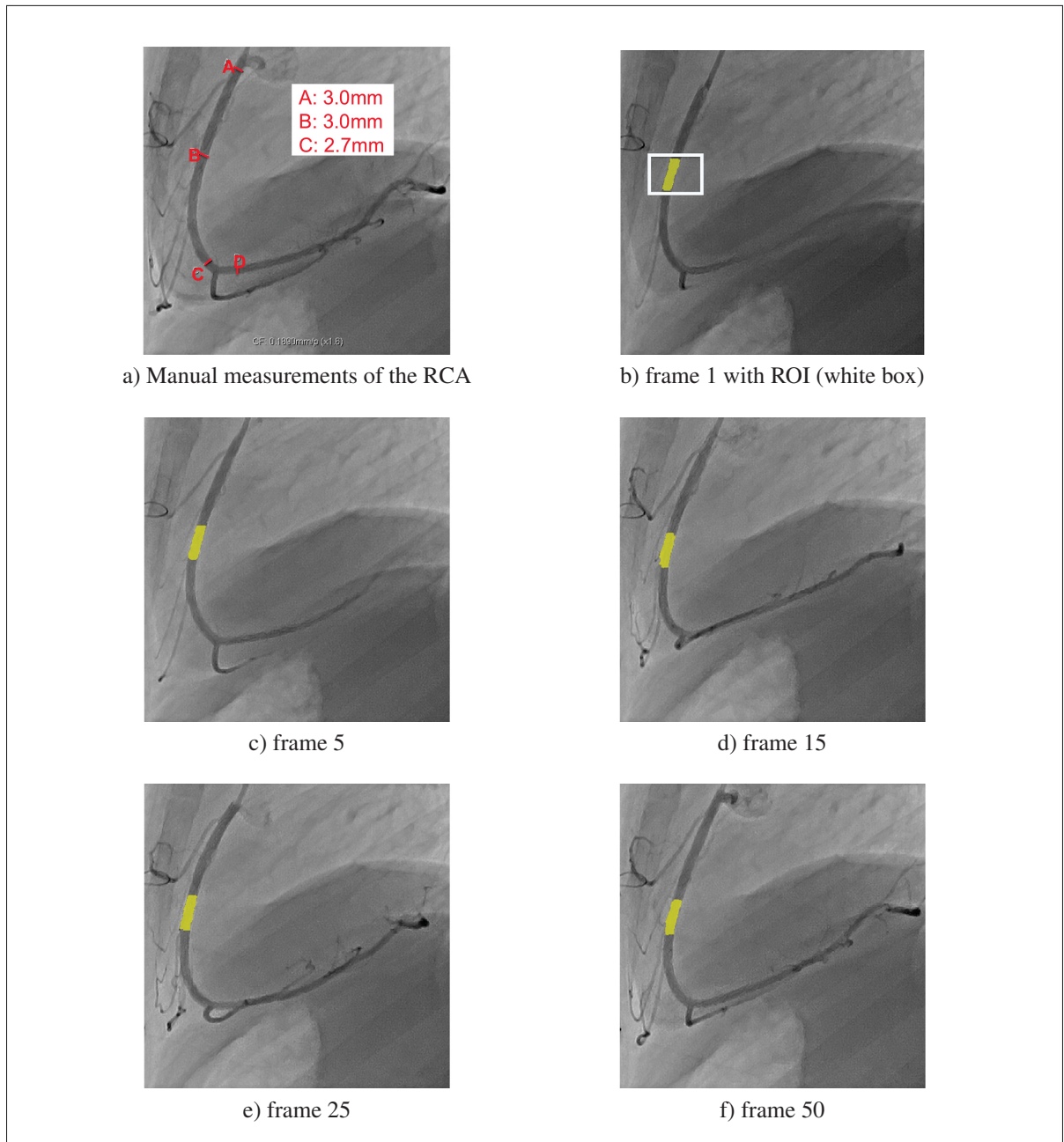
Figure 5.11   Segmentation results of the part of interest in the
right coronary artery at four different frames in sequence 4.
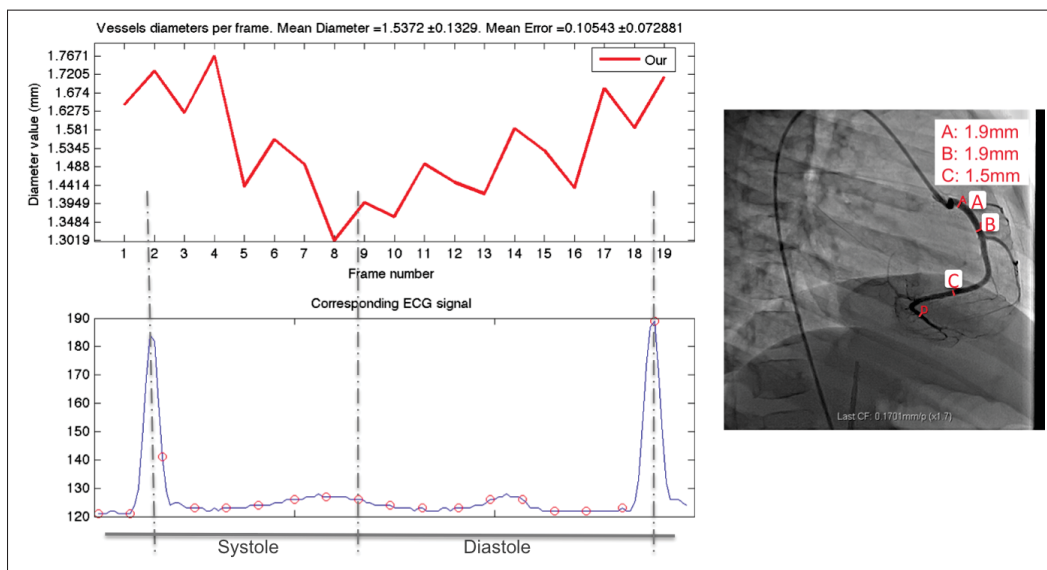
Figure 5.12   Left: Diameter values per frame using the proposed approach on sequence 2 of the coronary arteries dataset with the corresponding ECG signal (the blue curve with the red circles. The circles corresponds to the frame acquisition times). Right: Manually computed diameter by a medical expert from Sainte Justine's hospital.

Figure 5.12 shows, on the left, the computed diameter at each frame of the second sequence of the dataset with its corresponding electrocardiography (ECG) signal on the bottom. The diameter values decrease and then increase depending on the changes in the ECG signal. The diameter curve starts with a maximum value at the first three frames of the sequence and decreases after frame 4. The decrease of diameter happens at the first spike in the ECG signal (near the QRS complex), which corresponds to the systole phase of the cardiac cycle. At that time, the blood is ejected from the heart and therefore the blood flow is limited in the CAs. After the first peak, the diameter starts to increase again around frame 10 of the sequence. This corresponds in the ECG signal to the diastole, when the arteries are filled with blood. The diameter curve reaches a maximum again before the second spike in the ECG signal. This shows that the proposed automatic method can capture the diameter variation corresponding to the cardiac cycle. The image on the right in Fig. 5.13 shows that the diameter manually measured around segments A and B is 1.9mm which is close to our computed mean diameter value of 1.555 ± 0.13mm.

Figure 5.13 shows the segmented section of the vessel (overlaid in yellow) at four different frames of the sequence. We can notice the method brings encouraging results in segmenting and tracking accurately the part of the vessel as defined in the ROI in 5.13a. At frame 10 the method retrieve the wrong section of the artery. This is again caused by the abrupt change of vessel location from one frame to the next. This is corrected accordingly at frame 19 of the sequence. Overall, we can conclude the proposed method has encouraging result to segment, track and measure the diameter of the vessel. Results are precise enough to capture the vessel diameter changes in the cardiac cycle, which is the objective of the research.

In spite of that, more work has to be done on the method to accurately capture the section of the artery despite the large motion. This can be done by adapting the neighbourhood search of the temporal vessel walker method depending on the nature of the coronary artery. Indeed, the right and left coronary motions are different and more tests should be done on that aspect. Besides, the neighbourhood size should be adapted depending on the frame rate and the frame acquisition times in the cardiac cycle.

a) frame 1 with ROI (white box) b) frame 4

c) frame 10 d) frame 19
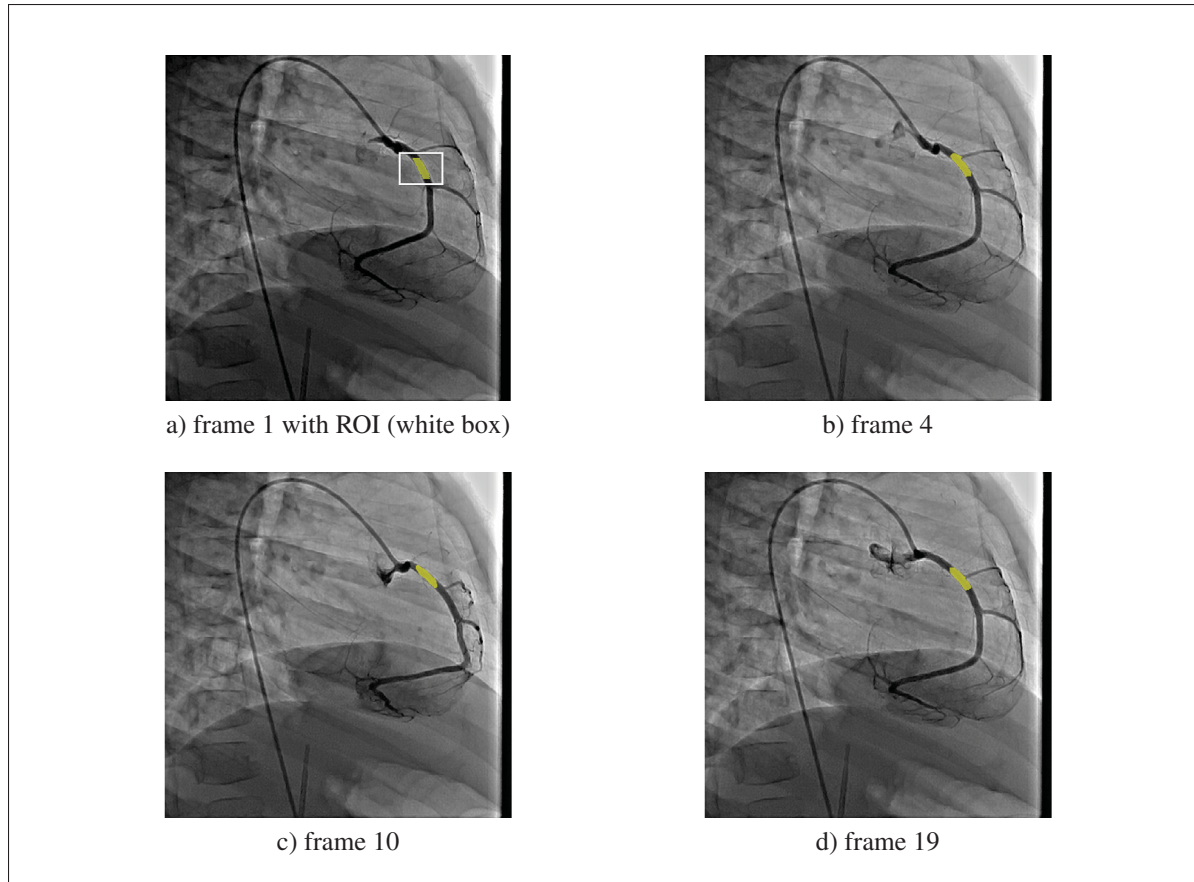
Figure 5.13   Segmentation result of the segment of interest at
four different frames in sequence 2

5.4   Discussion and conclusion

In this chapter, the temporal vessel walker (TVW) method was evaluated for segmenting and tracking a specific part of the coronary artery in 2D X-ray sequences. The result is used to capture the diameter changes in the artery according to heart contraction and relaxation. We proposed an efficient method to measure the diameter at different frames of the sequence. This proves to be more efficient than the existing method of Mirzaalian and Hamarneh (2010). The temporal vessel walker with a post-processing step showed encouraging result in segmenting and tracking not the whole artery but a section of an artery, which is a more challenging task. Experimental results showed that the proposed TVW with the diameter measurement method

brings encouraging performance and the results are close to the manually computed diameters with a low mean squared error. Moreover, the diameter changes seem to coincide with the changes in the cardiac cycle at systole and diastole, which is a crucial information to compute distensibility measure and evaluate vessel's elasticity. The tests were applied on simulated and real sequences of coronary arteries together with sequences displaying the ascending aorta. Experimental results illustrate the good performance of the method in tracking the right section of the artery and in measuring the diameter variations accurately. Finally, in this chapter we showed that an automatic method can be efficient to segment, track and measure coronary artery thickness from monoplane 2D X-ray sequences. This is a crucial information that can help clinicians in their work and eventually prevent some anomalies that can occur in the coronary arteries.

Future Works

Additional works have to be made in order to make the temporal vessel walker more robust to the location change of the coronary artery in the moving sequence. Moreover, a length term and a curvature term should be added to the model to guarantee that the method is tracking the same segment of the vessel in the sequence. Finally, other diameter measurements approaches should be considered to enhance the precision of the computations.

CONCLUSION

The presented research explores new methods to guide cardiologists in their task of treating congenital heart disease (CHD). CHD can lead to pathologies in the coronary arteries. To treat these coronary arteries, percutaneous catheter-based interventions (PCI) are used. To guide cardiologists while navigating through the arterial system, PCI is based on real-time 2D X-ray angiograms. These angiograms can be used not only for navigation guidance but also for diagnosing coronary arteries deformations. One of the measures used to detect CHD is arterial distensibility. Distensibility evaluates the ability of the coronary artery to expand and contract with cardiac contraction (systole) and relaxation (diastole). More precisely, the measure studies the artery's diameter changes in the cardiac cycle. Assessing the diameter of coronary arteries is usually done either manually by a technician after PCI or using other imaging modalities such as ultrasound images. The main question raised in this research is : Can we evaluate the changes of coronary artery's diameter, directly from monoplane 2D X-ray moving sequences?

To address this question, our research presented three main contributions. First, it introduced a new segmentation method combining the random walks method and topological features to segment coronary arteries in 2D X-ray images. Second, a spatio-temporal segmentation approach is proposed to segment and track the coronary artery in 2D X-ray moving sequence. These two contributions have led to the final work on evaluating the arteries' diameter changes within the cardiac cycle, automatically from monoplane 2D X-ray sequences. More precisely, our work evaluated three hypotheses.

Hypothesis 1 : *An automatic method to extract coronary arteries from 2D angiograms can be as accurate as an expert's manual segmentation.*

The objective is to propose an automatic segmentation approach for coronary arteries from 2D X-ray images. We introduced a new method that includes vesselness features with random walks formulation. The resulting method is called Vessel Walker (VW). It was compared to the random walks formulation and other existing methods have shown better quantitative and qualitative results in segmenting coronary arteries in 2D X-ray images, with a mean Dice value

of 70%. Despite the lack of contrast and the presence of noise, the method proved to bring accurate results, close to a manual segmentation.

Hypothesis 2 : *Using temporal information in 2D X-ray moving sequence helps segmenting and tracking a specific coronary artery.*

At this stage, we designed a framework for segmenting and tracking one coronary artery in the 2D X-ray moving sequence. To do so, a new formulated approach adds to the Vessel Walker equation a temporal prior. This prior describes the segmentation result of the coronary artery acquired from one frame of the sequence to guide the segmentation in the following frame. The new approach, defined as the Temporal Vessel Walker, also used superpixel grouping which makes the approach more robust while dealing with the respiratory and cardiac motions. We argue that the proposed framework can track and segment a vessel simultaneously without any pre-processing step to deal with the respiratory motion or cardiac motion alone. The method has more accurate quantitative results than existing methods, in tracking the centerline and in segmenting the lumen of the artery.

Hypothesis 3 : *Distensibility measure can be computed directly from monoplane 2D X-ray angiograms.*

Our objective is to automatically compute vessel's diameter from 2D X-ray angiogram sequences as accurately as expert measurements. We used both the Vessel Walker and Temporal Vessel Walker to segment and track a specific coronary artery in the X-ray sequence. Experimental results proved that the method has accurate performance in segmenting, tracking and measuring the vessel's diameter. The method was evaluated on simulated X-ray angiograms and patient's angiograms displaying the aorta and coronary arteries. Our results were compared to manual measurements and showed that diameter computations were close to manual ground truth. The results confirmed the hypothesis that it is possible to capture the small changes during the cardiac cycle in an artery's diameter from monoplane 2D X-ray sequences. Such results can be used to compute distensibility index. This is a crucial information that can help

clinicians in their work and eventually prevent some anomalies that can occur in the coronary arteries.

The main objective of this thesis is segmenting and tracking coronary arteries from 2D X-ray images to compute biophysical measurements. We focus on coronary arteries but we assume that the proposed methods can be applied on any vascular structure, such as pulmonary arteries.

We believe that all the research objectives were achieved. Each objective was validated through several experiments. However there is abundant room for further progress in some parts of the proposed work. First, to further evaluate the efficiency of these methods, tests on larger dataset should be made. Such dataset should include coronary arteries displaying local deformation such as stenosis or aneurysms. This will help evaluate the efficiency of the methods in detecting such cases. Moreover, adding other features besides intensity and vesselness information can enhance the performance of the proposed segmentation method. Besides, Vessel Walker and Temporal Vessel Walker rely on different parameters to process images. We notice that these parameters could be different depending on the nature of the dataset and the quality of the X-rays. Future work will consider defining an automatic approach to tune these parameters depending on the contrast level in the image. Furthermore, our work focus on 2D X-ray sequences. We assume that the proposed methods can be applied on other 2D or 3D moving sequences such as ultrasounds or MRI. Additional tests should be considered to validate this hypothesis.

To conclude, we believe that having an automatic pipeline to evaluate the elasticity of coronary arteries may lead to early detection of cardiac pathologies in newborns. Additional tests are needed to validate this assumption. Moreover, the research in congenital heart defects still has various questions that remain unanswered according to the Canadian Congenital Heart Alliance (2010). To address these questions, research engineers and computer scientists need to collaborate with cardiologists. Such collaboration would lead to bring new technologies and to improve protocols in cardiac interventions, making a better life for children.

APPENDIX I

PUBLICATIONS

Journal Article

Mhiri, F.; Duong, L.; Desrosiers, C.; Leye, M.; Miró, J. and Cheriet, M. *A graph-based approach for spatio temporal segmentation of coronary arteries in X-ray angiographic sequences* (under review for Elsevier's international journal "Computers in Biology and Medicine")

M'hiri, F.; Duong, L.; Desrosiers, C.; Dahdah, N.; Miró, J. and Cheriet, M. *Automatic method to extract and measure blood vessels diameter variation from 2D X-ray angiography in healthy children and young adult* (ready for submission)

Conference Proceedings

M'hiri, F.; Hoang, N.; Duong, L. and Cheriet, M. *A new adaptive framework for tubular structures segmentation in X-ray angiography.* Information Science, Signal Processing and their Applications (ISSPA), 2012 11th International Conference on, 2012, 496-500

M'hiri, F.; Duong, L. and Desrosiers, C. *Combining Laplacian eigenmaps and vesselness filters for vessel segmentation in X-ray angiography.* Computer Vision and Pattern Recognition Workshops (CVPRW), 2012 IEEE Computer Society Conference on, 2012, 70-75

M'hiri, F.; Duong, L.; Desrosiers, C. and Cheriet, M. *Vessel Walker: Coronary arteries segmentation using random walks and hessian-based vesselness filter.* Biomedical Imaging (ISBI), 2013 IEEE 10th International Symposium on, 2013, 918-921

M'hiri, F.; Hoang, N.; Duong, L. and Cheriet, M. *Hierarchical Segmentation and Tracking of Coronary Arteries in 2d X-ray Angiography Sequences.* International Conference on Image Processing (ICIP), 2015

BIBLIOGRAPHY

Achanta, R., A. Shaji, K. Smith, A. Lucchi, P. Fua, and S. Susstrunk. 2012. "SLIC super-pixels compared to state-of-the-art superpixel methods". *Pattern Analysis and Machine Intelligence, IEEE Transactions on*, vol. 34, n° 11, p. 2274–2282.

Ahmadi, N., D. Shavelle, V. Nabavi, F. Hajsadeghi, S. Moshrefi, F. Flores, S. Azmoon, S. S. Mao, R. Ebrahimi, and M. Budoff. clincal, measurement, CT 2010. "Coronary distensibility index measured by computed tomography is associated with the severity of coronary artery disease". *Journal of cardiovascular computed tomography*, vol. 4, n° 2, p. 119–126.

Anderson, R. 2007. "The surgical anatomy of the aortic root". *Multimedia Manual of Cardio-thoracic Surgery*, vol. 2007, n° 0219, p. 2527.

Andrews, S., G. Hamarneh, and A. Saad. 2010. Fast random walker with priors using precomputation for interactive medical image segmentation. *Medical Image Computing and Computer-Assisted Intervention–MICCAI 2010*, p. 9–16. Springer.

Arici, T., S. Dikbas, and Y. Altunbasak. 2009. "A histogram modification framework and its application for image contrast enhancement". *Trans. Img. Proc.*, vol. 18, n° 9, p. 1921–1935.

Ashley, E. A. and J. Niebauer, 2004. *Cardiology Explained*. Remedica Explained Series.

Auvray, V., P. Bouthemy, and J. Liénard. 2009. "Jointmotion estimation and layer segmentation in transparent image sequenc: application to noise reduction in X-ray image sequences". *EURASIP Journal on Advances in Signal Processing*, vol. 2009, p. 19.

Bauer, C. and H. Bischof. 2008. A novel approach for detection of tubular objects and its application to medical image analysis. Rigoll, G., editor, *Pattern Recognition*, volume 5096 of *Lecture Notes in Computer Science*, p. 163-172. Springer Berlin / Heidelberg.

Belkin, M. and P. Niyogi. 2003. "Laplacian eigenmaps for dimensionality reduction and data representation". *Neural computation*, vol. 15, n° 6, p. 1373–1396.

Bellemare, C. and J. Meunier. 2004. "Structural method for tracking coronary arteries in coronary cineangiograms". In *Computer and Robot Vision, 2004. Proceedings. First Canadian Conference on*. p. 378–384. IEEE.

Ben, S., A. Mitiche, and A. Ben. 2010. "Multiregion Image Segmentation by Parametric Kernel Graph Cuts.". *IEEE transactions on image processing: a publication of the IEEE Signal Processing Society*.

Benmansour, F. and L. Cohen. 2011. "Tubular Structure Segmentation Based on Minimal Path Method and Anisotropic Enhancement". *Int. J. Comput. Vision*, vol. 92, n° 2, p. 192–210.

Benovoy, M., F. Cheriet, R. L. Maurice, and N. Dahdah. 2015. "Automated Angiographic Assessment Of Coronary Artery Vasomotion In Kawasaki Disease Patients". *Circulation*, vol. 131, n° Suppl 2, p. A153–A153.

Benovoy, M., A. Dionne, F. Cheriet, R. L. Maurice, and N. Dahdah. 2016. "Correlation between automatic angio-based coronary artery stiffness assessment and visual OCT pathology scoring". *Journal of the American College of Cardiology*, vol. 67, n° 13_S, p. 1672–1672.

Bezold, L. I. Jan 2010. Coronary artery anomalies. University of Kentucky College of Medicine. <http://emedicine.medscape.com/article/895854-overview>.

BLOCH, I. 2000. Reconstruction d'images de tomographie. Enst Paris. <http://perso. telecom-paristech.fr/~bloch/ATIM/>.

Bouix, S., K. Siddiqi, and A. Tannenbaum. 2005. "Flux driven automatic centerline extraction". *Medical Image Analysis*, vol. 9, n° 3, p. 209–221.

Boykov, Y. and G. Funka-Lea. 2006. "Graph cuts and efficient nd image segmentation". *International Journal of Computer Vision*, vol. 70, n° 2, p. 109–131.

Boykov, Y. and V. Kolmogorov. sept. 2004. "An experimental comparison of min-cut/max-flow algorithms for energy minimization in vision". *Pattern Analysis and Machine Intelligence, IEEE Transactions on*, vol. 26, n° 9, p. 1124 -1137.

Boykov, Y. and O. Veksler. 2006. "Graph cuts in vision and graphics: Theories and applications". *The Handbook of Mathematical Models in Computer Vision. Springer*.

Brenner, D. J. and E. J. Hall. 2007. "Computed Tomography : An Increasing Source of Radiation Exposure". *New England Journal of Medicine*, vol. 357, n° 22, p. 2277–2284.

BruceBlaus. October 2013. "Illustration of coronary arteries".

BruceBlaus. February 2016. "Balloon-Tipped Catheter". <https://commons.wikimedia.org/ wiki/File:Balloon-Tipped_Catheter.png>.

Bui, T. D. and G. Chen. 1999. "Invariant Fourier-Wavelet Descriptor For Pattern Recognition". *Pattern Recognition*, vol. 32, p. 1083–1088.

Bunyak, F. and K. Palaniappan. 2009. "Efficient segmentation using feature-based graph partitioning active contours". In *Computer Vision, 2009 IEEE 12th International Conference on*. p. 873–880. IEEE.

Canadian Congenital Heart Alliance. 2010. "About Congenital Heart Defects CHD Facts and Issues". Online. <http://www.cchaforlife.org/facts-issues>.

Canny, J. 1986. "A computational approach to edge detection". *Pattern Analysis and Machine Intelligence, IEEE Transactions on*, , p. 679–698.

Cao, S., A. Bharath, K. Parker, J. Ng, J. Arnold, A. McGregor, and A. Hill. 2011. "Joint spatio-temporal registration and microvasculature segmentation of retinal angiogram sequences". In *Engineering in Medicine and Biology Society, EMBC, 2011 Annual International Conference of the IEEE*. p. 2618–2621. IEEE.

Cao, S., A. Bharath, K. Parker, J. Ng, J. Arnold, A. McGregor, and A. Hill. 2012. "Microvasculature segmentation of co-registered retinal angiogram sequences". *Annals of British Machine Vision Association, vol*.

Cesarelli, M., P. Bifulco, T. Cerciello, M. Romano, and L. Paura. 2013. "X-ray fluoroscopy noise modeling for filter design". *International journal of computer assisted radiology and surgery*, vol. 8, n° 2, p. 269–278.

Chan, T. and L. Vese. 2001. "Active contours without edges". *Image Processing, IEEE Transactions on*, vol. 10, n° 2, p. 266–277.

Chen, X., J. Graham, C. Hutchinson, and L. Muir. 2011. "Inferring 3D kinematics of carpal bones from single view fluoroscopic sequences". *Medical Image Computing and Computer-Assisted Intervention–MICCAI 2011*, p. 680–687.

Cheng, H. and Y. Sun. 2000. "A hierarchical approach to color image segmentation using homogeneity". *Image Processing, IEEE Transactions on*, vol. 9, n° 12, p. 2071–2082.

Cheung, Y., P. Brogan, C. Pilla, M. Dillon, and A. Redington. 2002. "Arterial distensibility in children and teenagers: normal evolution and the effect of childhood vasculitis". *Archives of disease in childhood*, vol. 87, n° 4, p. 348–351.

Cigla, C. and A. A. Alatan. 2010. "Efficient graph-based image segmentation via speeded-up turbo pixels". In *Image Processing (ICIP), 2010 17th IEEE International Conference on*. p. 3013 -3016.

Çiğla, C. and A. A. Alatan. 2010. "Efficient graph-based image segmentation via speeded-up turbo pixels". In *Image Processing (ICIP), 2010 17th IEEE International Conference on*. p. 3013–3016. IEEE.

Compas, C., T. Syeda-Mahmood, P. McNeillie, and D. Beymer. April 2014. "Automatic detection of coronary stenosis in X-ray angiography through spatio-temporal tracking". In *Biomedical Imaging (ISBI), 2014 IEEE 11th International Symposium on*. p. 1299-1302.

Couet, J., D. Rivest-Henault, J. Miro, C. Lapierre, L. Duong, and M. Cheriet. 2012. "Intensity-based 3D/2D registration for percutaneous intervention of major aorto-pulmonary collateral arteries". In *SPIE Medical Imaging*. p. 831629–831629. International Society for Optics and Photonics.

Cousty, J., L. Najman, M. Couprie, S. Clément-Guinaudeau, T. Goissen, and J. Garot. 2010. "Segmentation of 4D cardiac MRI: Automated method based on spatio-temporal watershed cuts". *Image and Vision Computing*, vol. 28, n° 8, p. 1229–1243.

120

Cremers, D. 2015. "Image Segmentation with Shape Priors: Explicit versus Implicit Representations". *Handbook of Mathematical Methods in Imaging*, p. 1909–1944.

Dalal, N. and B. Triggs. 2005. "Histograms of oriented gradients for human detection". In *Computer Vision and Pattern Recognition, 2005. CVPR 2005. IEEE Computer Society Conference on*. p. 886–893. IEEE.

david stutz. 2014. "superpixel algorithms overview comparison". <http://davidstutz.de/superpixel-algorithms-overview-comparison/>.

Desrosiers, C. 2015. "Unsupervised segmentation using dynamic superpixel random walks". In *International Conference on Image Processing (ICIP)*.

Dijkstra, E. W. 1959. "A note on two problems in connexion with graphs". *Numerische Mathematik*, vol. 1, n° 1, p. 269–271.

Ding, S., M. I. Miga, T. S. Pheiffer, A. L. Simpson, R. C. Thompson, and B. M. Dawant. 2011. "Tracking of vessels in intra-operative microscope video sequences for cortical displacement estimation". *Biomedical Engineering, IEEE Transactions on*, vol. 58, n° 7, p. 1985–1993.

Drake, R., W. Vogl, and A. Mitchell, 2009. *Dorland's/gray's pocket atlas of anatomy*.

Duan, Y., X. Wang, Z. Cheng, D. Wu, and L. Wu. 2012. "Application of prospective ECG-triggered dual-source CT coronary angiography for infants and children with coronary artery aneurysms due to Kawasaki disease". *British Journal of Radiology*, vol. 85, n° 1020, p. e1190–e1197.

Dubuisson-Jolly, M.-P., C.-C. Liang, and A. Gupta. 1998. "Optimal polyline tracking for artery motion compensation in coronary angiography". In *ICCV*. p. 414–419. IEEE.

Duncan, J. S., S. Member, and N. Ayache. 2000. "Medical image analysis: progress over two decades and the challenges ahead". *IEEE Transactions on Pattern Analysis and Machine Intelligence*, vol. 22, p. 85–106.

Duong, L. 2007. "Detection et classification automatique de la colonne vertebrale a partir d'images a rayons-X". PhD thesis, Ecole Polytechnique, Montreal (Canada).

El-Zehiry, N. Y. and L. Grady. 2016. "Contrast Driven Elastica for Image Segmentation". *IEEE Transactions on Image Processing*, vol. 25, n° 6, p. 2508–2518.

Fallavollita, P. and F. Cheriet. 2008. "Optimal 3D reconstruction of coronary arteries for 3D clinical assessment". *Computerized Medical Imaging and Graphics*, vol. 32, n° 6, p. 476 - 487.

Fischer, B. and J. Modersitzki. 2008. "Ill-posed medicine—an introduction to image registration". *Inverse Problems*, vol. 24, p. 034008.

Fleming, R. M., R. L. Kirkeeide, R. W. Smalling, K. Gould, and Y. Stuart. 1991. "Patterns in visual interpretation of coronary arteriograms as detected by quantitative coronary arteriography". *Journal of the American College of Cardiology*, vol. 18, n° 4, p. 945-951.

Ford, L. and D. Fulkerson. 1956. "Maximal flow through a network". *Canadian Journal of Mathematics*, vol. 8, n° 3, p. 399–404.

Franchi, D., P. Gallo, L. Marsili, and G. Placidi. 2009. "A shape-based segmentation algorithm for X-ray digital subtraction angiography images". *Computer Methods and Programs in Biomedicine*, vol. 94, n° 3, p. 267 - 278.

Frangi, A., W. Niessen, K. Vincken, and M. Viergever. 1998. "Multiscale vessel enhancement filtering". *Medical Image Computing and Computer-Assisted Intervention MICCAI98*, p. 130.

Freiman, M., N. Broide, M. Natanzon, E. Nammer, O. Shilon, L. Weizman, L. Joskowicz, and J. Sosna. 2009. Vessels-cut: A graph based approach to patient-specific carotid arteries modeling. Magnenat-Thalmann, N., editor, *Modelling the Physiological Human*, volume 5903 of *Lecture Notes in Computer Science*, p. 1-12. Springer Berlin / Heidelberg. ISBN 978-3-642-10468-8.

Freiman, M., L. Joskowicz, N. Broide, M. Natanzon, E. Nammer, O. Shilon, L. Weizman, and J. Sosna. 2012. "Carotid vasculature modeling from patient CT angiography studies for interventional procedures simulation". *International journal of computer assisted radiology and surgery*, vol. 7, n° 5, p. 799–812.

Friman, O., C. Kühnel, and H.-O. Peitgen. 2008. "Coronary centerline extraction using multiple hypothesis tracking and minimal paths". In *Proc MICCAI*.

Funka-Lea, G., Y. Boykov, C. Florin, M. Jolly, R. Moreau-Gobard, R. Ramaraj, and D. Rinck. 2006. "Automatic heart isolation for CT coronary visualization using graph-cuts". In *Biomedical Imaging: Nano to Macro, 2006. 3rd IEEE International Symposium on*. p. 614–617. IEEE.

Gao, Y. and H. Sundar. 2012. "Coronary arteries motion modeling on 2D x-ray images". In *SPIE Medical Imaging*. p. 83161A–83161A. International Society for Optics and Photonics.

Garg, S., L. Tang, A. Traboulsee, and R. Tam. 2015. "A Sensitive And Efficient Method For Measuring Change In Cortical Thickness Using Fuzzy Correspondence In Alzheimer's Disease". In *International Conference on Image Processing (ICIP)*.

Garreau, M., J. Coatrieux, R. Collorec, and C. Chardenon. 1991. "A knowledge-based approach for 3-D reconstruction and labeling of vascular networks from biplane angiographic projections". *Medical Imaging, IEEE Transactions on*, vol. 10, n° 2, p. 122–131.

Geman, S. and D. Geman. 1984. "Stochastic relaxation, Gibbs distributions, and the Bayesian restoration of images". *Pattern Analysis and Machine Intelligence, IEEE Transactions on*, , p. 721–741.

Girasis, C., J. Schuurbiers, T. Muramatsu, J.-P. Aben, Y. Onuma, S. Soekhradj, M. Morel, R.-J. van Geuns, J. J. Wentzel, and P. W. Serruys. 2013. "Advanced three-dimensional quantitative coronary angiographic assessment of bifurcation lesions: methodology and phantom validation". *EuroIntervention*, vol. 8, n° 12, p. 1451–1460.

Godia, E. C., R. Madhok, J. Pittman, S. Trocio, R. Ramas, D. Cabral, R. L. Sacco, and T. Rundek. 2007. "Carotid artery distensibility a reliability study". *Journal of Ultrasound in Medicine*, vol. 26, n° 9, p. 1157–1165.

Grady, L. June 2005. "Multilabel random walker image segmentation using prior models". In *CVPR 2005*. p. 763-770 vol. 1.

Grady, L. 2006. "Random walks for image segmentation". *Pattern Analysis and Machine Intelligence, IEEE Transactions on*, vol. 28, n° 11, p. 1768–1783.

Grady, L., V. Sun, and J. Williams. 2006a. Interactive graph-based segmentation methods in cardiovascular imaging. *Handbook of Mathematical Models in Computer Vision*, p. 453–469. Springer.

Grady, L., Y. Sun, and J. Williams. 2006b. "Three interactive graph-based segmentation methods applied to cardiovascular imaging". *Handbook of Mathematical Models in Computer Vision*, p. 453–469.

Grady, L. and C. V. Alvino. 2009. "The piecewise smooth Mumford–Shah functional on an arbitrary graph". *Image Processing, IEEE Transactions on*, vol. 18, n° 11, p. 2547–2561.

Greig, D., B. Porteous, and A. Seheult. 1989. "Exact maximum a posteriori estimation for binary images". *Journal of the Royal Statistical Society. Series B (Methodological)*, vol. 51, n° 2, p. 271–279.

Gronenschild, E., J. Janssen, and F. Tijdens. 1994. "CAAS II: A second generation system for off-line and on-line quantitative coronary angiography". *Catheterization and cardiovascular diagnosis*, vol. 33, n° 1, p. 61–75.

Grube, E., L. Buellesfeld, R. Mueller, B. Sauren, B. Zickmann, D. Nair, H. Beucher, T. Felderhoff, S. Iversen, and U. Gerckens. 2008. "Progress and current status of percutaneous aortic valve replacement: results of three device generations of the CoreValve Revalving system". *Circulation: Cardiovascular Interventions*, vol. 1, n° 3, p. 167.

Hadida, J., C. Desrosiers, and L. Duong. 2012. "Stochastic 3d motion compensation of coronary arteries from monoplane angiograms". In *Medical Image Computing and Computer-Assisted Intervention–MICCAI 2012*. p. 651–658. Springer.

Hagen, L. and A. Kahng. 1992. "New spectral methods for ratio cut partitioning and clustering". *Computer-aided design of integrated circuits and systems, ieee transactions on*, vol. 11, n° 9, p. 1074–1085.

HealthCanada. 2002. "Congenital anomalies in Canada - a perinatal health report". <http://www.phac-aspc.gc.ca/publicat/cac-acc02/pdf/cac2002_e.pdf>.

Hernández-Vela, A., C. Gatta, S. Escalera, L. Igual, V. Martin-Yuste, M. Sabaté, and P. Radeva. 2012. "Accurate coronary centerline extraction, caliber estimation and catheter detection in angiographies". *Information Technology in Biomedicine, IEEE Transactions on*, vol. 16, n° 6, p. 1332–1340.

Hill, D. L., P. G. Batchelor, M. Holden, and D. J. Hawkes. 2001. "Medical image registration". *Physics in medicine and biology*, vol. 46, n° 3, p. R1.

Hipwell, J., G. Penney, R. McLaughlin, K. Rhode, P. Summers, T. Cox, J. Byrne, J. Noble, and D. Hawkes. 2003. "Intensity-based 2-D-3-D registration of cerebral angiograms". *Medical Imaging, IEEE Transactions on*, vol. 22, n° 11, p. 1417–1426.

2001. *Grouping connected components using minimal path techniques. application to reconstruction of vessels in 2D and 3D images*, volume 2. IEEE.

Ionasec, R., B. Georgescu, E. Gassner, S. Vogt, O. Kutter, M. Scheuering, N. Navab, and D. Comaniciu. 2008. "Dynamic model-driven quantitative and visual evaluation of the aortic valve from 4D CT". *Medical Image Computing and Computer-Assisted Intervention– MICCAI 2008*, p. 686–694.

Jain, A. K., R. P. W. Duin, and J. Mao. 2000. "Statistical pattern recognition: A review". *IEEE TRANSACTIONS ON PATTERN ANALYSIS AND MACHINE INTELLIGENCE*, vol. 22, n° 1, p. 4–37.

Janssen, J. P., A. Rares, J. C. Tuinenburg, G. Koning, A. J. Lansky, and J. H. Reiber. 2010. "New approaches for the assessment of vessel sizes in quantitative (cardio-) vascular X-ray analysis". *The international journal of cardiovascular imaging*, vol. 26, n° 3, p. 259–271.

Kaeppler, S., A. Brost, M. Koch, W. Wu, F. Bourier, T. Chen, K. Kurzidim, J. Hornegger, and N. Strobel. 2012. "Motion estimation model for cardiac and respiratory motion compensation". In *Information Processing in Computer-Assisted Interventions*. p. 94–103. Springer.

Kalpathy-Cramer, J. and W. Hersh. 2007. "Automatic image modality based classification and annotation to improve medical image retrieval". *Studies in health technology and informatics*, vol. 129, n° 2, p. 1334.

Kass, M., A. Witkin, and D. Terzopoulos. 1988. "Snakes: Active contour models". *International journal of computer vision*, vol. 1, n° 4, p. 321–331.

Kelle, S., A. G. Hays, G. A. Hirsch, G. Gerstenblith, J. M. Miller, A. M. Steinberg, M. Schär, J. H. Texter, E. Wellnhofer, R. G. Weiss, and M. Stuber. 2011. "Coronary Artery Distensibility Assessed by 3.0 Tesla Coronary Magnetic Resonance Imaging in Subjects With and Without Coronary Artery Disease". *The American Journal of Cardiology*, vol. 108, n° 4, p. 491 - 497.

Kirbas, C. and F. Quek. 2004. "A review of vessel extraction techniques and algorithms". *ACM Comput. Surv.*, vol. 36, n° 2, p. 81–121.

Kondo, C., M. Hiroe, T. Nakanishi, and A. Takao. 1989. "Detection of coronary artery stenosis in children with Kawasaki disease. Usefulness of pharmacologic stress 201Tl myocardial tomography.". *Circulation*, vol. 80, n° 3, p. 615–624.

Kroon, D. J. March 2010. "Hessian based Frangi Vesselness filter implementation". [Online] Availabe : http://www.mathworks.com/matlabcentral/fileexchange/24409-hessian-based-frangi-vesselness-filter.

Kroon, D.-J., C. Slump, and T. Maal. 2010. Optimized anisotropic rotational invariant diffusion scheme on cone-beam ct. Jiang, T., Nassir Navab, Josien Pluim, and Max Viergever, editors, *Medical Image Computing and Computer-Assisted Intervention – MICCAI 2010*, volume 6363 of *Lecture Notes in Computer Science*, p. 221-228. Springer Berlin / Heidelberg.

Laguitton, S., C. Boldak, and C. Toumoulin. 2007. "Temporal tracking of coronaries in multi-slice computed tomography". In *EMBS*. p. 4512–4515. IEEE.

Lankton, S. and A. Tannenbaum. 2008. "Localizing region-based active contours". *Image Processing, IEEE Transactions on*, vol. 17, n° 11, p. 2029–2039.

Larralde, A., C. Boldak, M. Garreau, C. Toumoulin, D. Boulmier, and Y. Rolland. 2003. "Evaluation of a 3D segmentation software for the coronary characterization in multi-slice computed tomography". *Functional Imaging and Modeling of the Heart*, p. 1005–1005.

Lathen, G., J. Jonasson, and M. Borga. 2010. "Blood vessel segmentation using multi-scale quadrature filtering". *Pattern Recognition Letters*, vol. 31, n° 8, p. 762–767.

Lehmann, T., M. Gold, C. Thies, B. Fischer, K. Spitzer, D. Keysers, H. Ney, M. Kohnen, H. Schubert, and B. Wein. 2004. "Content-based image retrieval in medical applications". *Methods of Information in Medicine*, vol. 43, n° 4, p. 354–361.

Lesage, D., E. Angelini, I. Bloch, and G. Funka-Lea. 2009. "A review of 3D vessel lumen segmentation techniques: Models, features and extraction schemes". *Medical Image Analysis*, vol. 13, n° 6, p. 819 - 845.

Lewis, J. H. and S. B. Jiang. 2009. "A theoretical model for respiratory motion artifacts in free-breathing CT scans". *Physics in medicine and biology*, vol. 54, n° 3, p. 745.

Li, C., C. Xu, C. Gui, and M. Fox. 2005. "Level set evolution without re-initialization: A new variational formulation". In *Computer Vision and Pattern Recognition, 2005. CVPR 2005. IEEE Computer Society Conference on*. p. 430–436. IEEE.

Li, C., C. Kao, J. Gore, and Z. Ding. 2008. "Minimization of region-scalable fitting energy for image segmentation". *Image Processing, IEEE Transactions on*, vol. 17, n° 10, p. 1940–1949.

Li, C., C.-Y. Kao, J. C. Gore, and Z. Ding. 2007. "Implicit active contours driven by local binary fitting energy". In *Computer Vision and Pattern Recognition, 2007. CVPR'07. IEEE Conference on*. p. 1–7. IEEE.

Liao, R., L. Duong, Y. Sun, and K. Kirchberg. 2010. "3-D reconstruction of the coronary artery tree from multiple views of a rotational X-ray angiography". *The International Journal of Cardiovascular Imaging (formerly Cardiac Imaging)*, vol. 26, n° 7, p. 733–749.

Ling, H. and D. Jacobs. 2007. "Shape classification using the inner-distance". *Pattern Analysis and Machine Intelligence, IEEE Transactions on*, vol. 29, n° 2, p. 286–299.

Lombaert, H. 2012. "Atlas Construction for Measuring the Variability of Complex Anatomical Structures". PhD thesis, École Polytechnique de Montréal.

Lowe, D. G. 2004. "Distinctive Image Features from Scale-Invariant Keypoints". *Int. J. Comput. Vision*, vol. 60, n° 2, p. 91–110.

Mackay, J. and G. Mensah. 2004. The atlas of heart disease and stroke (who).

Manniesing, R., B. Velthuis, M. Van Leeuwen, I. Van der Schaaf, P. Van Laar, and W. Niessen. 2006. "Level set based cerebral vasculature segmentation and diameter quantification in CT angiography". *Medical Image Analysis*, vol. 10, n° 2, p. 200–214.

Markelj, P., D. Tomaževič, B. Likar, and F. Pernuš. 2010. "A review of 3D/2D registration methods for image-guided interventions". *Medical image analysis*.

Maurice, R. L., L. Vaujois, N. Dahdah, N. Chibab, A. Maurice, A.-M. Nuyt, É. Lévy, and J.-L. Bigras. 2014. "Carotid Wall Elastography to Assess Midterm Vascular Dysfunction Secondary to Intrauterine Growth Restriction: Feasibility and Comparison with Standardized Intima-Media Thickness". *Ultrasound in medicine & biology*, vol. 40, n° 5, p. 864–870.

Medis. "QAngio XA". <http://www.medis.nl/Products/QAngioXA>.

Mendis, S., P. Puska, and B. Norrving. 2011. *Global Atlas on Cardiovascular Disease Prevention and Control*. World Health Organization, Geneva, ed. Shanthi Mendis, Pekka Puska and Bo Norrving. <http://www.who.int/cardiovascular_diseases/publications/atlas_cvd/en/index.html>.

M'hiri, F., L. Duong, and C. Desrosiers. 2012a. "Combining Laplacian eigenmaps and vesselness filters for vessel segmentation in X-ray angiography". In *Computer Vision and Pattern Recognition Workshops (CVPRW), 2012 IEEE Computer Society Conference on*. p. 70–75. IEEE.

M'hiri, F., N. Hoang, L. Duong, and M. Cheriet. 2012b. "A new adaptive framework for tubular structures segmentation in X-ray angiography". In *Information Science, Signal Processing and their Applications (ISSPA), 2012 11th International Conference on*. p. 496–500. IEEE.

M'hiri, F., L. Duong, C. Desrosiers, and M. Cheriet. 2013. "Vessel Walker: Coronary arteries segmentation using random walks and hessian-based vesselness filter". In *ISBI*. p. 918-921.

M'hiri, F., N. Hoang, L. Duong, and M. Cheriet. 2015. "Hierarchical Segmentation and Tracking of Coronary Arteries in 2d x-ray Angiography Sequences". In *International Conference on Image Processing (ICIP)*.

Mirhassani, S., M. Hosseini, and A. Behrad. 2010. "Improvement of Hessian based vessel segmentation using two stage threshold and morphological image recovering". In *Innovations in Information Technology, 2009. IIT'09. International Conference on*. p. 50–54. IEEE.

Mirzaalian, H. and G. Hamarneh. 2010. "Vessel scale-selection using mrf optimization". In *Computer Vision and Pattern Recognition (CVPR), 2010 IEEE Conference on*. p. 3273–3279. IEEE.

Mori, G. 2005. "Guiding model search using segmentation". In *Computer Vision, 2005. ICCV 2005. Tenth IEEE International Conference on*. p. 1417–1423. IEEE.

Mumford, D. and J. Shah. 1989. "Optimal approximations by piecewise smooth functions and associated variational problems". *Communications on pure and applied mathematics*, vol. 42, n° 5, p. 577–685.

Nieuwenhuis, C., E. Toeppe, L. Gorelick, O. Veksler, and Y. Boykov. 2014. "Efficient squared curvature". In *Proceedings of the IEEE Conference on Computer Vision and Pattern Recognition*. p. 4098–4105.

Oberhoffer, R., D. Lang, and K. Feilen. 1989. "The diameter of coronary arteries in infants and children without heart disease". *European journal of pediatrics*, vol. 148, n° 5, p. 389–392.

Osher, S. and J. Sethian. 1988. "Fronts propagating with curvature-dependent speed: algorithms based on Hamilton-Jacobi formulations". *Journal of computational physics*, vol. 79, n° 1, p. 12–49.

Otsu, N. 1979. "A threshold selection method from gray-level histograms". *IEEE Transactions on Systems, Man and Cybernetics*, vol. 9, n° 1, p. 62–66.

Pamulapati, V., B. Wood, and M. Linguraru. 2011. "Intra-hepatic vessel segmentation and classification in multi-phase CT using optimized graph cuts". In *Biomedical Imaging: From Nano to Macro, 2011 IEEE International Symposium on*. p. 1982–1985. IEEE.

Paragios, N. 2005. "Curve Propagation, Level Set Methods and Grouping".

Peter WG, T., P. Mark S, B. Mary, and R. Judith. 2010. "20-year survival of children born with congenital anomalies: a population-based study". *The Lancet*, vol. 375, n° 9715, p. 649 - 656.

pie medical imaging. 02 2013a. *Quantification of diameters can improve bioresorbable stent therapies (White paper)*. pie medical imaging.

pie medical imaging. 02 2013b. *CAAS QCA The applications and benefits of quantitative coronary angiography (White paper)*. pie medical imaging, http://www.piemedicalimaging.com/wp-content/uploads/2013/02/White-paper-CAAS-QCA.pdf.

PIEMedical. "CAAS". <http://www.piemedicalimaging.com/partner/caas/>.

Preim, B. and D. Bartz, 2007. *Visualization in Medicine. Theory, Algorithms, and Applications. Series in Computer Graphics*.

Ren, X. and J. Malik. 2003. "Learning a classification model for segmentation". In *Computer Vision, 2003. Proceedings. Ninth IEEE International Conference on*. p. 10–17. IEEE.

Rivest-Henault, D. and M. Cheriet. 2013. "3-D curvilinear structure detection filter via structure-ball analysis". *Image Processing, IEEE Transactions on*, vol. 22, n° 7, p. 2849–2863.

Rivest-Hénault, D., C. Lapierre, S. Deschênes, and M. Cheriet. 2010. "Length increasing active contour for the segmentation of small blood vessels". In *20th International Conference on Pattern Recognition*.

Rivest-Henault, D., H. Sundar, and M. Cheriet. 2012. "Nonrigid 2D/3D registration of coronary artery models with live fluoroscopy for guidance of cardiac interventions". *Medical Imaging, IEEE Transactions on*, vol. 31, n° 8, p. 1557–1572.

Rousson, M. and N. Paragios. March 2008. "Prior Knowledge, Level Set Representations & Visual Grouping". *Int. J. Comput. Vision*, vol. 76, p. 231–243.

Rudyanto, R. D., S. Kerkstra, E. M. Van Rikxoort, C. Fetita, P.-Y. Brillet, C. Lefevre, W. Xue, X. Zhu, J. Liang, İ. Öksüz, et al. 2014. "Comparing algorithms for automated vessel segmentation in computed tomography scans of the lung: the VESSEL12 study". *Medical image analysis*, vol. 18, n° 7, p. 1217–1232.

Rueckert, D. and P. Aljabar. 2015. Non-rigid registration using free-form deformations. Paragios, N., James Duncan, and Nicholas Ayache, editors, *Handbook of Biomedical Imaging*, p. 277-294. Springer US. ISBN 978-0-387-09748-0. doi: 10.1007/978-0-387-09749-7_15. <http://dx.doi.org/10.1007/978-0-387-09749-7_15>.

Rueckert, D. and J. Schnabel. 2014. Registration and segmentation in medical imaging. Cipolla, R., Sebastiano Battiato, and Giovanni Maria Farinella, editors, *Registration and Recognition in Images and Videos*, volume 532 of *Studies in Computational Intelligence*, p. 137-156. Springer Berlin Heidelberg. ISBN 978-3-642-44906-2. doi: 10.1007/978-3-642-44907-9_7. <http://dx.doi.org/10.1007/978-3-642-44907-9_7>.

Ruijters, D., B. ter Haar Romeny, and P. Suetens. 2009. "Vesselness-based 2D–3D registration of the coronary arteries". *International journal of computer assisted radiology and surgery*, vol. 4, n° 4, p. 391–397.

Sadick, V., W. Reed, L. Collins, N. Sadick, R. Heard, and J. Robinson. 2014. "Impact of biplane versus single-plane imaging on radiation dose, contrast load and procedural time in coronary angioplasty". *The British journal of radiology*.

Sato, Y., S. Nakajima, N. Shiraga, H. Atsumi, S. Yoshida, T. Koller, G. Gerig, and R. Kikinis. 1998. "Three-dimensional multi-scale line filter for segmentation and visualization of curvilinear structures in medical images". *Medical Image Analysis*, vol. 2, n° 2, p. 143 - 168.

Schaap, M., L. Neefjes, C. Metz, A. van der Giessen, A. Weustink, N. Mollet, J. Wentzel, T. van Walsum, and W. Niessen. 2009. "Coronary lumen segmentation using graph cuts and robust kernel regression". In *Information Processing in Medical Imaging*. p. 528–539. Springer.

Schoenemann, T., F. Kahl, and D. Cremers. 2009. "Curvature regularity for region-based image segmentation and inpainting: A linear programming relaxation". In *2009 IEEE 12th International Conference on Computer Vision*. p. 17–23. IEEE.

Segars, W. P. and B. M. Tsui. 2009. "MCAT to XCAT: The evolution of 4-D computerized phantoms for imaging research". *Proceedings of the IEEE*, vol. 97, n° 12, p. 1954–1968.

Serra, J., 1982. *Image Analysis and Mathematical Morphology*.

Shahzad, R., H. Kirişli, C. Metz, H. Tang, M. Schaap, L. van Vliet, W. Niessen, and T. van Walsum. 2013. "Automatic segmentation, detection and quantification of coronary artery stenoses on CTA". *The international journal of cardiovascular imaging*, vol. 29, n° 8, p. 1847–1859.

Shechter, G., F. Devernay, E. Coste-Manière, A. Quyyumi, and E. R. McVeigh. 2003. "Three-dimensional motion tracking of coronary arteries in biplane cineangiograms". *Medical Imaging, IEEE Transactions on*, vol. 22, n° 4, p. 493–503.

Shechter, G., C. Ozturk, J. R. Resar, and E. R. McVeigh. 2004. "Respiratory motion of the heart from free breathing coronary angiograms". *Medical Imaging, IEEE Transactions on*, vol. 23, n° 8, p. 1046–1056.

Shen, J., Y. Du, W. Wang, and X. Li. 2014. "Lazy random walks for superpixel segmentation". *Image Processing, IEEE Transactions on*, vol. 23, n° 4, p. 1451–1462.

Shi, J. and J. Malik. 2000. "Normalized cuts and image segmentation". *Pattern Analysis and Machine Intelligence, IEEE Transactions on*, vol. 22, n° 8, p. 888–905.

Smets, C., G. Verbeeck, P. Suetens, and A. Oosterlinck. 1988. "A knowledge-based system for the delineation of blood vessels on subtraction angiograms". *Pattern recognition letters*, vol. 8, n° 2, p. 113–121.

Soares, J., J. Leandro, R. Cesar, H. Jelinek, and M. Cree. 2006. "Retinal vessel segmentation using the 2-D Gabor wavelet and supervised classification". *Medical Imaging, IEEE Transactions on*, vol. 25, n° 9, p. 1214–1222.

2007. *An ontology-based technique for validation of MRI brain segmentation methods*. Springer.

Sumengen, B. and B. Manjunath. 2006. "Graph partitioning active contours (GPAC) for image segmentation". *IEEE transactions on pattern analysis and machine intelligence*, p. 509–521.

Sumengen, B., S. Bhagavathy, and B. Manjunath. 2004. "Graph Partitioning Active Contours for Knowledge-Based Geo-Spatial Segmentation". In *Computer Vision and Pattern Recognition Workshop, 2004. CVPRW '04. Conference on*. p. 54.

Sun, K., Z. Chen, and S. Jiang. 2012. "Local morphology fitting active contour for automatic vascular segmentation". *Biomedical Engineering, IEEE Transactions on*, vol. 59, n° 2, p. 464–473.

Sundar, H. 3 2015. "Non-rigid 2D/3D registration of coronary artery models with live fluoroscopy images". <https://www.google.com/patents/US8948487>. US Patent 8,948,487.

Sundar, H., A. Khamene, C. Xu, F. Sauer, and C. Davatzikos. 2006. "A novel 2D-3D registration algorithm for aligning fluoro images with 3D pre-op CT/MR images". In *Medical Imaging*. p. 61412K–61412K. International Society for Optics and Photonics.

Syeda-Mahmood, T., D. Beymer, F. Wang, A. Mahmood, R. Lundstrom, N. Shafee, and T. Holve. 2010. "Automatic selection of keyframes from angiogram videos". In *Pattern Recognition (ICPR), 2010 20th International Conference on*. p. 4008–4011. IEEE.

Syeda-Mahmood, T., F. Wang, R. Kumar, D. Beymer, Y. Zhang, R. Lundstrom, and E. Mc-Nulty. 2012. Finding similar 2d x-ray coronary angiograms. *Medical Image Computing and Computer-Assisted Intervention–MICCAI 2012*, p. 501–508. Springer.

Tingelhoff, K., A. Moral, M. Kunkel, M. Rilk, I. Wagner, K. Eichhorn, F. Wahl, and F. Bootz. 2007. "Comparison between manual and semi-automatic segmentation of nasal cavity and paranasal sinuses from ct images". In *Engineering in Medicine and Biology Society, 2007. EMBS 2007. 29th Annual International Conference of the IEEE*. p. 5505–5508. IEEE.

Tomasello, S. D., A. R. Galassi, and L. Costanzo, 2011. *Advances in the Diagnosis of Coronary Atherosclerosis*, chapter Quantitative Coronary Angiography in the Interventional Cardiology, p. 255-272. INTECH Open Access Publisher.

Tomkowiak, M. T., A. N. Raval, M. S. Van Lysel, T. Funk, and M. A. Speidel. 2014. "Calibration-free coronary artery measurements for interventional device sizing using inverse geometry x-ray fluoroscopy: in vivo validation". *Journal of Medical Imaging*, vol. 1, n° 3, p. 033504–033504.

Van Bemmel, C., L. Spreeuwers, M. Viergever, and W. Niessen. 2002. Level-set based carotid artery segmentation for stenosis grading. Dohi, T. and Ron Kikinis, editors, *Medical Image Computing and Computer-Assisted Intervention MICCAI 2002*, volume 2489 of *Lecture Notes in Computer Science*, p. 36-43. Springer Berlin / Heidelberg.

Vasilevskiy, A. and K. Siddiqi. 2002. "Flux Maximizing Geometric Flows". *IEEE Trans. Pattern Anal. Mach. Intell.*, vol. 24, n° 12, p. 1565–1578.

Vaujois, L., F. Dallaire, R. L. Maurice, A. Fournier, C. Houde, J. Thérien, D. Cartwright, and N. Dahdah. 2013. "The Biophysical Properties of the Aorta Are Altered Following Kawasaki Disease". *Journal of the American Society of Echocardiography*, vol. 26, n° 12, p. 1388–1396.

Viard, R. 2009. "Présentation des différentes avancées techniques en imagerie interventionnelle par résonance magnétique". *IRBM*, vol. 30, n° 2, p. 85 - 91.

Von Luxburg, U. 2007. "A tutorial on spectral clustering". *Statistics and computing*, vol. 17, n° 4, p. 395–416.

Wang, C., R. Moreno, and Ö. Smedby. 2012. "Vessel segmentation using implicit model-guided level sets". In *MICCAI Workshop" 3D Cardiovascular Imaging: a MICCAI segmentation Challenge", Nice France, 1st of October 2012*.

Wang, K., R. Dutton, and C. Taylor. 1999. "Improving geometric model construction for blood flow modeling". *Engineering in Medicine and Biology Magazine, IEEE*, vol. 18, n° 6, p. 33–39.

Wang, L., C. Li, Q. Sun, D. Xia, and C. Kao. 2009. "Active contours driven by local and global intensity fitting energy with application to brain MR image segmentation". *Computerized Medical Imaging and Graphics*, vol. 33, n° 7, p. 520–531.

Wang, S. and J. Siskind. 2003. "Image segmentation with ratio cut". *Pattern Analysis and Machine Intelligence, IEEE Transactions on*, vol. 25, n° 6, p. 675–690.

Weickert, J., 1998. *Anisotropic diffusion in image processing*, volume 256.

Weinberg, E. J. and M. R. K. Mofrad. 2008. "A multiscale computational comparison of the bicuspid and tricuspid aortic valves in relation to calcific aortic stenosis". *Journal of Biomechanics*, vol. 41, n° 16, p. 3482 - 3487.

WHO, W. H. O. May 2014. "The top 10 causes of death : Fact sheet N 310". <http://who.int/mediacentre/factsheets/fs310/en/index2.html>.

Williams, J., R. Coeytaux, A. Wang, and D. Glower. August 2010. *Percutaneous heart valve replacement. technical brief no. 2.* Technical report.

Wong, D., J. Liu, Y. Fengshou, Q. Tian, W. Xiong, J. Zhou, Y. Qi, T. Han, S. Venkatesh, and S. Wang. 2009. "A semi-automated method for liver tumor segmentation based on 2D region growing with knowledge-based constraints". In *Proceedings of MICCAI workshop on 3D segmentation in the clinic: a grand challenge II. New York, NY, USA.*

Xu, C. and J. Prince. 2002. "Snakes, shapes, and gradient vector flow". *Image Processing, IEEE Transactions on*, vol. 7, n° 3, p. 359–369.

Yang, F., H. Lu, and M.-H. Yang. 2014. "Robust superpixel tracking". *Image Processing, IEEE Transactions on*, vol. 23, n° 4, p. 1639–1651.

Yang, Y., A. Tannenbaum, and D. Giddens. 2004. "Knowledge-based 3D segmentation and reconstruction of coronary arteries using CT images". In *Engineering in Medicine and Biology Society, 2004. IEMBS'04. 26th Annual International Conference of the IEEE*. p. 1664–1666. IEEE.

Yang, Y., A. Tannenbaum, D. Giddens, and A. Stillman. 2007. "Automatic segmentation of coronary arteries using Bayesian driven implicit surfaces". In *Biomedical Imaging: From Nano to Macro, 2007. ISBI 2007. 4th IEEE International Symposium on*. p. 189–192. IEEE.

Yi, J. and J. Ra. 2003. "A locally adaptive region growing algorithm for vascular segmentation". *International journal of imaging systems and technology*, vol. 13, n° 4, p. 208–214.

Yumei, W. 2011. "Tracking of coronary arteries in angiogram sequence by structural matching of junctions". Master's thesis.

Zhang, D. P., L. Risser, O. Friman, C. Metz, L. Neefjes, N. Mollet, W. Niessen, and D. Rueckert. 2010a. Nonrigid registration and template matching for coronary motion modeling from 4d cta. *Biomedical Image Registration*, p. 210–221. Springer.

Zhang, K., L. Zhang, H. Song, and W. Zhou. 2010b. "Active contours with selective local or global segmentation: A new formulation and level set method". *Image and Vision Computing*, vol. 28, n° 4, p. 668–676.

Zhao, M., H.-Y. Lin, C.-H. Yang, C.-Y. Hsu, J.-S. Pan, and M.-J. Lin. 2015a. "Automatic threshold level set model applied on MRI image segmentation of brain tissue". *Appl. Math*, vol. 9, n° 4, p. 1971–1980.

Zhao, Y., L. Rada, K. Chen, S. P. Harding, and Y. Zheng. 2015b. "Automated Vessel Segmentation Using Infinite Perimeter Active Contour Model with Hybrid Region Information with Application to Retinal Images". *Medical Imaging, IEEE Transactions on*, vol. 34, n° 9, p. 1797–1807.

Zhao, Y. Q., X. H. Wang, X. F. Wang, and F. Y. Shih. 2014. "Retinal vessels segmentation based on level set and region growing". *Pattern Recognition*, vol. 47, n° 7, p. 2437–2446.

Zheng, Y., A. Barbu, B. Georgescu, M. Scheuering, and D. Comaniciu. 2007. "Fast automatic heart chamber segmentation from 3D CT data using marginal space learning and steerable features". In *Proc. ICCV*. p. 31–94. Citeseer.

Zhu, N. and A. C. Chung. 2013. Random walks with adaptive cylinder flux based connectivity for vessel segmentation. *Medical Image Computing and Computer-Assisted Intervention–MICCAI 2013*, p. 550–558. Springer.

ZooFari. March 2010. "Human heart diagram". <https://en.wikipedia.org/wiki/File:Heart_diagram-en.svg>.